



UNIVERSIDADE FEDERAL DO CEARÁ
CENTRO DE CIÊNCIAS
DEPARTAMENTO DE BIOQUÍMICA E BIOLOGIA MOLECULAR
PROGRAMA DE PÓS-GRADUAÇÃO EM BIOQUÍMICA

**BIOINFORMÁTICA APLICADA AO DESENVOLVIMENTO DE DROGAS
CONTRA O CÂNCER GÁSTRICO**

DAIANE MARIA DA SILVA BRITO

FORTALEZA
2024

DAIANE MARIA DA SILVA BRITO

**BIOINFORMÁTICA APLICADA AO DESENVOLVIMENTO DE DROGAS
CONTRA O CÂNCER GÁSTRICO**

Dissertação apresentada ao Programa de Pós-Graduação em Bioquímica da Universidade Federal do Ceará, como parte dos requisitos para obtenção do título de Mestre em Bioquímica.

Orientador: Professor Dr. Pedro Filho
Noronha de Souza

FORTALEZA
2024

Dados Internacionais de Catalogação na Publicação
Universidade Federal do Ceará
Sistema de Bibliotecas
Gerada automaticamente pelo módulo Catalog, mediante os dados fornecidos pelo(a) autor(a)

B875b Brito, Daiane Maria da Silva.

Bioinformática aplicada ao desenvolvimento de drogas contra o câncer gástrico / Daiane Maria da Silva Brito. – 2024.

120 f. : il. color.

Dissertação (mestrado) – Universidade Federal do Ceará, Centro de Ciências, Programa de Pós-Graduação em Bioquímica, Fortaleza, 2024.

Orientação: Prof. Dr. Pedro Filho Noronha de Souza.

1. Células cancerosas. 2. Alvos terapêuticos. 3. Peptídeos antimicrobianos sintéticos. I. Título.

CDD 572

DAIANE MARIA DA SILVA BRITO

**BIOINFORMÁTICA APLICADA AO DESENVOLVIMENTO DE DROGAS
CONTRA O CÂNCER GÁSTRICO**

Aprovado em: ____/____/____.

BANCA EXAMINADORA

Prof.^ª Dr.^ª Raquel Carvalho Montenegro
Universidade Federal do Ceará

Prof. Dr. Rafael Wesley Bastos
Universidade Federal do Rio Grande do Norte

Prof. Dr. Pedro Filho Noronha de Souza (Orientador)
Universidade Federal do Ceará

À minha família,
por todo seu amor,
e paciência.

RESUMO

O câncer gástrico (CG) representa um desafio significativo para a saúde pública, sendo classificado como a quinta neoplasia maligna mais comum e a quarta principal causa de mortalidade relacionada com câncer em todo o mundo. Em 2020, ano em que foram divulgadas as últimas estimativas pelo Globocan, foi estimado 1.089.103 novos casos e 768.793 mortes por câncer gástrico. Estes dados destacam a necessidade urgente de avanços no tratamento para combater o CG. Embora o tratamento tenha melhorado gradualmente nas últimas décadas, a sobrevida mediana dos pacientes com CG avançado ainda é muito baixa, inferior a 12 meses. A heterogeneidade dos tumores, a resistência aos agentes quimioterápicos, a falta de seletividade e, conseqüente, toxicidade às células saudáveis dos pacientes limitam o tratamento desta neoplasia e contribuem para que o prognóstico da carcinogênese gástrica seja bastante desafiador. Neste contexto, é urgente a busca por moléculas com baixos níveis de toxicidade que explorem novos alvos terapêuticos no câncer, para isso, estudos de transcriptoma de *microarrays* combinados à técnica de SBVS (do inglês, *Structure-Based Virtual Screening*) se mostram promissores. Adicionalmente, outra estratégia importante é o reposicionamento de peptídeos antimicrobianos sintéticos (SAMPs) para o tratamento do câncer gástrico. Estes quais, representam uma alternativa de intervenção terapêutica para CG por serem estrategicamente projetados, a partir de sequências de proteínas, para terem baixos níveis de toxicidade, desempenho multifacetado e alta seletividade. Portanto, o presente trabalho teve dois principais objetivos (1) desenvolver, por bioinformática, uma *pipeline* eficiente para identificar novos alvos terapêuticos no câncer gástrico, além de buscar compostos inibidores para os alvos identificados; (2) realizar estudos *in silico*, *in vitro* e *in vivo* para investigar o reposicionamento dos SAMPs como potencial abordagem terapêutica no CG. Na primeira parte deste trabalho, os dados foram coletados no banco *Gene Expression Omnibus (GEO)* de três matrizes de conjuntos de dados que analisaram tecido tumoral gástrico *versus* tecido gástrico normal, realizados por microarranjos usando a plataforma GPL570. Os dados foram analisados pela ferramenta GEPIA para expressão diferencial e *KMPlot* para análise de sobrevivência de pacientes. Para maior robustez, foram utilizados dados de CG presentes no banco de dados do TCGA (do inglês, *The Cancer Genome Atlas Program*) para corroborar a análise do GEO. Os genes encontrados na análise *in silico*, através do GEO e TCGA, foram confirmados em diferentes linhagens celulares de CG por RT-qPCR. O banco de dados *AlphaFold* foi usado para encontrar a estrutura 3D das proteínas codificadas pelos genes superexpressos. Em seguida, a técnica de SBVS foi empregada para encontrar moléculas com alta afinidade de ligação com as proteínas selecionadas, e, portanto, a análise de *docking* molecular foi realizada utilizando o servidor *DockThor*. Na segunda parte deste trabalho, os conhecimentos adquiridos por meio dos estudos de bioinformática foram empregados para avaliar o reposicionamento de peptídeos sintéticos antimicrobianos contra o câncer gástrico. Utilizando as sequências dos peptídeos sintéticos, foi possível conduzir uma análise preditiva sobre o seu potencial anticâncer. Além disso, por meio da bioinformática, realizou-se um estudo de predição de toxicidade com diferentes parâmetros, incluindo LD₅₀. Os peptídeos selecionados pelos testes *in silico* foram testados através de experimentos *in vitro* contra diversas linhagens de CG. Os peptídeos que demonstraram uma CI₅₀ contra as células tumorais gástricas foram então utilizados nos estudos de mecanismos de ação, os quais incluíram avaliações do aumento da permeabilidade e formação de poros na membrana, análises morfológicas por microscopia de força atômica (AFM) e inibição da migração celular. Ainda *in vitro*, foram realizados testes de toxicidade contra células humanas saudáveis para avaliar a segurança do(s) peptídeo(s) com ação anticâncer. Testes de toxicidade *in vivo* contra peixe-zebra foram realizados para avaliar a potencial aplicação desse(s) peptídeo(s) na terapia contra o CG. Por último, o(s) peptídeo(s)

selecionado(s) foi submetido a ensaios de *docking* molecular para avaliar sua interação com os novos alvos identificados na parte I deste trabalho e superexpressos na linhagem AGP-01. Com relação aos resultados, na primeira parte do trabalho, as análises *in silico* e por RT-qPCR (*in vitro*) confirmaram a alta expressão dos genes *AJUBA*, *CD80* e *NOLCI* em linhagens gástricas tumorais. Posteriormente, as estruturas 3D das proteínas correspondentes a esses genes foram utilizadas na análise de SBVS, resultando na seleção de três moléculas, uma para cada alvo: MCULE-2386589557-0-6, MCULE-9178344200-0-1 e MCULE-5881513100-0-29. Todas as moléculas demonstraram propriedades farmacocinéticas, farmacodinâmicas e toxicológicas favoráveis. A análise de *docking* molecular revelou que as moléculas interagiram com proteínas-alvo em locais críticos para sua atividade, alterando suas estruturas tridimensionais e, possivelmente, sua função nas células gástricas tumorais. Na segunda parte do estudo, seis peptídeos sintéticos foram avaliados por bioinformática em relação ao seu potencial anticâncer e obtiveram resultados positivos de predição. Assim, todos eles foram submetidos a ensaios *in vitro* contra diferentes linhagens celulares de câncer gástrico. Quatro desses peptídeos apresentaram valores de CI_{50} contra células de CG. Entre esses quatro, o peptídeo *RcAlb-PepI* demonstrou um valor de CI_{50} baixo (53,87 $\mu\text{g/mL}$) contra a linha de CG metastática AGP-01. Além disso, o *RcAlb-PepI* exibiu baixa toxicidade em células gástricas saudáveis (MNP-01) em comparação com os outros peptídeos. Este peptídeo induziu um aumento na permeabilidade da membrana, seguido pela formação de um poro de 6 kDa na membrana da célula AGP-01. As análises de AFM revelaram que o *RcAlb-PepI* foi capaz de modificar as propriedades ultraestruturais e nanomecânicas das células AGP-01, resultando em aumento de rugosidade, adesão, área e volume celular, bem como redução da plasticidade celular e organização do citoesqueleto. Estes dados corroboraram com o efeito inibitório, observado no ensaio de migração celular, do *RcAlb-PepI* sobre a célula AGP-01. Os resultados de toxicidade *in vitro* e *in vivo* mostraram que o *RcAlb-PepI* não exibe toxicidade contra células saudáveis, embriões ou larvas de peixe-zebra, confirmando sua segurança. O ensaio de *docking* molecular demonstrou que o *RcAlb-PepI* apresentou forte interação com as proteínas *AJUBA* e *NOLCI*, identificadas na parte I deste trabalho e superexpressas na linhagem AGP-01. Como conclusão, este trabalho apresenta uma *pipeline* construída por bioinformática que se mostrou eficiente na identificação de novos alvos terapêuticos no CG e de compostos inibidores para os alvos identificados, havendo possibilidade de extensão dessa *pipeline* para outros tipos de câncer. Além disso, revela a potencial aplicação do *RcAlb-PepI* contra a linhagem gástrica metastática AGP-01 e fornece *insights* sobre o mecanismo de ação desse peptídeo sintético por trás de sua atividade anticancerígena.

Palavras-chave: Células cancerosas; Alvos terapêuticos; Peptídeos antimicrobianos sintéticos; Triagem virtual; Reposicionamento de peptídeos; Resistência às drogas.

ABSTRACT

Gastric cancer (GC) represents a significant public health challenge, being ranked as the fifth most common malignancy and the fourth leading cause of cancer-related mortality worldwide. In 2020, the year in which the latest estimates were released by Globocan, there were an estimated 1,089,103 new cases and 768,793 deaths from gastric cancer. These data highlight the urgent need for advances in treatment to combat GC. Although treatment has gradually improved in recent decades, the median survival of patients with advanced GC is still very low, less than 12 months. The heterogeneity of tumors, resistance to chemotherapy agents, lack of selectivity and, consequently, toxicity to patients' healthy cells limit the treatment of this neoplasm and contribute to the prognosis of gastric carcinogenesis being quite challenging. In this context, it is urgent to search for molecules with low levels of toxicity that explore new therapeutic targets in cancer. To this end, microarray transcriptome studies combined with the SBVS technique (Structure-Based Virtual Screening) show promise. Additionally, another important strategy is the repositioning of synthetic antimicrobial peptides (SAMPs) for the treatment of gastric cancer. These represent an alternative therapeutic intervention for GC as they are strategically designed, based on protein sequences, to have low levels of toxicity, multifaceted performance and high selectivity. Therefore, the present work had two main objectives (1) to develop, through bioinformatics, an efficient pipeline to identify new therapeutic targets in gastric cancer, in addition to searching for inhibitory compounds for the identified targets; (2) carry out *in silico*, *in vitro* and *in vivo* studies to investigate the repositioning of SAMPs as a potential therapeutic approach in GC. In the first part of this work, data were collected in the Gene Expression Omnibus (GEO) database from three arrays of data sets that analyzed gastric tumor tissue versus normal gastric tissue, performed by microarrays using the GPL570 platform. Data were analyzed using the GEPIA tool for differential expression and KMPlot for patient survival analysis. For greater robustness, GC data from the TCGA database (The Cancer Genome Atlas Program) were used to corroborate the GEO analysis. The genes found in the *in silico* analysis, through GEO and TCGA, were confirmed in different GC cell lines by RT-qPCR. The AlphaFold database was used to find the 3D structure of the proteins encoded by the overexpressed genes. Then, the SBVS technique was used to find molecules with high binding affinity to the selected proteins, and, therefore, molecular docking analysis was performed using the DockThor server. In the second part of this work, the knowledge acquired through bioinformatics studies was used to evaluate the repositioning of synthetic antimicrobial peptides against gastric cancer. Using the sequences of synthetic peptides, it was possible to conduct a predictive analysis on their anticancer potential. Furthermore, using bioinformatics, a toxicity prediction study was carried out with different parameters, including LD50. The peptides selected by *in silico* tests were tested through *in vitro* experiments against several GC strains. The peptides that demonstrated an IC₅₀ against gastric tumor cells were then used in studies of mechanisms of action, which included assessments of increased permeability and formation of pores in the membrane, morphological analyzes by atomic force microscopy (AFM) and inhibition of migration cell phone. Still *in vitro*, toxicity tests were carried out against healthy human cells to evaluate the safety of the peptide(s) with anticancer action. *In vivo* toxicity tests against zebrafish were performed to evaluate the potential application of this peptide(s) in GC therapy. Finally, the selected peptide(s) were subjected to molecular docking assays to evaluate their interaction with the new targets identified in part I of this work and overexpressed in the AGP-01 strain. Regarding the results, in the first part of the work, *in silico* and RT-qPCR (*in vitro*) analyzes confirmed the high expression of the AJUBA, CD80 and NOLC1 genes in gastric tumor lines. Subsequently, the 3D structures of the proteins corresponding to these genes were used in the SBVS analysis,

resulting in the selection of three molecules, one for each target: MCULE-2386589557-0-6, MCULE-9178344200-0-1 and MCULE-5881513100- 0-29. All molecules demonstrated favorable pharmacokinetic, pharmacodynamic and toxicological properties. Molecular docking analysis revealed that the molecules interacted with target proteins at sites critical for their activity, altering their three-dimensional structures and, possibly, their function in gastric tumor cells. In the second part of the study, six synthetic peptides were evaluated by bioinformatics in relation to their anticancer potential and obtained positive prediction results. Thus, all of them were subjected to in vitro assays against different gastric cancer cell lines. Four of these peptides showed IC₅₀ values against GC cells. Among these four, the RcAlb-PepI peptide demonstrated a low IC₅₀ value (53.87 µg/mL) against the metastatic GC line AGP-01. Furthermore, RcAlb-PepI exhibited low toxicity in healthy gastric cells (MNP-01) compared to the other peptides. This peptide induced an increase in membrane permeability, followed by the formation of a 6 kDa pore in the AGP-01 cell membrane. AFM analyzes revealed that RcAlb-PepI was able to modify the ultrastructural and nanomechanical properties of AGP-01 cells, resulting in increased roughness, adhesion, cell area and volume, as well as reduced cellular plasticity and cytoskeletal organization. These data corroborated the inhibitory effect, observed in the cell migration assay, of RcAlb-PepI on the AGP-01 cell. In vitro and in vivo toxicity results showed that RcAlb-PepI does not exhibit toxicity against healthy zebrafish cells, embryos or larvae, confirming its safety. The molecular docking assay demonstrated that RcAlb-PepI showed a strong interaction with the AJUBA and NOLC1 proteins, identified in part I of this work and overexpressed in the AGP-01 strain. In conclusion, this work presents a pipeline built by bioinformatics that proved to be efficient in identifying new therapeutic targets in GC and inhibitory compounds for the identified targets, with the possibility of extending this pipeline to other types of cancer. Furthermore, it reveals the potential application of RcAlb-PepI against the metastatic gastric lineage AGP-01 and provides insights into the mechanism of action of this synthetic peptide behind its anticancer activity.

Keywords: Cancer cells; Therapeutic targets; Synthetic antimicrobial peptides; Virtual screening; Repositioning of peptides; Resistance to drugs.

LISTA DE ILUSTRAÇÕES

CAPÍTULO I

Figura 1 - <i>Hallmarks</i> do câncer	16
Figura 2 - Taxa de incidência global do câncer gástrico em 2022	20
Figura 3 - Fonte e estrutura de peptídeos antimicrobianos.....	27
Figura 4 - Comparação entre membranas de células bacterianas, células eritrocitárias e células cancerígenas.	29
Figura 5 - Microscopia de Força Atômica.....	32
Figura 6 - Alvos celulares de peptídeos.....	33

CAPÍTULO II

Figure 1 - Batch effect corrected among the studies and volcano plot of differentially expressed genes in gastric tumors	16
Figure 2 - Differentially expressed genes were found using GSEA	53
Figure 3 - TCGA (RNA-seq) expression data for selected genes using GEPIA.....	16
Figure 4 - Survival analysis for the genes using KM plotter.....	55
Figure 5 - The relative expression level of AJUBA, CD80, NOLC1 and KNL1 genes.....	55
Figure 6 - Molecular docking analysis of AJUBA, CD80, NOLC1 proteins.....	57
Figure 7 - Graphic representation of the network of protein interactions	59
Figure 8 - Re-docking analysis.....	16

CAPÍTULO III

Figure 1 - Analysis of membrane permeabilization, pore formation and ROS overaccumulation.....	84
Figure 2 - AFM analysis of AGP-01 cells control and treated with RcAlb-PepI.....	85
Figure 3 - Ultrastructural parameters obtained by AFM maps.....	86
Figure 4 - Nanomechanical parameters obtained from AFM maps	87
Figure 5 - Vibrational Signature of AGP-01 cells.....	88
Figure 6 - Migration assay of AGP-01 cells.....	90
Figure 7 - Molecular docking analysis between AJUBA and RcAlb-PepI	92
Figure 8 - Molecular docking analysis between NOLC1 and RcAlb-PepI	93
Figure 9 - Toxicity of RcAlb-PepI to human cell lines	95
Figure 10 - In vivo toxicity of RcAlb-PepI to Zebrafish embryos	96

LISTA DE ABREVIATURAS E SIGLAS

TEM	Transição Epitélio-Mesenquimal
IARC	International Agency for Research on Cancer
OMS	Organização Mundial da Saúde
INCA	Instituto Nacional do Câncer
EBV	Vírus Epstein-Barr
AJCC	American Joint Committee on Cancer
UICC	International Union Against Cancer Classification
TCGA	The Cancer Genome Atlas
CF	Cisplatina infusional
ECF	5-fluoruracil+cisplatina+epirrubicina
FDA	Food and Drug Administration
CI50	Concentração inibitória em 50% de atividade celular
GC	Gastric cancer
DMEM	Dulbecco's Modified Eagle's Medium
FBS	Fetal bovine serum
DMSO	Dimethyl sulfoxide
PDB	Protein Databank
ANOVA	Analysis of variance
HR	Hazard ratio
GEO	Gene Expression Omnibus
GEAP	Gene Expression Analysis Platform
DEGs	differentially expressed genes
GSEA	Gene Set Enrichment Analysis
FDR	False Discovery Rate
FC	Fold change
ES	Enrichment scor
AGS	Gastric adenocarcinoma tumors of a Caucasian patient
MNP-01	Célula gástrica saudável
AGP01	Células de ascite maligna
ACP02	Células tumorais de adenocarcinoma gástrico do tipo difuso
ACP03	Células tumorais de adenocarcinoma gástrico do tipo intestinal
qRT-PCR	Real-Time Quantitative PCR
SBVS	Structure-based virtual screening
SAMPs	Synthetic antimicrobial peptides
AFM	Atomic force microscopy
AMPs	Antimicrobial peptides
YM	Young's modulus
MSigDB	Molecular Signatures Database
MGHPC	Massachusetts Green High-Performance Computing Center
GPU	Graphic Processing Unit
MD	Molecular docking
Rq	Quantification of roughness
GLOBOCAN	Global Cancer Statistics
KM plotter	Kaplan–Meier plotter
GEPIA	Gene Expression Profiling Interactive Analysis
CADD	Computer-aided drug design
FUNCAP	Fundação Cearense de Apoio ao Científico e Tecnológico

SUMÁRIO

CAPÍTULO I

1 FUNDAMENTAÇÃO TEÓRICA	16
1.1 Um panorama geral do câncer	16
1.2 Câncer gástrico	18
1.2.1 <i>Fatores de risco</i>	18
1.2.2 <i>Epidemiologia do câncer gástrico</i>	19
1.2.3 <i>Classificação histológica e molecular do câncer gástrico</i>	20
1.2.4 <i>Tratamento do câncer gástrico</i>	22
1.3 Bioinformática aplicada ao desenho de drogas	23
1.4 Reposicionamento de peptídeos antimicrobianos para o câncer	26
1.5 Alvos e efeitos dos peptídeos nas células cancerígenas	32
2 OBJETIVOS	36
2.1 Objetivo geral	36
2.2 Objetivos específicos.....	36
2.2.1 <i>Capítulo II</i>	36
2.2.2 <i>Capítulo III</i>	37
REFERÊNCIAS	38

CAPÍTULO II

1 Introduction	45
2 Methodology	47
2.1 <i>Selection of Microarray Transcriptome Studies</i>	47
2.2 <i>Data Acquisition and Processing</i>	47
2.3 <i>Metadata Construction</i>	47
2.4 <i>Gene Set Enrichment Analysis</i>	47
2.5 <i>Selection of Microarray Transcriptome Studies</i>	48
2.6 <i>Primer Designer</i>	48
2.7 <i>Cell Culture</i>	48
2.8 <i>Gene Expression by qRT-PCR</i>	48
2.9 <i>Three-Dimensional Structure Obtention</i>	49
2.10 <i>Virtual Screening</i>	49
2.11 <i>In Silico Toxicity Prediction</i>	50
2.12 <i>Prediction of ADME Parameters</i>	50
2.13 <i>Molecular Docking (MD) Assays</i>	50
2.14 <i>Protein-Protein Interaction Network</i>	51
2.15 <i>Re-Docking</i>	51

2.16 <i>Statistical Analysis</i>	51
3 Results	51
3.1 <i>Differential Gene Expression in Gastric Tumor Meta-Dataset</i>	51
3.2 <i>Gastric Tumor Group Involved in Multiple Cancer Progression Pathways</i>	52
3.3 <i>Expression and Prognostic Value of Genes Involved in Gastric Cancer Progression</i> ... 53	
3.4 <i>Validation of Relevant Genes in Gastric Tumor Cell Lines Compared to Normal Gastric</i> . 54	
3.5 <i>In Silico High-Throughput Virtual Screening</i>	54
3.6 <i>Molecular Docking (MD) Validation</i>	55
3.7 <i>In Silico Pharmacokinetics Prediction</i>	57
3.8 <i>Protein–Protein Interaction Network</i>	57
4 Discussion	59
5 Conclusions	62
References	63

CAPÍTULO III

1 Introduction	69
2 Methodology	70
2.1 <i>Ethical Statement</i>	70
2.2 <i>Synthetic Peptides</i>	70
2.3 <i>Bioinformatics analysis</i>	71
2.4 <i>Cell Culture and Cytotoxicity by Alamar Blue Assay</i>	72
2.5 <i>Membrane Damage induced by peptides</i>	18
2.6 <i>Induction of Reactive Oxygen Species (ROS)</i>	74
2.7 <i>Atomic Force Microscopy (AFM) Analysis</i>	74
2.8 <i>Raman spectroscopic analysis</i>	75
2.9 <i>Wound healing assay</i>	76
2.10 <i>Evaluation of Cytotoxicity to non-cancerous cells</i>	76
2.11 <i>Comet assay</i>	77
2.12 <i>Morphological characterization of apoptotic cells</i>	78
2.13 <i>Zebrafish toxicity</i>	78
2.14 <i>Statistical analysis</i>	79
3 Results	79
3.1 <i>Bioinformatics Analysis of Synthetic Peptides</i>	79
3.2 <i>Cytotoxicity of peptides against gastric cancer lines</i>	81
3.3 <i>RcAlb-PepI induces membrane damage in AGP-01 cells</i>	83
3.4 <i>RcAlb-PepI induces morphological, nanomechanical and ultrastructural changes in AGP-01 cells</i>	84

<i>3.5 RcAlb-PepI alters the vibrational signature of AGP-01 cells</i>	87
<i>3.6 RcAlb-PepI reduces the migration of AGP-01</i>	89
<i>3.7 Molecular Docking Assay</i>	91
<i>3.8 RcAlb-PepI is not toxic to healthy cells and zebra-fish</i>	93
4 Discussion	96
5 Conclusions	106
References	107

CAPÍTULO I

FUNDAMENTAÇÃO TEÓRICA

Daiane Maria da Silva Brito

1 FUNDAMENTAÇÃO TEÓRICA

1.1 Um panorama geral do câncer

O câncer é uma doença multifatorial em que o seu processo de desenvolvimento é causado por influências de fatores genéticos, epigenéticos e ambientais. É considerado um dos principais problemas de saúde pública no mundo e representa uma grande barreira para o aumento da expectativa de vida global (JOSHI; BADGWELL, 2021; SIEGEL et al., 2023).

Com relação à carcinogênese, é um processo que ocorre em várias etapas. De modo geral, envolve a transformação de um fenótipo normal em maligno, permitindo a proliferação descontrolada e a resistência aos mecanismos regulatórios. Isto é, a célula evita os mecanismos regulatórios que normalmente a levariam à apoptose, permitindo, portanto, a progressão do tumor. Além disso, adquire autonomia em relação aos sinais que regulam o crescimento celular, não respondendo mais aos sinais que normalmente a induziriam à fase quiescente (G0) ou abandonar o ciclo celular. O avanço tumoral é comumente acompanhado pela perda da adesão celular e pelo aumento da capacidade de migração e invasão, que são características marcantes da formação de metástases (HANAHAN, 2022; HANAHAN; WEINBERG, 2000, 2011; WELCH; HURST, 2019).

A transição epitélio-mesenquimal (TEM) desempenha também um papel crucial na progressão dos tumores epiteliais, especialmente na ativação de perfis metastáticos em tumores malignos. Durante a TEM, as células epiteliais tumorais sofrem uma transformação na qual adquirem características de células mesenquimais, aumentando assim sua capacidade de migração e invasão (BAJ et al., 2020; LEE et al., 2006; THIERY; SLEEMAN, 2006).

As características citadas anteriormente compõem algumas das alterações essenciais para que o câncer se desenvolva e atinja um estado avançado da doença conhecidos como “*The Hallmarks of Cancer*”. Refere-se a um dos mais importantes estudos sobre o câncer, publicados por Hanahan e Weinberg. Em sua revisão bibliográfica, foi proposto que um conjunto de capacidades funcionais teriam de ser adquiridas para que as células fizessem o seu caminho da normalidade para estados de desenvolvimento neoplásico e formação de tumores malignos (HANAHAN; WEINBERG, 2000). Trata-se de um estudo que sintetiza as seis principais características que diferem uma célula cancerosa de uma célula normal, são elas: sustentação de sinais proliferativos; insensibilidade a sinais antiproliferativos; resistência à morte celular programada (apoptose); potencial de replicação ilimitado; angiogênese sustentada; invasão e

metástase tecidual. Foi proposto, em 2000, que essas seis capacidades eram compartilhadas pela maioria dos tipos de tumores humanos (HANAHAN; WEINBERG, 2000).

Décadas depois, à medida que o conhecimento dos mecanismos dos tumores progredia, foram acrescentadas mais características: reprogramação epigenética não mutacional, evasão ao sistema imune, instabilidade genômica e mutações e promoção de inflamação pelo tumor (HANAHAN; WEINBERG, 2011) Em 2022, houve mais uma atualização sobre essa temática, sendo adicionadas quatro características: desbloqueio da plasticidade fenotípica; reprogramação epigenética não mutacional; microbiomas polimórficos e células senescentes (HANAHAN, 2022). A Figura 1 exibe todos os *Hallmarks* do câncer.

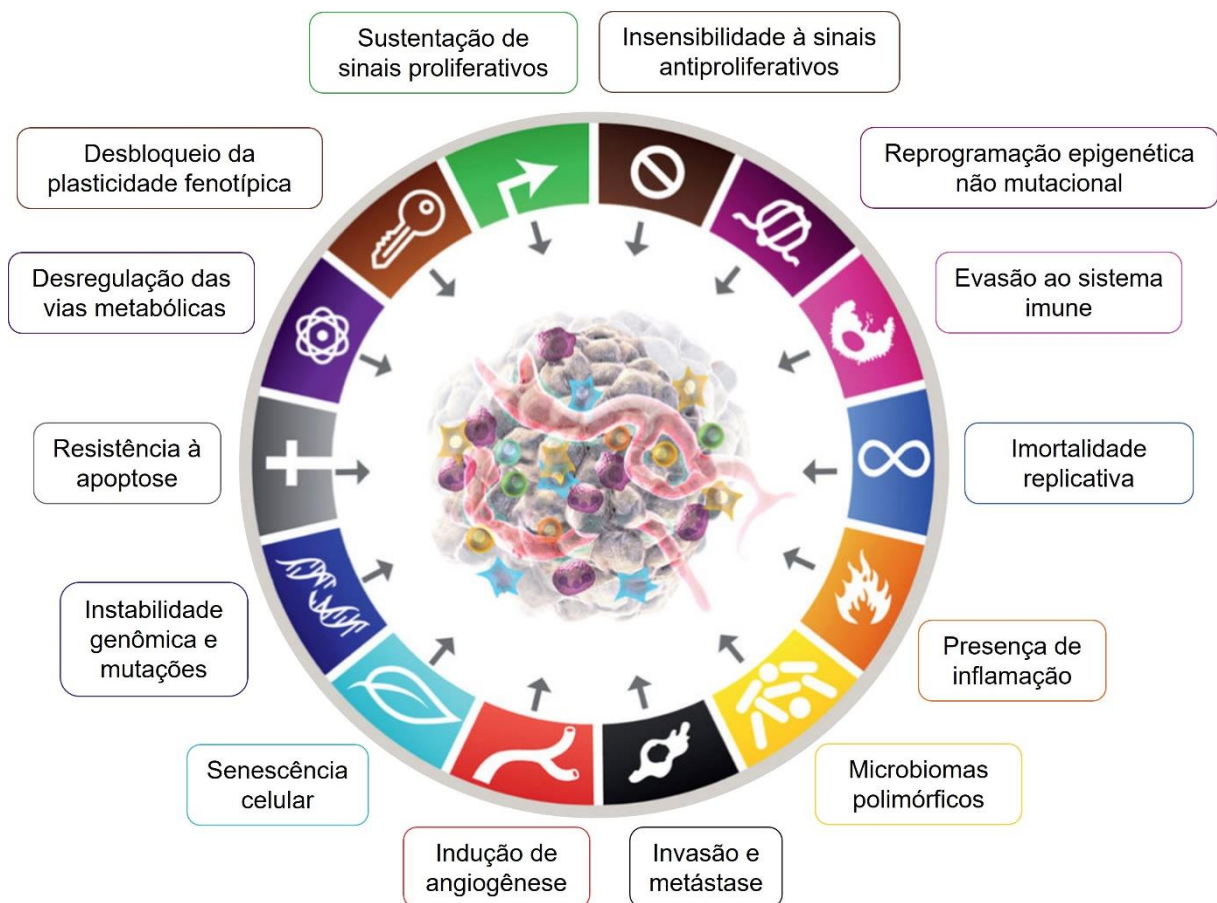


Figura 1 – *Hallmarks* do câncer. Figura adaptada de *Hallmarks of Cancer: New Dimensions* (HANAHAN, 2022).

Em relação ao impacto do câncer no mundo, esta condição representa a segunda maior causa de morte global, sendo superada apenas pelas doenças cardíacas (SIEGEL et al., 2023). Em 2020, ano em que foram divulgadas as últimas estimativas do Global Cancer Observatory (Globocan), elaboradas pela International Agency for Research on Cancer (Iarc), estimava-se 19,3 milhões de novos casos e 10 milhões de mortes por câncer em todo o mundo. Isso

representa que um em cada cinco indivíduos terão câncer durante sua vida (FERLAY et al., 2021; SUNG et al., 2021).

Os dez principais tipos de câncer representam mais de 60% do total de casos novos. Entre os tipos mais comuns, o câncer de mama feminino é o mais comumente diagnosticado, representando 11,7% de todos os casos de câncer, seguido de perto pelos cânceres de pulmão (11,4%), colorretal (10,0%), próstata (7,3%) e estômago (5,6%). Em termos de mortalidade, o câncer de pulmão é a principal causa, responsável por 18,0% de todas as mortes por câncer, seguido pelos cânceres colorretal (9,4%), hepático (8,3%), estômago (7,7%) e mama feminino (6,9%) (SUNG et al., 2021).

No âmbito nacional, o Instituto Nacional do Câncer (INCA) estimou para o triênio de 2023/2025 mais de 704 mil casos novos de câncer no Brasil por ano, concentrados principalmente na região Sul e Sudeste (70% da incidência). Estima-se que os tipos de câncer mais frequentes em homens, no Brasil, serão pele não melanoma (29,9%); próstata (21,0%); cólon e reto (6,4%); pulmão (5,3%); estômago (3,9%); e cavidade oral (3,2%). Enquanto, em mulheres, serão os cânceres de pele não melanoma (32,7%); mama (20,3%); cólon e reto (6,5%); colo do útero (4,7%); pulmão (4,0%); e tireoide (3,9%) (ESTIMATIVA 2023: INCIDÊNCIA DE CÂNCER NO BRASIL | INCA - INSTITUTO NACIONAL DE CÂNCER, [s.d.]).

1.2 Câncer gástrico

1.2.1 Fatores de risco

A infecção crônica pela bactéria *Helicobacter pylori* é considerada a principal causa de câncer gástrico, particularmente prevalente na África, na América Latina e na Ásia (WILD; WEIDERPASS; STEWART, 2020). A prevalência da infecção por *H. pylori* é bastante alta, infectando 50% da população mundial e sua variação geográfica correlaciona-se com a incidência de câncer de estômago. No entanto, considera-se que menos que 5% dos hospedeiros infectados desenvolverão câncer, provavelmente devido a diferenças na genética bacteriana, genética do hospedeiro, idade de aquisição da infecção e fatores ambientais (ALIPOUR, 2021; BAJ et al., 2020).

Outros fatores de risco estão associados às características genéticas e hereditárias do hospedeiro, como anemia perniciosa e lesões pré-cancerosas, condições associadas ao comportamento, como excesso de peso e obesidade, consumo de alimentos preservados no sal,

alto consumo de carne processada, alimentação com baixa ingestão de frutas, vegetais e fibra integral, consumo de álcool e tabaco. Fatores ocupacionais, como trabalho na produção da borracha e exposição a radiações, por exemplo raios X e gama também são considerados fatores de risco para o câncer gástrico (POOROLAJAL et al., 2020; RAWLA; BARSOUK, 2019).

O sucesso na prevenção e tratamento de infecções por *H. pylori*, juntamente com os avanços nas técnicas de conservação e armazenamento de alimentos, bem como a adoção de hábitos alimentares e estilo de vida mais saudáveis pela população, têm sido identificados como fatores que contribuíram significativamente para o declínio das taxas de incidência e mortalidade do câncer gástrico ao longo do último meio século, em grande parte das populações (Alipour, 2021; Sung et al., 2021).

1.2.2 Epidemiologia do câncer gástrico

Apesar de um declínio mundial nas taxas de incidência e mortalidade ter sido observado nas últimas décadas, o câncer gástrico (CG) ainda representa um grande impacto em todo o mundo, especialmente, nas populações de países em desenvolvimento. As estatísticas atuais revelam que o CG é a quinta neoplasia maligna mais comum e a quarta principal causa de mortalidade relacionada ao câncer em todo o mundo, responsável por mais de 768 mil mortes em 2020 (Ferlay et al., 2021; Sung et al., 2021).

A incidência de câncer gástrico é altamente variável por região e cultura. As taxas de incidência são mais elevadas na Ásia Oriental (Japão e Mongólia, os países com maior incidência em homens e mulheres, respectivamente) e na Europa Oriental, enquanto as taxas na América do Norte e no Norte da Europa são geralmente baixas (Figura 2) (RAWLA; BARSOUK, 2019; SUNG et al., 2021).

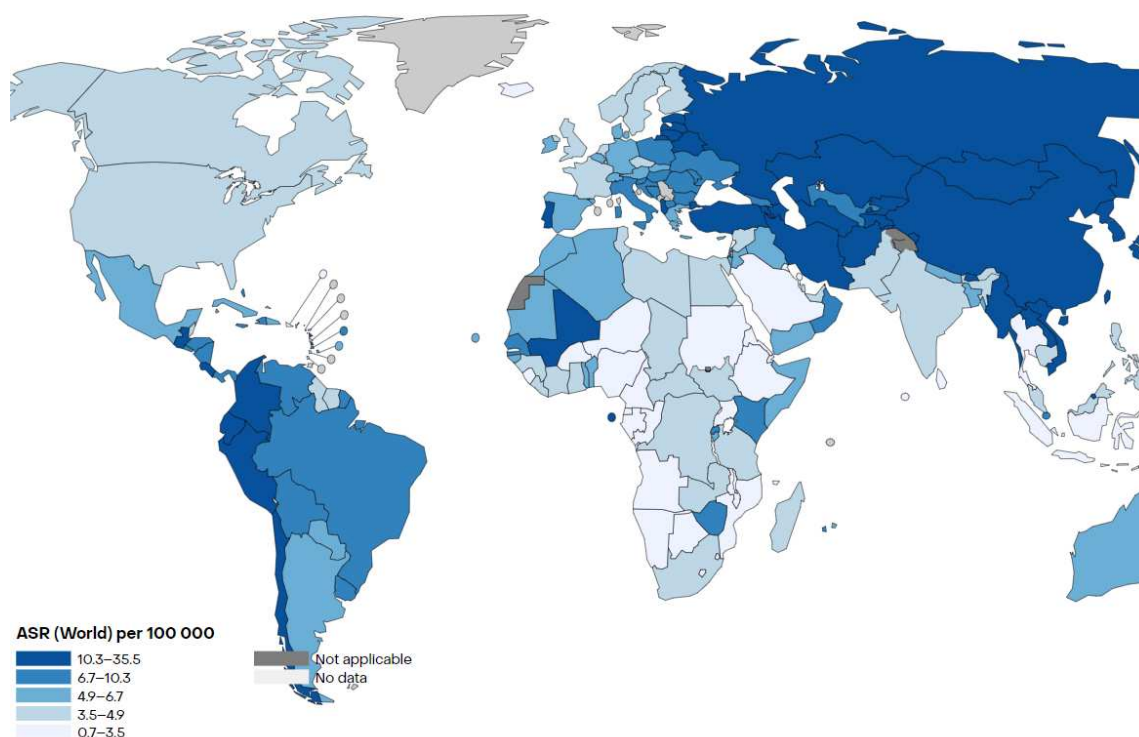


Figura 2 – Taxa de incidência global do câncer gástrico em 2022. Representada em mapa, considerando ambos os sexos e todas as idades. Reproduzido a partir de <http://globocan.iarc.fr/>.

No âmbito nacional, o Instituto Nacional do Câncer (INCA) estima para o Brasil 13.340 casos novos de GC em homens e 8.140 em mulheres no triênio de 2023 a 2025, totalizando 21.480 casos por ano. Esses valores correspondem a um risco estimado de 12,63 casos novos a cada 100 mil homens e 7,36 a cada 100 mil mulheres (ESTIMATIVA 2023: INCIDÊNCIA DE CÂNCER NO BRASIL | INCA - INSTITUTO NACIONAL DE CÂNCER, [s.d.]).

Em termos de mortalidade, em 2020, houve um total de 13.850 mortes devido ao câncer gástrico no Brasil, o que representa uma taxa de mortalidade de 6,54 por 100 mil habitantes. Entre os homens, foram registrados 8.772 óbitos, resultando em uma taxa de mortalidade de 8,47 por 100 mil homens. Entre as mulheres, ocorreram 5.078 mortes, com uma taxa de mortalidade de 4,69 por 100 mil mulheres. (BRASIL, 2022; INSTITUTO NACIONAL DE CÂNCER JOSÉ ALENCAR GOMES DA SILVA, 2020a).

1.2.3 Classificação histológica e molecular do câncer gástrico

A grande maioria dos cânceres gástricos são adenocarcinomas. Estes quais, representam mais de 95% de todas as neoplasias gástricas malignas e podem ser subdivididos segundo a classificação de *Laurén* (1965) com base na histologia do tumor, um sistema de classificação

amplamente utilizado até os dias atuais. Segundo esta classificação, os carcinomas gástricos são divididos em dois tipos histológicos principais: tipo difuso e intestinal. Estes dois tipos histológicos de adenocarcinoma apresentam diferenças em relação a aspectos etiológicos, epidemiológicos, patogênese e comportamento biológico (CHEN et al., 2016; LAURÉN, 1965).

Morfologicamente, o tipo intestinal consiste em um câncer diferenciado com tendência a se agrupar em formações glandulares e progride principalmente através de sucessivas modificações na mucosa gástrica normal, iniciando com uma gastrite crônica ativa, progredindo para gastrite atrófica, metaplasia intestinal, displasia, até desencadear, finalmente, o desenvolvimento de uma neoplasia maligna gástrica. Observa-se que o tipo intestinal acomete comumente pacientes mais idosos, com predileção pelo sexo masculino. Ao comparar as frequências relativas, verifica-se que o tipo intestinal é mais frequente e mais amplamente associado à infecção por *H. pylori* em relação ao tipo difuso (LAURÉN, 1965; MA et al., 2016).

Em contraste, a forma difusa consiste em um tecido pouco diferenciado que apresenta baixa coesão celular e tende a substituir a mucosa gástrica por células em anel de sinete. Atinge pacientes mais jovens, com distribuição igualitária entre os sexos. A série de eventos que originam o CG de tipo difuso ainda não é completamente estabelecida. No entanto, é observado que o seu desenvolvimento parece ser independentemente da gastrite atrófica ou metaplasia intestinal, parecendo estar mais correlacionado à mutação somática do gene CDH1, um gene supressor tumoral que codifica a proteína de adesão celular E-caderina. As diferenças observadas nas características clínico-patológicas entre os dois tipos histológicos indicam que o desenvolvimento ocorre por vias moleculares distintas (CHEN et al., 2016; LAURÉN, 1965; MA et al., 2016).

Com relação ao perfil molecular do câncer gástrico, uma classificação proposta pela *The Cancer Genome Atlas* (TCGA) categorizou os tumores gástricos em quatro subtipos: 1) tumores positivos para Epstein-Barr, com frequente hipermetilação do DNA; 2) tumores com instabilidade microssatélite, caracterizados por apresentar hipermutação, fenótipo metilador de ilhotas CpG e frequente silenciamento MLH1; 3) tumores genomicamente estáveis, apresentando histologia difusa, frequentes mutações no CDH1 e RHOA, e fusão do CLDN18-ARHGAP; 4) tumores com instabilidade cromossomal, a qual apresenta características a histologia intestinal, frequentes mutação da p53, aneuploidia e amplificação dos receptores de tirosina quinase. Nessa classificação foi observado que, embora considerada uma doença molecular e fenotipicamente heterogênea, há um padrão existente para as alterações moleculares presentes nos tumores de câncer gástrico (BASS et al., 2014).

As alterações moleculares são consideradas uma fonte importante para o desenvolvimento do câncer de estômago. Desse modo, variações na expressão de genes que desempenham importantes papéis em funções celulares, tais como transdução do sinal, diferenciação, adesão celular, desenvolvimento ou reparo do DNA se tornam alvos promissores para estudo.

1.2.4 Tratamento do câncer gástrico

O tratamento padrão para o câncer gástrico é baseado na tríade: cirurgia, quimioterapia e radioterapia. As alternativas e intervenções terapêuticas empregadas em pacientes oncológicos são determinadas a partir de alguns componentes, que incluem: estágio da doença, avaliação do perfil molecular e presença de biomarcadores, inclinações do paciente, avaliação do risco, assim como o seu bem-estar geral. O sistema de estadiamento do câncer (cTNM) do *American Joint Committee on Cancer* (AJCC) otimizou, significativamente, as decisões sobre o tratamento do câncer gástrico. Este sistema descreve a invasão do tumor através das camadas da parede do estômago (T), envolvimento de linfonodos (N) e se há presença de metástases à distância (M) (SEXTON, 2020). Para tumores gástricos, as terapias de modalidade combinada (cirurgia, quimioterapia e radioterapia) têm sido amplamente aplicadas (BHARDWAJ *et al.*, 2022).

A ressecção cirúrgica é considerada o principal método de tratamento em estágio inicial e a única abordagem potencialmente curativa no tratamento do câncer gástrico. Todavia, é frequentemente observado o fenômeno de recidiva em uma proporção significativa dos pacientes mesmo após a ressecção. Diante desta problemática, um estudo realizado com 206 pacientes com câncer gástrico revelou que os pacientes nos estágios II e III tinham melhores taxas de sobrevida com quimioterapia adjuvante em comparação com a cirurgia isolada (SASAKO *et al.*, 2011). Estudos clínicos de fase II, há mais de duas décadas, têm demonstrado que o emprego da quimioterapia neoadjuvante é capaz de aumentar a taxa de sucesso da ressecção do tumor em 72 a 87% (AJANI *et al.*, 1999; GUAN; HE; XU, 2023; JOSHI; BADGWELL, 2021; RAJDEV, 2010). Diante das evidências, a adição de quimioterapia pré (neoadjuvante), pós (adjuvante) ou perioperatória representa atualmente um benefício de sobrevida, sendo utilizada como parte de uma abordagem multimodal.

Há uma grande variedade de quimioterápicos e esquemas terapêuticos aprovados para o tratamento farmacológico do câncer gástrico. Alguns destes esquemas terapêuticos são bem descritos na literatura: o esquema FLOT (5-fluorouracil, leucovorin, oxaliplatina e taxano), o

esquema ECF (epirrubicina, cisplatina e fluorouracil), FOLFOX (5-fluorouracil, leucovorin e oxaliplatina), cisplatina infusional (CF) e regime monofármaco com irinotecano (MESQUITA, *et al.* 2021; SEXTON, 2020). Na prática clínica, o FLOT tornou-se o regime padrão perioperatória em pacientes com câncer gástrico e gastroesofágico ressecáveis que apresentam bom estado de desempenho e sem comorbidades (JOSHI; BADGWELL, 2021).

Apesar dos avanços e das diversas opções terapêuticas disponíveis atualmente, o prognóstico de pacientes com CG continua desfavorável. A sobrevida mediana dos pacientes com CG avançado ainda é muito baixa, inferior a 12 meses (DIGKLIA, 2016). Fatores como o predomínio do diagnóstico em fases avançadas do tumor primário ou metástase; a heterogeneidade tumoral; a resistência quimioterapêutica; a falta de seletividade das terapias e, conseqüente, toxicidade às células saudáveis dos pacientes constituem os maiores desafios para o controle do CG e limitam o tratamento desta neoplasia (LONGLLEY; JOHNSTON, 2005; MELLOR; CALLAGHAN, 2008).

Embora a terapia monoclonal não apresente forte toxicidade em comparação à quimioterapia convencional, seu uso é restrito. Trastuzumabe é a escolha padrão para pacientes com CG avançado com superexpressão de HER2; entretanto, a expressão de HER2 no câncer gástrico (GC) é inferior a 20%. Além disso, a presença de heterogeneidade tumoral e resistência ao trastuzumabe impõe limitações consideráveis ao uso deste tratamento (GUAN; HE; XU, 2023; POUS *et al.*, 2023; SATO *et al.*, 2023).

Com relação à quimiorresistência, o câncer pode desenvolver resistência praticamente a todos os tipos de terapias, como radioterapia, quimioterapia e até mesmo terapias direcionadas (VASAN; BASELGA; HYMAN, 2019). Para superar este desafio, é urgente a busca por moléculas com baixos níveis de toxicidade que explorem novos alvos terapêuticos no câncer. Adicionalmente, outra estratégia importante é o reposicionamento de moléculas que apresentem mecanismos de ação distintos dos das drogas quimioterápicas convencionais. Visto que as células cancerosas desenvolveram resistência aos mecanismos utilizados pela maioria das drogas citotóxicas e pelas terapias molecularmente direcionadas disponíveis atualmente.

1.3 Bioinformática aplicada ao desenho de drogas

Atualmente, dois problemas relacionados aos medicamentos para GC precisam ser resolvidos: (1) a alta toxicidade dos medicamentos para os pacientes e (2) a resistência das células do GC a esses medicamentos. Em relação a estes problemas, a bioinformática tem sido

levantada como uma ferramenta poderosa para identificar novos alvos ou novas moléculas para um alvo.

Na busca por novos alvos terapêuticos e na descoberta de novos candidatos a medicamentos, as metodologias de *design* de medicamentos auxiliados por computador (CADD) se destacam como uma tecnologia poderosa e promissora para um *design* de drogas mais rápido, barato e eficaz (PRIETO-MARTÍNEZ et al., 2019). Além disso, fornece um ponto de partida absoluto para a descoberta de alvos de medicamentos. Diante do alto custo e do tempo necessário para pesquisa e desenvolvimento de medicamentos na área de oncologia, os modelos computacionais representam uma alternativa eficiente, pois são capazes de prever parâmetros físico-químicos, farmacocinéticos, farmacodinâmicos e toxicológicos a partir de uma determinada estrutura molecular, bem como como otimizar a etapa de teste *in vitro* (PRIETO-MARTÍNEZ et al., 2019).

A análise de predição das propriedades ADMET é uma técnica de grande relevância no desenvolvimento do *design* de medicamentos, comumente aplicada ainda nas fases iniciais do processo de descoberta de drogas. ADMET refere-se aos processos de absorção (A), distribuição (D), metabolismo (M), excreção (E) e toxicidade (T). Esta análise reduz drasticamente a fração de falha relacionada à farmacocinética nas fases clínicas e os efeitos tóxicos associados aos medicamentos (DAINA; ZOETE, 2016).

Os resultados obtidos até o momento na obtenção de novos fármacos através de estudos *in silico* são bem conhecidos. Por exemplo, há o desenvolvimento do medicamento captopril, o primeiro inibidor da enzima de conversão da angiotensina (ECA) e um dos primeiros medicamentos bem-sucedidos produzidos usando ferramentas computacionais para otimizar o planejamento de medicamentos na década de 1980 (ANTHONY; KANDING; SELVAN, 2020). Após este estudo, o desenvolvimento de medicamentos baseados em estrutura exibiu um impacto significativo no *design* de medicamentos com um número crescente de aplicações, e foi observado um rápido crescimento de ferramentas computacionais para descoberta de medicamentos, incluindo terapias anticâncer.

Por exemplo, Miller et al., (2015) realizaram uma triagem virtual baseada em estrutura (SBVS) para encontrar novas moléculas com atividade contra o proteossomo de células cancerosas pancreáticas. A triagem virtual baseada em estrutura (SBVS) é uma técnica robusta que permite a identificação rápida de compostos biologicamente ativos, fornecendo uma alternativa eficiente e econômica às triagens experimentais de alto rendimento. Esta técnica permite prever o melhor modo de interação entre duas moléculas para formar um complexo estável, utiliza funções de pontuação para estimar a força de uma interação não covalente entre

um ligante e um alvo molecular. No estudo, os autores analisaram 380 mil compostos contra uma subunidade do proteassoma. Após análise SBVS, dos 288 compostos testados *in vitro*, 1 foi selecionado para análise experimental (MILLER et al., 2015). Este caso é um exemplo de como a bioinformática pode ajudar rapidamente na descoberta de medicamentos.

Outro estudo de Rohr et al. (2021) desenvolveram um *pipeline* empregando *scripts* de pacote R para analisar dados de análise transcricional de um *microarray* de câncer colorretal pré e pós-maligno. Usando esta pipeline, foi possível realizar a análise de um conjunto de dados contendo 231 amostras de tecido normal, 132 de adenoma e 342 de câncer de cólon em doze estudos independentes analisados por microarranjo depositado no *Gene Expression Omnibus* (GEO) (ROHR et al., 2021). O estudo mencionado foi desenvolvido pelo nosso grupo a fim de investigarmos quais são os genes envolvidos na gravidade e progressão do CG, bem como para buscarmos novos alvos para o tratamento do câncer colorretal.

Um estudo desenvolvido por Lima et al., (2023) identificou moléculas potencialmente inibidoras da Aurora quinase A (AURKA), uma proteína hiperexpressa em células malignas de pacientes com LLA que participa de várias etapas do processo de mitose. Através de triagem virtual baseada em estrutura (SBVS) e estudos de *docking* molecular duas moléculas foram identificadas. Estas quais, interagiram com o sítio ativo da AURKA, atuando como inibidores ou bloqueadores do sítio catalítico, e foram apontadas como moléculas promissoras no combate ao câncer.

Estudos de Silva et al., (2023) evidenciaram o mecanismo antitumoral e citotóxico do fármaco mebendazol (MBZ) em células gástricas tumorais com o uso da bioinformática. Os resultados deste trabalho revelaram que os genes SLC2A1, HK1, GAPDH e LDHA são superexpressos em amostras de câncer gástrico (CG), e que esse aumento está fortemente associado à diminuição da sobrevida global dos pacientes acometidos por esta doença. Estudos de *docking* molecular revelaram que o MBZ modifica a estrutura proteica dos alvos mencionados, promovendo possíveis alterações na função dos mesmos. Desse modo, análises *in silico* realizadas neste trabalho auxiliaram na descoberta de novos alvos farmacológicos para o CG.

No trabalho desenvolvido por Mesquita et al., (2023) a bioinformática foi aplicada para analisar a proteína ACE2 de diferentes espécies animais e fornecer novos *insights* sobre a transmissão de espécies de SARS-CoV-2. Modelos computacionais foram utilizados para analisar as relações filogenéticas entre o ACE2 de humanos e de outros animais e investigou a potencial interação entre o domínio de ligação ao receptor (RBD) do SARS-CoV-2 e ACE2 de diferentes espécies. Neste estudo, utilizando somente bioinformática, foi possível a

identificação de 11 espécies com um encaixe perfeito para a interação entre o ACE2 e o RBD do SARS-CoV-2, este resultado apresentou grande relevância ao prever potenciais hospedeiros para SARS-CoV-2, compreender o seu ciclo epidemiológico e propor estratégias de vigilância em um período pandêmico de SARS-CoV-2.

Os diferentes exemplos bem-sucedidos de aplicações de análises *in silico* relatados na literatura evidenciam que a bioinformática tem contribuído significativamente na descoberta de moléculas e alvos que possam ser aplicados ao câncer. Sendo assim, a bioinformática desempenha um papel fundamental no avanço da pesquisa sobre o câncer, mostrando-se promissora em oferecer novas perspectivas e abordagens para o desenvolvimento de biomarcadores, alvos terapêuticos, bem como, terapias mais eficazes contra os variados tipos de câncer.

1.4 Reposição de peptídeos antimicrobianos para o câncer

A resistência aos medicamentos é um problema para os profissionais de saúde, pois a cada ano há uma diminuição na produção de novos medicamentos e os disponíveis no mercado perdem cada vez mais os seus efeitos. Uma das resistências aos medicamentos mais conhecidas é a antimicrobiana, que tem sido considerada um problema de saúde pública (HANEY; MANSOUR; HANCOCK, 2017). De acordo com dados da Organização Pan-Americana da Saúde, nos últimos anos, observou-se um aumento significativo nos níveis de resistência das principais bactérias responsáveis pela sepse hospitalar aos antibióticos empregados no tratamento padrão contra essa condição (RUSIECKA; GAĞAŁO; KOCIĆ, 2022)

Outro desafio significativo diz respeito à resistência aos tratamentos contra o câncer. Neste caso, a resistência é atribuída à inativação de medicamentos, alterações no direcionamento de drogas, desenvolvimento de bombas de efluxo para reduzir a concentração intracelular de medicamentos e reparo de danos ao DNA causados pelos agentes quimioterápicos (HOUSMAN et al., 2014). Para superar este desafio, é necessário a busca ou o desenvolvimento de moléculas que explorem novos alvos terapêuticos e apresentem mecanismos de ação distintos da quimioterapia convencional. Nesse contexto, os peptídeos antimicrobianos se mostram como uma alternativa terapêutica e apresentam vantagens sobre vários medicamentos. Estes quais, são formados por sequências de aminoácidos unidas por ligações peptídicas e desempenham diversas funções, como atividades antimicrobianas, antibiofilme e anticancerígenas (HANEY; MANSOUR; HANCOCK, 2017; HOPPENZ; ELS-HEINDL; BECK-SICKINGER, 2020; LIU et al., 2021).

Os peptídeos antimicrobianos são encontrados em todos os organismos vivos como componentes dos sistemas de defesa (Figura 3A) e assumem diversas estruturas tridimensionais (3D). As estruturas 3D mais comuns assumidas são α -helicoidal, desordenada, cadeia β e mista (Figura 3B).

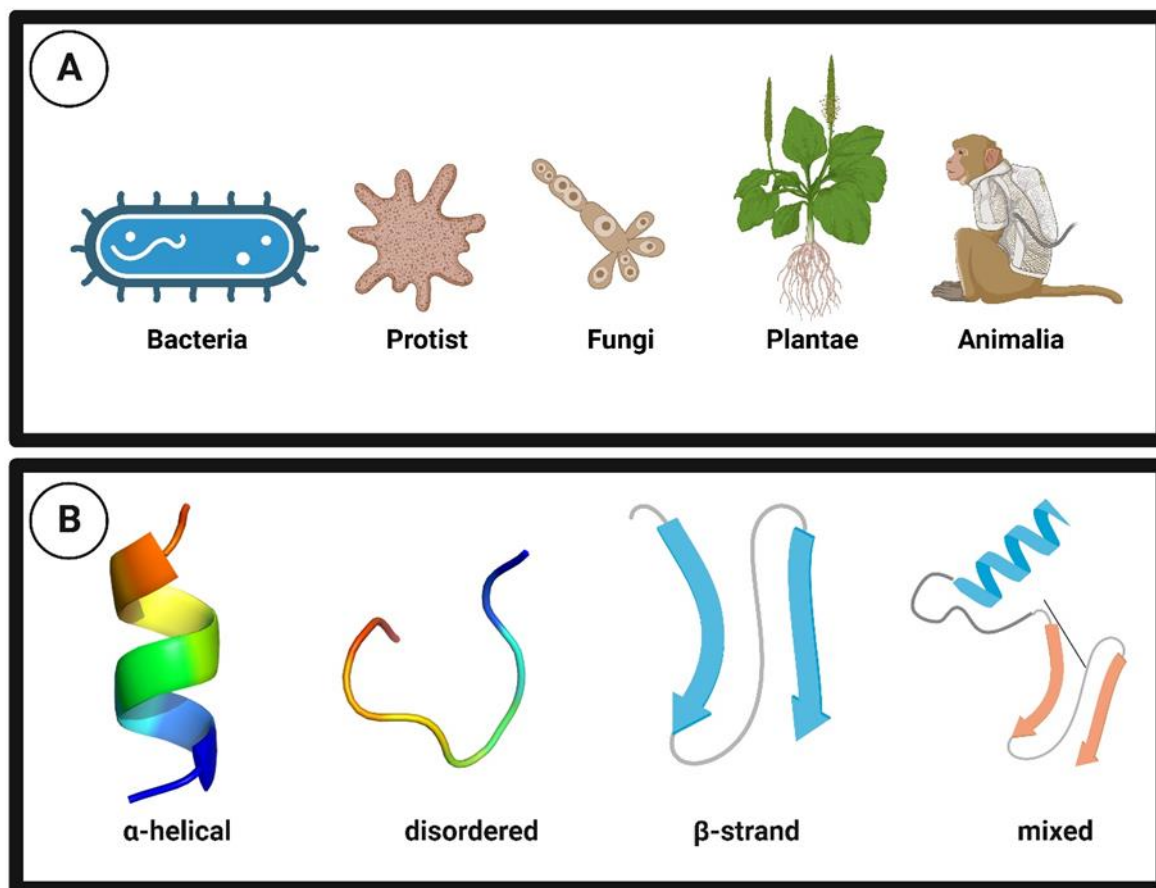


Figura 3 – Fonte e estrutura de peptídeos antimicrobianos. (A) Os peptídeos antimicrobianos estão presentes em todos os reinos. (B) estruturas tridimensionais mais comuns assumidas pelos peptídeos

As perspectivas de utilização de peptídeos em tratamentos contra doenças têm crescido ultimamente. Entretanto, algumas dificuldades foram observadas em seu uso, como baixa biodisponibilidade oral, meia-vida plasmática curta e solubilidade. O avanço nas ferramentas de bioinformática tornou possível a modulação de sequências peptídicas para produzir peptídeos sintéticos para superar os problemas mencionados anteriormente (LAU; DUNN, 2018). Assim, a atenção a essas moléculas e ao seu reposicionamento é uma excelente alternativa para o tratamento de outras patologias, como o câncer. A pesquisa científica busca meios árduos para o tratamento do câncer, visando eficácia e boa qualidade de vida ao paciente.

Os peptídeos antimicrobianos (AMPs) têm sido estudados para sua utilização contra células cancerígenas, visando a capacidade de alguns AMPs também apresentarem ações

consideráveis contra essas células a partir do seu mecanismo de ação por semelhanças entre essas duas células, uma vez que tanto as células bacterianas quanto as cancerígenas compartilham lipídios carregados negativamente fora da bicamada da membrana (RĂILEANU; BACALUM, 2023; WANG et al., 2022).

Para uma melhor aplicação dos AMPs como peptídeos anticâncer, é necessário identificar as características das células cancerígenas e como os AMPs irão interferir no comportamento destas células. Nos últimos anos, tem sido postulado e aceite que as células cancerígenas têm lipídios carregados negativamente nas suas membranas, assim como as células bacterianas. Isto é possível devido à hipóxia e aos altos níveis de ERO, criando um microambiente ácido e favorável para a proliferação de células cancerígenas (BAXTER et al., 2017; TORNESELLO et al., 2020).

Alguns peptídeos antimicrobianos são moléculas catiônicas e anfipáticas que possuem afinidade por lipídios negativos presentes nas membranas de patógenos e estabelecem interações iônicas (RIEDL; ZWEYTICK; LOHNER, 2011; TORNESELLO et al., 2020). Com base nessas características, os AMPs atuam formando poros na membrana e modificando a estrutura dos canais iônicos transmembrana, levando à ruptura da membrana e à indução de apoptose celular. Esse mecanismo é eficaz contra membranas e paredes celulares carregadas negativamente em fungos e bactérias (BAXTER et al., 2017).

As células cancerosas alteram seu microambiente para sobreviver e proliferar, tornando sua carga líquida mais negativa do que as células normais (BAXTER et al., 2017). Essa modificação é o resultado de uma combinação de aumento da concentração de espécies reativas de oxigênio (EROs), hipóxia (BAXTER et al., 2017; TORNESELLO et al., 2020), desregulação dos fosfolipídios que compõem as membranas celulares através da glicosilação irregular em glicoproteínas e glicolipídios, menor teor de colesterol entre os fosfolipídios, que contribui para a penetração de peptídeos nas células (BALASUBRAMANIAN; SCHROIT, 2003; HOSKIN; RAMAMOORTHY, 2008), e a presença de projeções celulares importantes para a comunicação celular (filopódios) e microvilosidades, que aumentam a superfície celular total.

As alterações mais comuns nas glicoproteínas são a superexpressão de mucinas O-glicosiladas e proteoglicatos de membrana, que favorecem ainda mais uma carga negativa da membrana e, mais importante, um aumento na concentração de fosfatidilserinas (PS) na membrana plasmática (BAXTER et al., 2017). As fosfatidilserinas são uma das várias classes de fosfolipídios que constituem as membranas celulares. Entre eles, as esfingomielinas e os fosfatidilcolinas, que são lipídios zwitteriônicos ou neutros, são encontrados principalmente na porção externa da membrana (BAXTER et al., 2017; TORNESELLO et al., 2020; WODLEJ et

al., 2019). Na região citoplasmática ou no folheto interno das células eucarióticas, predominam aminofosfolípidios, como fosfatidiletanolamina e fosfatidilserinas (WODLEJ et al., 2019). A indução de PS no folheto da membrana externa ocorre devido ao estresse oxidativo gerado por citocinas inflamatórias, aumento da acidez e trombina (TORNESELLO et al., 2020). Além disso, há também uma regulação negativa de uma translocase fosfolipídica dependente de ATP e de uma flipase dependente de Ca^{2+} , ambas responsáveis por controlar a simetria da membrana plasmática (BEVERS; COMFURIUS; ZWAAL, 1996; WODLEJ et al., 2019).

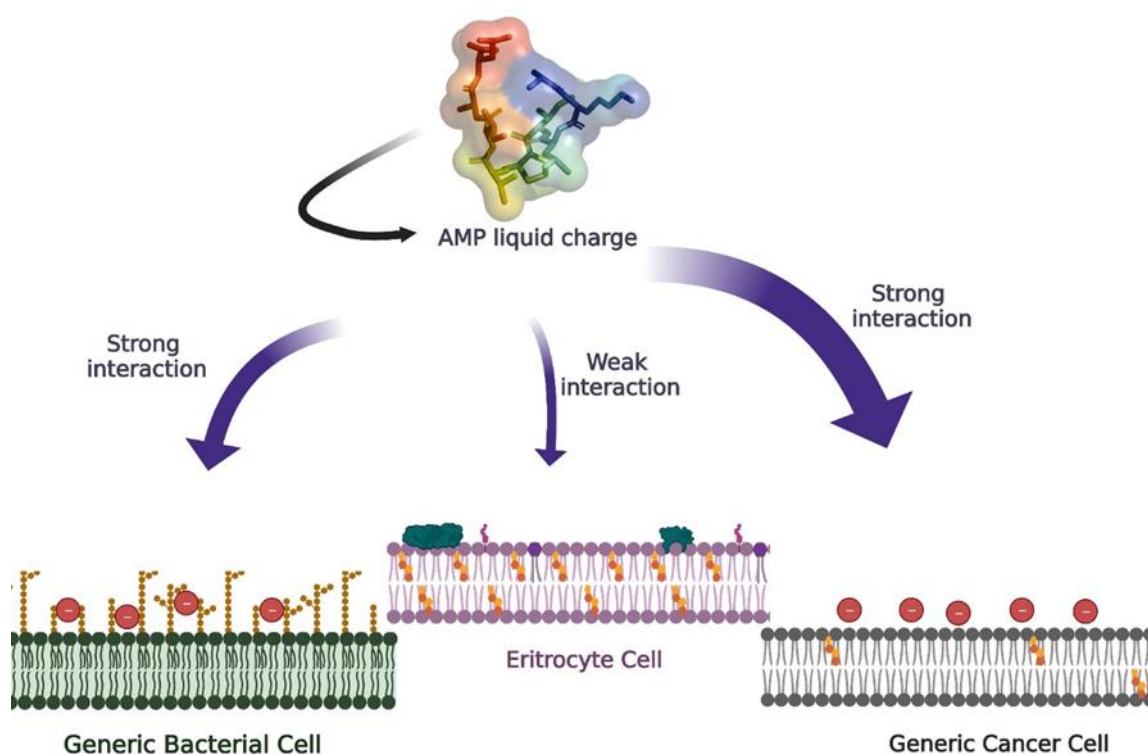


Figura 4 – Comparação entre membranas de células bacterianas, células eritrócitárias e células cancerígenas. O esquema representa a carga negativa das membranas das células bacterianas e cancerígenas e a membrana neutra das células eritrócitárias. A carga positiva do peptídeo interage fortemente com as membranas das células bacterianas e cancerígenas. No entanto, a ausência de carga na membrana das células eritrócitárias proporciona apenas uma interação fraca entre peptídeos e eritrócitos.

Devido às alterações no microambiente tumoral, o PS fica exposto e a membrana plasmática fica carregada negativamente, criando um espaço favorável para a interação entre a membrana tumoral e o peptídeo (KORDI et al., 2023; TORNESELLO et al., 2020). Esta mudança na carga da membrana também contribui para a seletividade dos peptídeos para interagir com as células cancerígenas, uma vez que a atração eletrostática será mais forte que a das células normais. Além disso, o uso de peptídeos antimicrobianos na terapia anticâncer

torna-se uma possibilidade para detectar células que ainda não são metabolicamente ativas, mas já possuem um microambiente alterado (BAXTER et al., 2017), bem como uma alternativa para casos de resistência microbiana a antibióticos (HOSKIN; RAMAMOORTHY, 2008; RIEDL; ZWEYTICK; LOHNER, 2011). Isso porque a ação alvo dos AMPs é um componente estrutural essencial para a célula, que, aliado às peculiaridades das células cancerígenas, potencializa o mecanismo de ação dos peptídeos.

Com base nessas informações, entende-se que a penetração e a seletividade são características fundamentais para a obtenção de resultados satisfatórios na descoberta e caracterização de peptídeos anticancerígenos, sejam eles naturais ou sintéticos. Auxiliados pela bioinformática, estudos sobre desenho racional de fármacos e *docking* molecular contribuem para a seleção desses peptídeos, otimizando tempo e custo em pesquisas. Por exemplo, o estudo sobre o desenho racional de um AMP anticâncer curto α -helicoidal, denominado At1-At12, realizado por Pan et al., (2022), teve como objetivo otimizar as propriedades físico-químicas da interação peptídeo-célula e a avaliação da atividade anticancerígena em um fator de virulência de *Leishmania spp.* para o tratamento do câncer de melanoma (SHARIFI et al., 2023).

Em um estudo de Sang et al., (2017) dois peptídeos antimicrobianos catiônicos naturais pertencentes à classe das cecropinas foram investigados para avaliar seu potencial como agentes anticancerígenos em células leucêmicas humanas e células normais. Os resultados revelaram que ambos os peptídeos mostraram seletividade para células cancerígenas das linhas celulares K562, U937 e THP-1. Em contraste, mesmo em concentrações elevadas, não mostraram citotoxicidade em células renais normais (HEK-293) e células mononucleares (PBMCs). Além disso, observou-se que estes peptídeos inibiram a proliferação de células de leucemia de uma forma dependente da dose. A análise realizada pelos pesquisadores identificou que o mecanismo de ação desses peptídeos envolvia danos à membrana celular das células leucêmicas, resultando em sua morte. O estudo concluiu que esses peptídeos têm potencial como agentes anticancerígenos no tratamento da leucemia, destacando sua notável capacidade de atingir seletivamente as células cancerígenas sem afetar as células normais do corpo (SANG; ZHANG; ZHUGE, 2017).

Em outro estudo realizado por Hsu et al. (2022), foram identificados dois peptídeos antimicrobianos, Ple e sua variante Ple-a, que apresentava uma modificação na forma de um grupo amida. Os resultados deste estudo revelaram que Ple-a apresentou eficácia superior em comparação com Ple na inibição do crescimento de várias linhagens celulares J5, Huh7 e Hep3B (hepatocarcinoma), A549 (adenocarcinoma pulmonar de células não pequenas), AGS (adenocarcinoma gástrico) e WiDr. (adenocarcinoma colorretal). Além disso, observou-se que

Ple-a exibiu notável seletividade em relação às células cancerígenas, com pouco impacto nas células normais.

Os resultados indicaram que Ple-a induziu apoptose e autofagia em células cancerígenas, levando ao encolhimento celular e à formação de vacúolos citoplasmáticos que alteraram a morfologia celular. Análises de Western blot sugeriram que Ple-a ativou o processo apoptótico ativando caspases. Além disso, foi observada uma possível interação do Ple-a com microtúbulos e proteínas de adesão focal, afetando a estrutura das células cancerígenas. Portanto, esses peptídeos apresentam potencial promissor como agentes anticancerígenos devido à sua seletividade e mecanismo de ação envolvendo apoptose e autofagia em células cancerígenas. No entanto, os pesquisadores relataram a necessidade de mais estudos para obter uma compreensão mais profunda dos alvos intracelulares desses peptídeos (HSU et al., 2022).

A linhagem celular de câncer gástrico AGP-01 foi avaliada por microscopia de força atômica (AFM) e comparada com MNP-01, uma célula gástrica normal para comprovar nossa hipótese. Os dados de AFM revelaram que a membrana do AGP-01 tem carga negativa em comparação com as células MNP-01. Devemos ressaltar que as curvas de força obtidas na análise de AFM foram adquiridas em 1000 Hz, resultando em milhares de curvas de força na membrana celular. Neste processo, a sonda sofre eletrificação devido ao atrito, e a contribuição das forças eletrostáticas na medição da adesão torna-se bastante relevante. Portanto, superfícies com cargas negativas terão menor resposta adesiva em relação à sonda (Fig. 5). É possível notar que esta interação é menor para células tumorais (Fig. 5B e D) em comparação com uma linhagem celular não tumoral do mesmo órgão (Fig. 5A e C). Esta redução nas forças de adesão na linhagem tumoral indica sua carga negativa (Fig. 5E). Adicionalmente, pela análise de AFM, foi possível avaliar que o peptídeo catiônico analisado apresentou maior afinidade para interagir com células de membrana de células AGP-01 do que MNP-01.

Portanto, acredita-se que a ação anticâncer desses peptídeos pode estar relacionada ao núcleo hidrofóbico dentro da membrana e aos lipídios carregados negativamente fora da membrana celular das células cancerígenas, o que contribui para a eficácia desses peptídeos como agentes anticâncer, conforme mencionado no texto anterior. Portanto, estes resultados sugerem que os peptídeos antimicrobianos têm potencial para se tornarem uma abordagem promissora no tratamento de pacientes com câncer devido à sua seletividade e mecanismos de ação específicos.

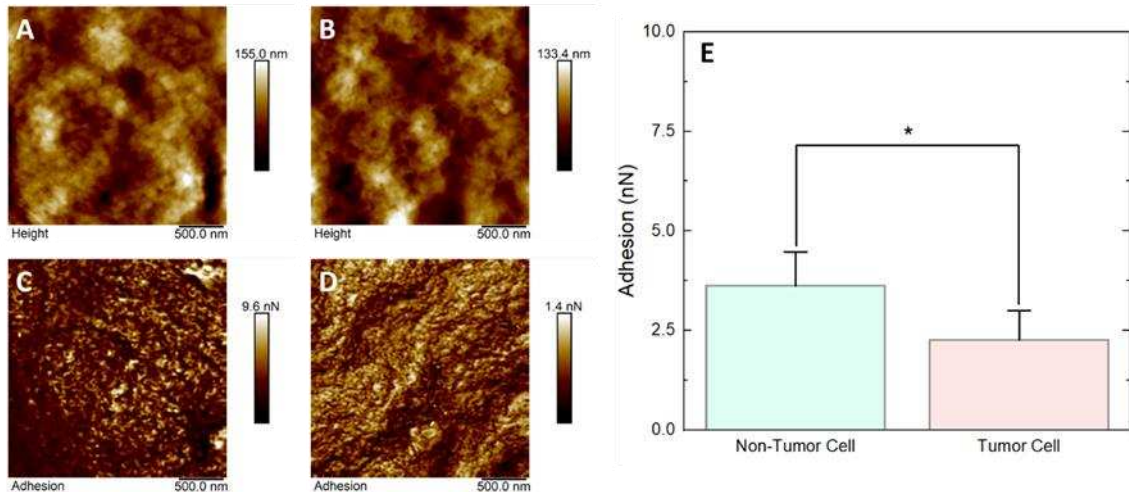


Figura 5 - Microscopia de Força Atômica. (A) imagem de 2,5 μm de altura sobre a região do corpo celular de uma célula intestinal não tumoral. (B) Mapa de altura de 2,5 μm sobre a região do corpo celular da linha celular de câncer intestinal. (C) Mapa de adesão correspondente à imagem topográfica mostrada em (A). (D) Mapa de forças de adesão correspondente à imagem topográfica mostrada em (B). (E) Gráfico de $n=10$ mapas de força de adesão de cada grupo com curvas de força 256 x 256 em cada mapa. Os valores médios são, respectivamente, para células não tumorais e tumorais: $3,7 \pm 0,7$ nN e $2,2 \pm 0,5$ nN. O asterisco no gráfico de adesão indica que os grupos apresentam diferenças significativas no teste ANOVA com *Turkey* para $p < 0,05$.

1.5 Alvos e efeitos dos peptídeos nas células cancerígenas

Os peptídeos têm atraído atenção no tratamento de tumores devido ao seu pequeno tamanho, alta afinidade, fácil modificação, facilidade de síntese e baixa imunogenicidade. Os peptídeos desenvolvidos no campo do tratamento do câncer exercem os seus efeitos antitumorais através de duas estratégias específicas (Fig. 6). Ligando-se a receptores alvo na superfície celular e permitindo a entrega de conjugados a um determinado tipo de célula (Fig. 6A). Pela interação com componentes carregados na membrana celular, ocorrendo a internalização do peptídeo ou complexo fármaco-peptídeo através de mecanismos previamente descritos. Portanto, os peptídeos terapêuticos podem ser classificados em proteínas de direcionamento celular (PCTP) e de penetração celular (CPP), respectivamente (CONIBEAR et al., 2020; LI et al., 2021).

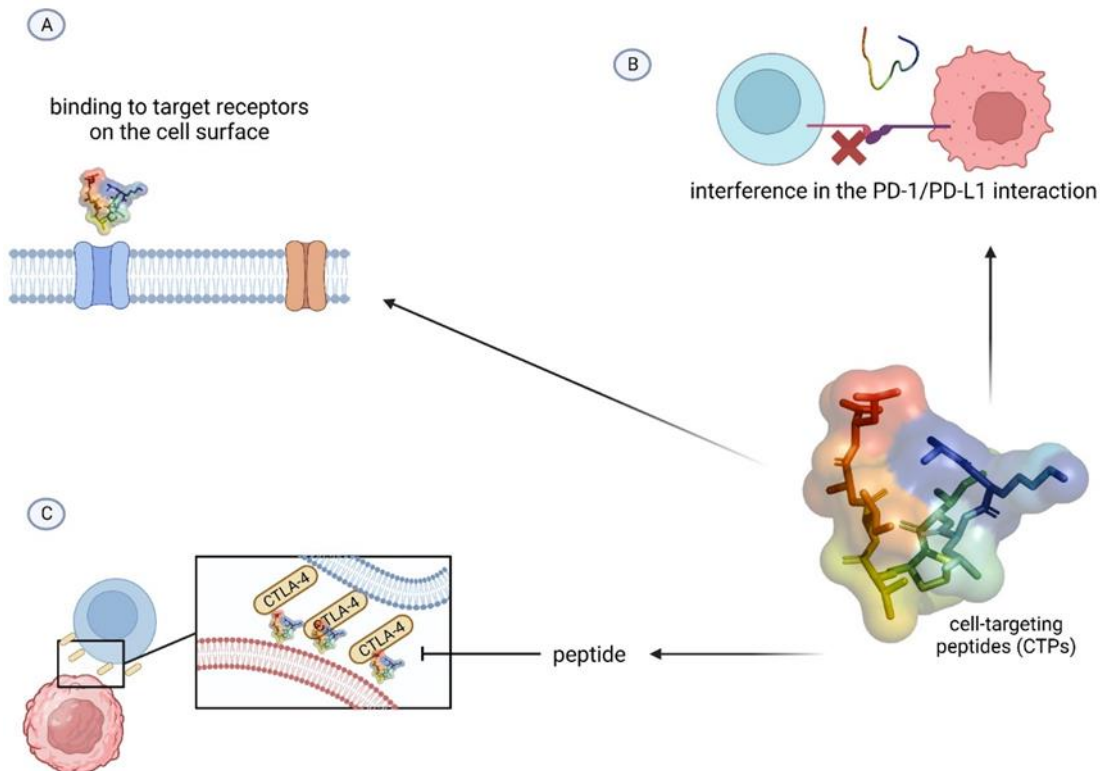


Figura 6 - Alvos celulares de peptídeos. Além de atingir as membranas das células cancerígenas, os peptídeos também podem interagir com outros alvos celulares e exibir seu efeito nas células cancerígenas. (A) os peptídeos poderiam interagir diretamente com um receptor de células cancerígenas ou impedir que as células cancerígenas se tornassem invisíveis ao sistema imunológico, interagindo com as proteínas PD-1/PD-L1 (B) e CTLA-4 (C).

Os PCTPs exercem seus efeitos interagindo especificamente com proteínas na superfície celular. Esta interação pode ativar ou inibir a sinalização do receptor e internalizar o complexo peptídeo-receptor. A cada dia, as proteínas são apontadas como alvos promissores no combate à carcinogênese. A identificação desses alvos é comumente baseada em dados de enriquecimento em células cancerígenas *versus* células normais. Assim, alvos para cada tipo de linhagem de câncer são melhor estudados no processo de desenvolvimento tumoral (LI et al., 2021; WANG et al., 2022). Entre os PCTPs, os peptídeos mais populares têm como alvo a via de sinalização PD-1/PD-L1 (Fig. 7B).

Há um interesse crescente no desenvolvimento de inibidores anti-PD-L1 baseados em peptídeos. Este interesse é justificado pelas limitações inerentes às imunoterapias baseadas em anticorpos, como o elevado custo de produção de anticorpos ou a sua longa semivida. Assim, a descoberta de terapêuticas baseadas em inibidores de moléculas pequenas da interação PD-1/PD-L1 representa uma perspectiva promissora no tratamento do câncer (GUZIK et al., 2019).

Em um estudo de Boohaker et al., (2018), um peptídeo imita PD-L1, denominado PL120131, foi projetado. Isso interfere na interação PD-1/PD-L1, ligando-se ao PD-1. Foi

demonstrado que o PL120131 pode inibir a via de sinalização apoptótica mediada por PD-1 e resgatar células Jurkat e linfócitos primários da apoptose. Também foi revelado que este peptídeo pode manter melhor capacidade de sobrevivência de células T e atividade de cocultura em um modelo de cocultura 3D do que o anticorpo bloqueador anti-PD-1 (BOOHAKER et al., 2018; GUZIK et al., 2019).

Um estudo proposto por Liu et al., (2021) também revelaram resultados positivos para pequenos inibidores de *checkpoint* baseados em peptídeos. Os resultados sugeriram que o peptídeo CLP002 representa um promissor inibidor de *checkpoint* de baixo peso molecular para imunoterapia contra o câncer, demonstrando que este peptídeo se liga especificamente ao PD-L1 nos resíduos onde o PD-L1 interage com o PD-1; previne a apoptose de células T que são co-cultivadas com células cancerígenas; inibe o crescimento tumoral; aumenta a sobrevivência de camundongos portadores de tumor CT26, exibe melhor penetração do tumor em um modelo 3D de tumor esferóide em comparação com o anticorpo (LIU et al., 2021).

O receptor do fator de crescimento epidérmico (EGFR) é um alvo peptídico popularmente estudado. Este é um alvo proteico da membrana celular superexpresso em tumores de origem epitelial, incluindo cânceres de mama de origem ductal ou lobular. Um estudo de Hoppenz et al., (2020) destacaram as vantagens do uso de conjugados peptídeo-droga (PDCs) em vez de conjugados anticorpo-droga (ADCs), uma terapia que tem sido efetivamente aplicada contra o alvo de EGFR no câncer de mama triplo negativo. As vantagens do uso de PDCs incluem a capacidade de penetrar facilmente nos tumores, baixa imunogenicidade, síntese fácil e acessível e menor propensão para acúmulo em órgãos excretórios. Considerando as vantagens da terapia peptídica, cada vez mais CTPs estão sendo desenvolvidos para atingir o alvo EGFR (HOPPENZ; ELS-HEINDL; BECK-SICKINGER, 2020).

Outro alvo relevante refere-se à CTLA-4 (Fig. 4C), proteína 4 associada a linfócitos T citotóxicos, que interage com receptores de células T (TCRs), impedindo o reconhecimento pelos linfócitos T e, assim, a destruição das células cancerígenas. Neste cenário, a imunoterapia com anticorpos monoclonais anti-CTLA-4 é altamente eficiente ao bloquear o CTLA4 e expor as células cancerígenas às células T. No entanto, é uma terapia cara e impossível de ser disponibilizada à população normal. Recentemente, foi demonstrado que os peptídeos sintéticos poderiam ser uma opção econômica para o tratamento com anticorpos monoclonais anti-CTLA-4 (AMARAL et al., 2020).

Utilizando uma abordagem *in silico*, Amaral et al. 2020 propôs o projeto de peptídeos sintéticos derivados de ipilimumabe que têm como alvo e bloqueiam CTLA-4, permitindo assim que as células cancerígenas expostas às células T as destruam. Com a ajuda da dinâmica

molecular e do cálculo bioquímico quântico foi possível avaliar a posição do *hotspot* de interação no complexo CTLA-4:Ipilimumab e utilizar esta região para projetar peptídeos. Esses peptídeos apresentaram a capacidade de interagir e formar um complexo com CTLA-4, levando à morte de células cancerígenas (AMARAL et al., 2020).

Por outro lado, os CPPs não têm como alvo uma proteína específica, mas sim membranas. Eles interagem com a camada externa da membrana celular através de forças eletrostáticas e interações hidrofóbicas. Esses peptídeos aderem e iniciam um processo de internalização na membrana das células cancerígenas, que se caracterizam por terem uma carga mais negativa do que as membranas das células normais. Observa-se que a diferença na eletronegatividade entre células saudáveis e cancerosas é essencial para a seletividade na terapia peptídica CPP e seu mecanismo de ação.

Os CPPs são caracterizados por possuírem em sua composição um alto percentual de aminoácidos básicos, que em pH fisiológico carregam carga positiva em sua cadeia lateral. Portanto, o CPP carregado positivamente pode aderir eletrostaticamente à membrana carregada negativamente das células cancerígenas. Assim como os CTPs, os CPPs também podem atuar como transportadores de medicamentos para células-alvo. Os CPPs também têm sido usados para fornecer proteínas, peptídeos, siRNAs, DNA plasmídico e medicamentos anticâncer.

2 OBJETIVOS

2.1 Objetivo geral

Aplicar a bioinformática na busca de novos alvos terapêuticos e no reposicionamento de peptídeos sintéticos antimicrobianos contra o câncer gástrico.

2.2 Objetivos específicos

2.2.1 Capítulo II

- Analisar datasets de RNAseq de pacientes com câncer gástrico e pacientes saudáveis na busca por novos alvos terapêuticos;
- Realizar uma análise de expressão diferencial tumor *versus* normal utilizando o pacote *limma*;
- Identificar os genes mais hipoexpressos e hiperexpressos em amostras tumorais e desenhar os *primers* dos mesmos;
- Analisar os dados de câncer gástrico presentes no banco de dados do TCGA (do inglês, *The Cancer Genome Atlas Program*) para validar a análise do GEO;
- Correlacionar a taxa de sobrevivência dos pacientes com a expressão dos genes identificados;
- Validar os dados *in silico* realizando expressão gênica por PCR quantitativo em tempo real (qRT-PCR);
- Obter a estrutura 3D das proteínas correspondentes aos genes mais hiperexpressos;
- Realizar a técnica de triagem virtual baseada em estrutura (SBVS) para encontrar ligantes com alta afinidade de ligação aos alvos identificados;
- Caracterizar as propriedades farmacocinéticas, farmacodinâmicas e toxicológicas dos ligantes encontrados com uso de *softwares* e ferramentas computacionais;
- Realizar o estudo de *docking* molecular para determinar a energia de ligação entre a molécula e o receptor;

2.2.2 Capítulo III

- Avaliar, por bioinformática, o potencial anticâncer de peptídeos sintéticos antimicrobianos;
- Realizar um estudo *in silico* de parâmetros toxicológicos e farmacocinéticos dos peptídeos sintéticos;
- Definir a CI_{50} e caracterizar o índice de seletividade de peptídeos sintéticos contra linhagens de câncer gástrico;
- Avaliar se o(s) peptídeo(s) alteram a permeabilidade da membrana e induzem a formação de poros nas células de câncer gástrico;
- Avaliar se o(s) peptídeo(s) induzem o acúmulo de espécies reativas de oxigênio (EROs) em células gástricas tumorais;
- Estudar, através de microscopia de força atômica, o efeito do(s) peptídeo(s) sobre a morfologia, propriedades ultraestruturais e nanomecânicas das células cancerígenas;
- Avaliar se o(s) peptídeo(s) são capazes de alterar a assinatura vibracional das células cancerígenas;
- Avaliar o efeito antimigratório do(s) peptídeo(s) sintéticos sobre as células cancerígenas;
- Analisar a toxicidade *in vitro* do(s) peptídeo(s) em células humanas saudáveis por meio dos ensaios de cometa e indução de apoptose;
- Analisar a toxicidade *in vivo* do(s) peptídeo(s) em embriões de peixe-zebra;
- Estudar por *docking* molecular a interação do(s) peptídeo(s) contra alvos moleculares do câncer gástrico.

REFERÊNCIAS

- AJANI, J. A. et al. Enhanced Staging and All Chemotherapy Preoperatively in Patients with Potentially Resectable Gastric Carcinoma. **Journal of Clinical Oncology**, v. 17, n. 8, p. 2403–2403, ago. 1999.
- ALIPOUR, M. Molecular Mechanism of Helicobacter pylori-Induced Gastric Cancer. **Journal of Gastrointestinal Cancer**, v. 52, n. 1, p. 23–30, 14 mar. 2021.
- AMARAL, J. L. et al. Quantum biochemistry in cancer immunotherapy: New insights about CTLA-4/ipilimumab and design of ipilimumab-derived peptides with high potential in cancer treatment. **Molecular Immunology**, v. 127, p. 203–211, nov. 2020.
- ANTHONY, L. F. W.; KANDING, B.; SELVAN, R. Carbontracker: Tracking and Predicting the Carbon Footprint of Training Deep Learning Models. 6 jul. 2020.
- BAJ, J. et al. Mechanisms of the Epithelial–Mesenchymal Transition and Tumor Microenvironment in Helicobacter pylori-Induced Gastric Cancer. **Cells**, v. 9, n. 4, p. 1055, 23 abr. 2020.
- BALASUBRAMANIAN, K.; SCHROIT, A. J. Aminophospholipid Asymmetry: A Matter of Life and Death. <https://doi.org/10.1146/annurev.physiol.65.092101.142459>, v. 65, p. 701–734, nov. 2003.
- BASS, A. J. et al. Comprehensive molecular characterization of gastric adenocarcinoma. **Nature**, v. 513, n. 7517, p. 202–209, 11 set. 2014.
- BAXTER, A. A. et al. Tumor cell membrane-targeting cationic antimicrobial peptides: novel insights into mechanisms of action and therapeutic prospects. **Cellular and Molecular Life Sciences** 2017 74:20, v. 74, n. 20, p. 3809–3825, ago. 2017.
- BEVERS, E. M.; COMFURIUS, P.; ZWAAL, R. F. A. Regulatory Mechanisms in Maintenance and Modulation of Transmembrane Lipid Asymmetry: Pathophysiological Implications. <http://dx.doi.org/10.1177/096120339600500531>, v. 5, n. 5, p. 480–487, out. 1996.
- BHARDWAJ, Priya *et al.* An investigational approach for the prediction of gastric cancer using artificial intelligence techniques: a systematic review. **Archives of Computational Methods in Engineering**, v. 29, n. 6, p. 4379–4400, 2022.
- BOOHAKER, R. J. et al. Rational design and development of a peptide inhibitor for the PD-1/PD-L1 interaction. **Cancer letters**, v. 434, p. 11–21, out. 2018.
- BRASIL. Ministério da Saúde. DATASUS. **Tabnet**. Brasília, DF: Ministério da Saúde, 2022. Disponível em: <https://datasus.saude.gov.br/informacoes-de-saude-tabnet/>. Acesso em: 3 jan. 2024.
- CHEN, Y.-C. et al. Clinicopathological Variation of Lauren Classification in Gastric Cancer. **Pathology & Oncology Research**, v. 22, n. 1, p. 197–202, 27 jan. 2016.

- CONIBEAR, A. C. et al. Recent Advances in Peptide-Based Approaches for Cancer Treatment. **Current medicinal chemistry**, v. 27, n. 8, p. 1174–1205, nov. 2020.
- DA SILVA, E. L. et al. Mebendazole targets essential proteins in glucose metabolism leading gastric cancer cells to death. **Toxicology and Applied Pharmacology**, v. 475, p. 116630, set. 2023.
- DAINA, A.; ZOETE, V. A BOILED-Egg To Predict Gastrointestinal Absorption and Brain Penetration of Small Molecules. **ChemMedChem**, v. 11, n. 11, p. 1117–1121, 6 jun. 2016.
- DE ALMEIDA GOMES, I. et al. Recalculating the Route: Repositioning Antimicrobial Peptides for Cancer Treatment. **Chemistry & Biodiversity**, 13 dez. 2023.
- DIGKLIA, A. Advanced gastric cancer: Current treatment landscape and future perspectives. **World Journal of Gastroenterology**, v. 22, n. 8, p. 2403, 2016.
- FERLAY, J. et al. Cancer statistics for the year 2020: An overview. **International Journal of Cancer**, v. 149, n. 4, p. 778–789, 15 ago. 2021.
- GUAN, W.-L.; HE, Y.; XU, R.-H. Gastric cancer treatment: recent progress and future perspectives. **Journal of Hematology & Oncology**, v. 16, n. 1, p. 57, 27 maio 2023.
- GUZIK, K. et al. Development of the Inhibitors that Target the PD-1/PD-L1 Interaction-A Brief Look at Progress on Small Molecules, Peptides and Macrocycles. **Molecules (Basel, Switzerland)**, v. 24, n. 11, maio 2019.
- HANAHAN, D. Hallmarks of Cancer: New Dimensions. **Cancer Discovery**, v. 12, n. 1, p. 31–46, 1 jan. 2022.
- HANAHAN, D.; WEINBERG, R. A. The Hallmarks of Cancer. **Cell**, v. 100, n. 1, p. 57–70, jan. 2000.
- HANAHAN, D.; WEINBERG, R. A. Hallmarks of Cancer: The Next Generation. **Cell**, v. 144, n. 5, p. 646–674, mar. 2011.
- HANEY, E. F.; MANSOUR, S. C.; HANCOCK, R. E. W. Antimicrobial peptides: An introduction. **Methods in Molecular Biology**, v. 1548, p. 3–22, 2017.
- HOPPENZ, P.; ELS-HEINDL, S.; BECK-SICKINGER, A. G. Peptide-Drug Conjugates and Their Targets in Advanced Cancer Therapies. **Frontiers in Chemistry**, v. 8, p. 545283, jul. 2020.
- HOSKIN, D. W.; RAMAMOORTHY, A. Studies on anticancer activities of antimicrobial peptides. **Biochimica et Biophysica Acta (BBA) - Biomembranes**, v. 1778, n. 2, p. 357–375, fev. 2008.
- HOUSMAN, G. et al. Drug resistance in cancer: An overview. **Cancers**, v. 6, n. 3, p. 1769–1792, 2014.
- HSU, H. C. et al. Antibacterial and Anticancer Activities of Pleurocidin-Amide, a Potent Marine Antimicrobial Peptide Derived from Winter Flounder, *Pleuronectes americanus*. **Marine Drugs** 2022, Vol. 20, Page 519, v. 20, n. 8, p. 519, ago. 2022.

INSTITUTO NACIONAL DE CÂNCER (Brasil). Câncer. Tipos de câncer. **Câncer de estômago**. Rio de Janeiro: INCA, 2022a. Disponível em: <https://www.gov.br/inca/pt-br/assuntos/cancer/tipos/estomago>. Acesso em: 13 jan. 2024.

INSTITUTO NACIONAL DE CÂNCER JOSÉ ALENCAR GOMES DA SILVA. **Atlas online de mortalidade**. [Rio de Janeiro: INCA, 2020a]. Disponível em: <https://www.inca.gov.br/MortalidadeWeb>. Acesso em: 1 dez. 2024.

JOSHI, S. S.; BADGWELL, B. D. Current treatment and recent progress in gastric cancer. **CA: A Cancer Journal for Clinicians**, v. 71, n. 3, p. 264–279, 16 maio 2021.

KORDI, M. et al. Antimicrobial peptides with anticancer activity: Today status, trends and their computational design. **Archives of Biochemistry and Biophysics**, v. 733, p. 109484, jan. 2023.

LAU, J. L.; DUNN, M. K. Therapeutic peptides: Historical perspectives, current development trends, and future directions. **Bioorganic & Medicinal Chemistry**, v. 26, n. 10, p. 2700–2707, jun. 2018.

LAURÉN, P. THE TWO HISTOLOGICAL MAIN TYPES OF GASTRIC CARCINOMA: DIFFUSE AND SO-CALLED INTESTINAL-TYPE CARCINOMA. **Acta Pathologica Microbiologica Scandinavica**, v. 64, n. 1, p. 31–49, 30 set. 1965.

LEE, J. M. et al. The epithelial–mesenchymal transition: new insights in signaling, development, and disease. **The Journal of Cell Biology**, v. 172, n. 7, p. 973–981, 27 mar. 2006.

LI, C. M. et al. Novel Peptide Therapeutic Approaches for Cancer Treatment. **Cells**, v. 10, n. 11, nov. 2021.

LIU, M. et al. Peptide-Enabled Targeted Delivery Systems for Therapeutic Applications. **Frontiers in bioengineering and biotechnology**, v. 9, jul. 2021.

LONGLEY, D.; JOHNSTON, P. Molecular mechanisms of drug resistance. **The Journal of Pathology**, v. 205, n. 2, p. 275–292, 10 jan. 2005.

MA, J. et al. Lauren classification and individualized chemotherapy in gastric cancer. **Oncology Letters**, v. 11, n. 5, p. 2959–2964, maio 2016.

MELLOR, H. R.; CALLAGHAN, R. Resistance to Chemotherapy in Cancer: A Complex and Integrated Cellular Response. **Pharmacology**, v. 81, n. 4, p. 275–300, 2008.

MESQUITA, F. P. et al. In silico analysis of ACE2 from different animal species provides new insights into SARS-CoV-2 species spillover. **Future Virology**, v. 18, n. 6, p. 359–371, abr. 2023.

MESQUITA, F. P. et al. Kinase inhibitor screening reveals aurora kinase is a potential therapeutic and prognostic biomarker of gastric cancer. **Journal of Cellular Biochemistry**, v. 1, p. 1, 2021.

MILLER, Z. et al. Proteasome Inhibitors with Pyrazole Scaffolds from Structure-Based Virtual Screening. **Journal of Medicinal Chemistry**, v. 58, n. 4, p. 2036–2041, 26 fev. 2015.

- PAN, F. et al. Anticancer effect of rationally designed α -helical amphiphilic peptides. **Colloids and Surfaces B: Biointerfaces**, v. 220, p. 112841, dez. 2022.
- POOROLAJAL, J. et al. Risk factors for stomach cancer: a systematic review and meta-analysis. **Epidemiology and Health**, v. 42, p. e2020004, 2 fev. 2020.
- POUS, A. et al. HER2-Positive Gastric Cancer: The Role of Immunotherapy and Novel Therapeutic Strategies. **International Journal of Molecular Sciences**, v. 24, n. 14, p. 11403, 13 jul. 2023.
- PRIETO-MARTÍNEZ, F. D. et al. Computational Drug Design Methods—Current and Future Perspectives. Em: **In Silico Drug Design**. [s.l.] Elsevier, 2019. p. 19–44.
- RĂILEANU, M.; BACALUM, M. Cancer Wars: Revenge of the AMPs (Antimicrobial Peptides), a New Strategy against Colorectal Cancer. **Toxins**, v. 15, n. 7, jul. 2023.
- RAJDEV, L. Treatment Options for Surgically Resectable Gastric Cancer. **Current Treatment Options in Oncology**, v. 11, n. 1–2, p. 14–23, 27 jun. 2010.
- RAWLA, P.; BARSOUK, A. **Epidemiology of gastric cancer: Global trends, risk factors and prevention**. **Przegląd Gastroenterologiczny** Termedia Publishing House Ltd., , 2019.
- RIEDL, S.; ZWEYTICK, D.; LOHNER, K. Membrane-active host defense peptides – Challenges and perspectives for the development of novel anticancer drugs. **Chemistry and Physics of Lipids**, v. 164, n. 8, p. 766–781, nov. 2011.
- ROHR, M. et al. A merged microarray meta-dataset for transcriptionally profiling colorectal neoplasm formation and progression. **Scientific Data**, v. 8, n. 1, p. 214, 11 ago. 2021.
- RUSIECKA, I.; GAĞAŁO, I.; KOCIĆ, I. Cell-penetrating peptides improve pharmacokinetics and pharmacodynamics of anticancer drugs. **Tissue Barriers**, v. 10, n. 1, 2022.
- SANG, M.; ZHANG, J.; ZHUGE, Q. Selective cytotoxicity of the antibacterial peptide ABP-dHC-Cecropin A and its analog towards leukemia cells. **European Journal of Pharmacology**, v. 803, p. 138–147, maio 2017.
- SASAKO, M. et al. Five-Year Outcomes of a Randomized Phase III Trial Comparing Adjuvant Chemotherapy With S-1 Versus Surgery Alone in Stage II or III Gastric Cancer. **Journal of Clinical Oncology**, v. 29, n. 33, p. 4387–4393, 20 nov. 2011.
- SATO, Y. et al. Overview of Chemotherapy for Gastric Cancer. **Journal of Clinical Medicine**, v. 12, n. 4, p. 1336, 7 fev. 2023.
- SEXTON, Rachel E. *et al.* Gastric cancer: a comprehensive review of current and future treatment strategies. **Cancer and Metastasis Reviews**, v. 39, p. 1179-1203, 2020.
- SHARIFI, F. et al. Bioinformatics evaluation of anticancer properties of GP63 protein-derived peptides on MMP2 protein of melanoma cancer. **Journal of Pathology Informatics**, v. 14, p. 100190, jan. 2023.
- SIEGEL, R. L. et al. Cancer statistics, 2023. **CA: A Cancer Journal for Clinicians**, v. 73, n. 1, p. 17–48, 12 jan. 2023.

SUNG, H. et al. Global Cancer Statistics 2020: GLOBOCAN Estimates of Incidence and Mortality Worldwide for 36 Cancers in 185 Countries. **CA: A Cancer Journal for Clinicians**, v. 71, n. 3, p. 209–249, 4 maio 2021.

THIERY, J. P.; SLEEMAN, J. P. Complex networks orchestrate epithelial–mesenchymal transitions. **Nature Reviews Molecular Cell Biology**, v. 7, n. 2, p. 131–142, fev. 2006.

TORNESELLO, A. L. et al. Antimicrobial Peptides as Anticancer Agents: Functional Properties and Biological Activities. **Molecules 2020, Vol. 25, Page 2850**, v. 25, n. 12, p. 2850, jun. 2020.

VASAN, N.; BASELGA, J.; HYMAN, D. M. A view on drug resistance in cancer. **Nature**, v. 575, n. 7782, p. 299–309, 14 nov. 2019.

WANG, L. et al. Therapeutic peptides: current applications and future directions. **Signal transduction and targeted therapy**, v. 7, n. 1, dez. 2022.

WELCH, D. R.; HURST, D. R. Defining the Hallmarks of Metastasis. **Cancer Research**, v. 79, n. 12, p. 3011–3027, 15 jun. 2019.

WODLEJ, C. et al. Interaction of two antitumor peptides with membrane lipids – Influence of phosphatidylserine and cholesterol on specificity for melanoma cells. **PLoS ONE**, v. 14, n. 1, jan. 2019.

CAPÍTULO II

A Shortcut from Genome to Drug: The Employment of Bioinformatic Tools to Find New Targets for Gastric Cancer Treatment

**Artigo publicado na Revista *Pharmaceutics*
(Fator de Impacto 5.4, Qualis A1)**

Daiane Maria da Silva Brito



Article





A Shortcut from Genome to Drug: The Employment of Bioinformatic Tools to Find New Targets for Gastric Cancer Treatment

Daiane M. S. Brito, Odnan G. Lima, Felipe P. Mesquita, Emerson L. da Silva, Maria E. A. de Moraes, Rommel M. R. Burbano, Raquel C. Montenegro and Pedro F. N. Souza



Article

A Shortcut from Genome to Drug: The Employment of Bioinformatic Tools to Find New Targets for Gastric Cancer Treatment

Daiane M. S. Brito ^{1,2}, Odnan G. Lima ², Felipe P. Mesquita ², Emerson L. da Silva ², Maria E. A. de Moraes ², Rommel M. R. Burbano ^{3,4}, Raquel C. Montenegro ^{2,5,*} and Pedro F. N. Souza ^{1,2,*}

¹ Department of Biochemistry and Molecular Biology, Federal University of Ceará, Fortaleza 60020-181, Brazil

² Pharmacogenetics Laboratory, Drug Research and Development Center, Department of Physiology and Pharmacology, Federal University of Ceará, Fortaleza 60430-160, Brazil

³ Department of Biological Sciences, Oncology Research Center, Federal University of Pará, Belém 66073-005, Brazil; rommel@ufpa.br

⁴ Molecular Biology Laboratory, Ophir Loyola Hospital, Belém 66063-240, Brazil

⁵ Red Latinoamericana de Implementación y Validación de Guías Clínicas Farmacogenómicas (RELIVAF), Cytel, 28015 Madrid, Spain

* Correspondence: rcm.montenegro@gmail.com (R.C.M.); pedrofilhobio@gmail.com or pedrofilhobio@ufc.br (P.F.N.S.)

Abstract: Gastric cancer (GC) is a highly heterogeneous, complex disease and the fifth most common cancer worldwide (about 1 million cases and 784,000 deaths worldwide in 2018). GC has a poor prognosis (the 5-year survival rate is less than 20%), but there is an effort to find genes highly expressed during tumor establishment and use the related proteins as targets to find new anticancer molecules. Data were collected from the Gene Expression Omnibus (GEO) bank to obtain three dataset matrices analyzing gastric tumor tissue versus normal gastric tissue and involving microarray analysis performed using the GPL570 platform and different sources. The data were analyzed using the GEPIA tool for differential expression and KMPlot for survival analysis. For more robustness, GC data from the TCGA database were used to corroborate the analysis of data from GEO. The genes found in in silico analysis in both GEO and TCGA were confirmed in several lines of GC cells by RT-qPCR. The AlphaFold Protein Structure Database was used to find the corresponding proteins. Then, a structure-based virtual screening was performed to find molecules, and docking analysis was performed using the DockThor server. Our in silico and RT-qPCR analysis results confirmed the high expression of the *AJUBA*, *CD80* and *NOLC1* genes in GC lines. Thus, the corresponding proteins were used in SBVS analysis. There were three molecules, one molecule for each target, MCULE-2386589557-0-6, MCULE-9178344200-0-1 and MCULE-5881513100-0-29. All molecules had favorable pharmacokinetic, pharmacodynamic and toxicological properties. Molecular docking analysis revealed that the molecules interact with proteins in critical sites for their activity. Using a virtual screening approach, a molecular docking study was performed for proteins encoded by genes that play important roles in cellular functions for carcinogenesis. Combining a systematic collection of public microarray data with a comparative meta-profiling, RT-qPCR, SBVS and molecular docking analysis provided a suitable approach for finding genes involved in GC and working with the corresponding proteins to search for new molecules with anticancer properties.

Keywords: transcriptional meta-analysis; molecular docking; RT-qPCR; bioinformatics; structure-based virtual screening



Citation: Brito, D.M.S.; Lima, O.G.; Mesquita, F.P.; da Silva, E.L.; de Moraes, M.E.A.; Burbano, R.M.R.; Montenegro, R.C.; Souza, P.F.N. A Shortcut from Genome to Drug: The Employment of Bioinformatic Tools to Find New Targets for Gastric Cancer Treatment. *Pharmaceutics* **2023**, *15*, 2303. <https://doi.org/10.3390/pharmaceutics15092303>

Academic Editor: David Barlow

Received: 8 August 2023

Revised: 28 August 2023

Accepted: 3 September 2023

Published: 12 September 2023



Copyright: © 2023 by the authors. Licensee MDPI, Basel, Switzerland. This article is an open access article distributed under the terms and conditions of the Creative Commons Attribution (CC BY) license (<https://creativecommons.org/licenses/by/4.0/>).

1. Introduction

Gastric cancer (GC) is a complex and multifactorial disease caused by genetic, epigenetic and environmental influences [1]. Although a worldwide decline in incidence and mortality rates has been observed in recent decades, GC still constitutes a significant burden

and significantly impacts populations in developing countries. Current statistics reveal that GC is the third most common malignancy and the fourth leading cause of cancer-related mortality worldwide, accounting for more than 768,000 deaths in 2020 [2,3]. The National Cancer Institute (INCA) estimates 13,340 new cases of GC in men and 8140 in women for Brazil in the three years from 2023 to 2025. These values correspond to an estimated risk of 12.63 new cases per 100,000 men and 7.36 per 100,000 women [4].

Most gastric cancers are adenocarcinomas. According to Lauren's classification, these represent more than 95% of all gastric malignancies and can be subdivided into intestinal and diffuse types. This classification is based on the histology of the tumor [5]. The intestinal type consists of differentiated cancer with a tendency to form glands. It progresses mainly through successive changes in the normal gastric mucosa, leading to acute and chronic gastritis, atrophic gastritis, intestinal metaplasia, dysplasia and a gastric tumor [5].

The standard treatment for gastric cancer is based on the triad of surgery, chemotherapy and radiotherapy. Surgical resection is considered the primary method of treatment at an early stage and the only potentially curative approach in treating gastric cancer. However, recurrence is frequently observed in many patients, even after resection. Faced with this problem, a study of 206 patients with gastric cancer revealed that patients in stages II and III had better survival rates with adjuvant chemotherapy than surgery alone [6]. Over two decades ago, Phase II clinical studies showed that neoadjuvant chemotherapy can increase tumor resection success rate by 72 to 87% [7,8].

Various chemotherapeutic drugs and therapeutic schemes are approved for the pharmacological treatment of gastric cancer. Some of these therapeutic schemes are well described in the literature: the FLOT scheme (5-fluorouracil, leucovorin, oxaliplatin and taxane), the ECF scheme (epirubicin, cisplatin and fluorouracil), FOLFOX (5-fluorouracil, leucovorin and oxaliplatin), infusional cisplatin (CF) and a single-drug regimen with irinotecan [9,10].

Nowadays, two problems related to drugs for GC need to be solved: (1) the high toxicity of drugs to patients and (2) the resistance of GC cells to these drugs. In relation to these problems, bioinformatics has been raised as a powerful tool to identify new targets or new molecules for a target. Over the last few years, bioinformatics has helped researchers worldwide to rapidly find molecules and targets that could be applied to cancer. For example, Miller et al. [11] performed a structure-based virtual screening (SBVS) to find new molecules with activity against the proteasome of pancreatic cancer cells. In the study, the authors analyzed 380,000 compounds against one proteasome subunit. After SBVS analysis, out of 288 compounds tested in vitro, 1 was selected for experiment analysis [11]. This case is an example of how bioinformatics can rapidly help drug discovery.

Another study by Rohr et al. [12] developed a pipeline employing R package scripts to analyze data from transcriptional analysis from a microarray from pre- and post-malignant colorectal cancer. Using the pipeline developed, it was possible to analyze a merged dataset containing 231 normal, 132 adenoma and 342 colon cancer tissue samples across twelve independent studies analyzed by microarray deposited in the Gene Expression Omnibus (GEO) [12]. The analysis was performed to understand the genes involved in the disease severity, progression, and new targets for treating colorectal cancer. Both studies employed bioinformatics to find new targets and molecules that could be useful in cancer treatment, corroborating bioinformatics applications in clinics.

The present study aimed to identify new potential targets involved in GC establishment in samples collected from different populations worldwide using bioinformatic tools. First, an R code script was employed to analyze the microarray metadata from healthy patients and with GC downloaded from GEO in a search for new genes involved in GC establishment.

2. Methodology

2.1. Selection of Microarray Transcriptome Studies

To minimize the number and impact of batch effects, Minimum Information About a Microarray Experiment (MIAME)-compliant microarray studies were selected based on predefined inclusion criteria: (1) collection of human tissue samples; (2) use of the GPL570 platform (Affymetrix Human Genome U133 Plus 2.0 array) for matching probe sets (Supplementary Table S1); and (3) inclusion of samples from gastric cancer (tumor) and healthy tissue (normal). In total, 3 independent studies were chosen from an initial list of 156 to construct the meta-data.

2.2. Data Acquisition and Processing

Data acquisition and processing were performed in the R studio (v 4.1.3). Raw data were downloaded from the GEO database (<https://www.ncbi.nlm.nih.gov/geo/>) (accessed on 10 January 2022) using the `getGEO` function of the `GEOquery` package (version 2.58.0) and the method described by Rohr et al. [12]. The `.cel` format files for each study were unpacked using the `R` `untar` function and loaded using the `ReadAffy` function of the `affy` package (version 1.68.0). Subsequently, the data were corrected and log-transformed by the frozen Robust Multiarray Averaging (fRMA) method using the `fRMA` package (version 1.42.0). Compared to traditional RMA, fRMA uses pre-calculated probe drifts to normalize the raw microarray data and has been shown to outperform RMA when preprocessing individual data sets for pooled analyses [12].

2.3. Metadata Construction

The construction of the metadata followed the script described and validated by Rohr and colleagues [12]. Following fRMA normalization, the matrices of individual datasets were merged by combining the microarray probes. The batch effect among studies was identified using the Uniform Manifold Approximation and Projection (UMAP) method using the `umap` package (version 0.2.7.0) and removed using the original ComBat parametric iteration within the `SVA` package (version 3.38.0). UMAP was used over traditional principal component analysis (PCA) to identify batch effects due to its ability to represent local relationships better while preserving the global structure [12]. The ComBat function was chosen due to its flexibility, reliability, and ability to define covariates of interest.

Next, probes with an expression variation in the 75th percentile were filtered from the meta-dataset using the `gene-filter` function in the `oligo` package (version 1.54.1). Finally, the maximum average expression using the `hgu133plus2` collapsed redundant probes to their corresponding human gene symbol.db package (version 3.2.3). The constructed metadata contain 601 samples, including 152 tumor and 449 normal patients from 3 independent studies.

Differential expression (DE) analysis for tumor versus normal comparison was performed using the `limma` package. Specifically, DE analysis was performed independently on 25% of the most variable genes between each group. Genes were considered differentially expressed if the q -value of $|\text{LogFC}| \geq 1.0$ and false discovery rate (FDR) < 0.01 .

2.4. Gene Set Enrichment Analysis (GSEA)

The significantly enriched tumor and normal phenotype gene sets were identified using Gene Set Enrichment Analysis (GSEA, [gsea-msigdb.org](https://www.broadinstitute.org/gsea)) (accessed on 15 January 2022). The H collection (hallmark gene set) available in the Molecular Signatures Database (MSigDB) 3.0 was chosen for the enrichment analysis [13]. The default parameters defined by Subramanian et al. [14] were used in this analysis. One hundred permutations determined the significance of the GSEA analysis (corrected p -value < 0.05 and false discovery rate (FDR) < 0.25). GraphPad Prism™ software version 5 (San Francisco, CA, USA) was also used to represent individual genes' enrichment scores and signal-to-noise values.

2.5. Differential Expression and Survival Analysis from TCGA

Based on tumor and normal samples from the TCGA (The Cancer Genome Atlas) databases, differential expression and overall survival analyses were performed for the three up- and downregulated genes in the differential expression analysis using the limma package and for the three most enriched genes in the analysis using the GSEA. Using the Gene Expression Profiling Interactive Analysis (GEPIA) tool, available at <http://gepia.cancer-pku.cn/> (accessed on 19 August 2023), an analysis of the differential expression of the mRNA levels of these proteins in gastric cancer (identified by STAD) was performed. The results are presented in box plots. The Kaplan–Meier plotter database (<https://kmplot.com/analysis/>) (accessed on 21 August 2023) was used to compare the expression profiles of the gene of interest in normal and tumor gastric tissue, classifying them as high or low/medium expression, which was then correlated with the probability of patient survival [15]. This tool can evaluate the correlation between the expression of all genes (mRNA, miRNA, protein) and survival in more than thirty thousand samples of different types of tumors. Therefore, the genes most significantly associated with patient survival can be identified.

2.6. Primer Designer

The ThermoFisher trading platform (<https://apps.thermofisher.com/apps/oligoperfect/#!/design>) (accessed on 15 March 2022) was chosen to design the perfect primers for polymerase chain reaction (PCR). For this, the mRNA codes had to be obtained from the NCBI databases (<https://www.ncbi.nlm.nih.gov/>) (accessed on 18 March 2022), providing the nucleotide sequence for all transcript variants of interest (Supplementary Table S2). The primer sequence was provided by the OligoAnalyzer™ Tool from Integrated DNA Technologies.

2.7. Cell Culture

The gastric cancer cell line AGP-01 was obtained from the malignant ascitic fluid of primary metastatic intestinal-type tumors. The ACP-02 and ACP-03 cell lines were established from Brazilian patients' diffuse-type and primary intestinal-type tumors, respectively. The AGS cell line was obtained from gastric adenocarcinoma tumors of a Caucasian patient [16,17]. The non-malignant gastric cell lineage MNP-01 was previously established from normal gastric mucosa and was used as a cell-type-specific control [18]. All cells were cultured in Dulbecco's modified Eagle's medium (DMEM; Gibco®), supplemented with 10% (*v/v*) fetal bovine serum (Gibco®), 1% (*v/v*) penicillin (100 U mL⁻¹) and streptomycin (100 mg mL⁻¹) (Invitrogen®), in a humidified atmosphere with 5% CO₂ at 37 °C. Cell confluence was observed under a conventional microscope.

2.8. Gene Expression by qRT-PCR

2.8.1. RNA Extraction

Total mRNA from gastric cell lines and tissue specimens was extracted using TRIzol™ reagent (Invitrogen, Carlsbad, CA, USA) as per the manufacturer's guidelines. Quantification was performed in a spectrophotometer (NanoDrop®, Thermo Scientific, Carlsbad, CA, USA), and mRNA was stored at –80 °C until conversion into cDNA.

2.8.2. Conversion of mRNA to cDNA

The mRNA was converted to cDNA using the High-Capacity cDNA Reverse Transcriptase® kit (Thermo Scientific, Carlsbad, CA, USA). A thermocycler was used to carry out the conversion reactions (Verity®, Thermo Scientific, Carlsbad, CA, USA).

2.8.3. Real-Time Quantitative PCR (qRT-PCR)

Gene expression was determined by qRT-PCR using PowerUp SYBR® Master Mix (Life Technologies, San Diego, CA, USA) on a QuantStudio5 Real-Time PCR system (Applied Biosystems®, Carlsbad, CA, USA). The primer efficiency was determined for all described

genes. The relative expression levels of the *AJUBA*, *CD80*, *NOLC1* and *KNL1* genes were normalized and determined using the *ACTB* gene as an endogenous control. Calculations were performed using the $2^{-\Delta\Delta CT}$ method. The requirements proposed in the Minimum Information for Publication of Quantitative Real-Time PCR Experiments (MIQE) Guidelines were followed [19].

2.9. Three-Dimensional Structure Obtention

The 3D structures of the proteins were obtained from the AlphaFold Protein Structure Database (<https://alphafold.com/>) (accessed on 15 June 2022), an artificial intelligence (AI) system developed by DeepMind and EMBL-EBI that predicts the 3D structure of proteins from an amino acid sequence with high precision. The predictions of the 3D structures related to the *AJUBA*, *CD80* and *NOLC1* genes were available in this database free of charge and with open access [20,21]. Even though they were produced by artificial intelligence, the structures had the quality assessed by Verify 3D and ERRATA servers.

The organism filter was applied to choose the structure for each protein, selecting the *Homo sapiens* option. Per-residue confidence score (pLDDT) and FASTA amino acid sequence coverage analysis were considered. The PyMOL Molecular Graphics System (version 2.5.4, Schrödinger, LLC, San Diego, CA, USA) [22] was employed to analyze the 3D structures of proteins. The 3D structures of the *AJUBA*, *CD80* and *NOLC1* proteins downloaded from the AlphaFold Protein Structure Database (<https://alphafold.com/>) (accessed on 25 June 2022) have the following Uniprot codes Q96IF1, P33681 and Q96J17, respectively [20,21].

2.10. Virtual Screening

To identify inhibitors of *AJUBA*, *CD80* and *NOLC1* proteins, a structure-based virtual screening (SBVS) analysis was performed on the Mcule online platform (<https://mcule.com/dashboard/>) (accessed on 10 August 2022). Mcule is a platform that provides information technology (IT) infrastructure containing drug discovery tools, a high-quality compound database, pharmacokinetic and toxicological prediction tools, and commercialization services for approximately 100+ million compounds [23,24].

On this platform, virtual screening workflows consisting of a set of filters and calculations can be created. Filters can remove compounds that are unlikely to bind to study targets or have undesirable properties. The calculations, in turn, rank the best candidates concerning the binding affinity between the protein and ligand complex. Additionally, it is possible to perform Hit Identification analyses, and then the Structure-Based Virtual Screen option was selected, generating the workflow. In the collection, Mcule Purchasable (Full) was selected, aiming to guarantee that the evaluated molecules would be available for commercialization. In the basic property filter, only the RO5 violation filter was changed, with an analysis performed with the maximum value of violations equal to 0 (RO5 violations 0) for each target. The other default settings preserved, such as sampling and diversity filters, were used to randomly select several different chemical structures with a maximum value of 10 rotating bonds, 5 chiral centers and 0 or 1 violation of Lipinski's rule of five.

Lipinski's rule of five allows a prediction of the oral bioavailability profile for new molecules. In this rule, it is established that for a compound to be a good drug candidate, it must present multiple values of 5 for the following 4 parameters: (1) log P greater than or equal to 5; (2) molecular mass less than or equal to 500; (3) number of hydrogen bond acceptors less than or equal to 10; (4) number of hydrogen bond donors less than or equal to 5. It is defined that a molecule may present only one violation of one of these parameters to be a promising drug candidate [25,26].

In summary, using the Mcule platform, it was possible to identify compounds that bind to the active or allosteric site of the targets under study, obtain results on the binding affinity of the protein–ligand complex (docking scores) and conduct an analysis of the toxicity of compounds from their chemical structure.

2.11. In Silico Toxicity Prediction

The top ten compounds with minimum target binding energy were selected in each virtual screening analysis performed in Mcule for the target proteins *AJUBA*, *CD80* and *NOLC1*. Toxicological parameters were estimated for these compounds using Mcule and ProTox-II.

On the Mcule platform, it is only possible to predict the toxicity of molecules contained in its compound database. This in silico prediction is based on the search for substructures commonly found in toxic and promiscuous ligands. This way, when a molecule is classified as toxic, the responsible fragment is flagged and identified [23]. All molecules analyzed in this tool were also evaluated in the ProTox-II server.

ProTox-II, freely available from https://tox-new.charite.de/protox_II/ (accessed on 4 September 2022), is a web server for in silico toxicity prediction incorporating molecular similarity, pharmacophores, fragment propensities and machine learning models for the prediction of toxicity endpoints, specifically acute toxicity, hepatotoxicity, cytotoxicity, carcinogenicity, mutagenicity, immunotoxicity, pathways of adverse outcomes (Tox21) and toxicity targets. It is worth mentioning that the predictive models of this server are built based on data from in vitro trials and in vivo cases [27].

For evaluating the toxicity profile in ProTox-II, the SMILE code was used as an input file for the construction of the two-dimensional chemical structure of the chemical products. Acute oral toxicity was determined using the toxicity class. Only compounds that showed prediction for toxicity class equal to or greater than IV and no prediction for toxicity endpoint models were selected for the next step.

2.12. Prediction of ADME Parameters

To evaluate pharmacokinetic parameters, the SwissADME tool was used. The SwissADME tool assesses the pharmacokinetics and structural similarity between molecules. This tool also allows for calculating physicochemical descriptors. It provides access to robust and fast predictive models for physicochemical properties, similarity to drugs and compatibility with medicinal chemistry [28,29].

2.13. Molecular Docking (MD) Assays

Only chemicals obtained after virtual screening that showed favorable toxicological properties (prediction for toxicity class equal to or greater than IV and no prediction for toxicity endpoint models) in the in silico toxicity prediction step were selected and virtually tested for potential binding against study targets using the DockThor server. This server presents a methodology using flexible ligands and rigid receptors through a genetic algorithm and the MMFF94s molecular force field to predict the score of each pose [30,31].

For each analysis, the 3D structure of the protein was loaded as a PDB file into the docking platform. In the protein preparation step, the internal program PdbThorBox automatically parameterizes the protein atoms according to the atomic type and partial charges of the MMFF94 force field, adding polar hydrogen atoms when necessary, reconstructing missing atoms from residual side chains and adjusting the protonation state. In the ligand preparation step, the internal MMFFLigand program parameterizes the atoms according to the atomic type and partial charges of the MMFF94s force field, adding polar hydrogen atoms if required by the user.

In the docking step, to find the protein cavities and the site of interaction between the molecules, blind docking was performed, with an option called Blind Docking. This option generates a grid box centered on the protein coordinate center with a size that covers the entire receptor. The prediction of affinity and total energy of the protein–ligand complexes was performed using the internal program DockTScore. At the end of the molecular docking assay, the final output compounds were ranked based on their minimum target binding energy. The PyMOL Molecular Graphics System (version 2.5.4, Schrödinger, LLC, San Diego, CA, USA) [22] and BIOVIA Discovery Studio Visualizer (version 21.1.0.20298)

tools were used to analyze the docking conformation of the protein–ligand complex and the types of connection involved.

2.14. Protein–Protein Interaction Network

To identify the protein interaction network of the *AJUBA*, *CD80* and *NOLC1* proteins, the STRING tool (version 11.5) was used. The STRING resource is available online at <https://string-db.org/> (accessed on 5 January 2023). The results obtained using this tool enabled the selection of protein complexes that later served as controls for the molecular docking (MD) assay.

2.15. Re-Docking

For the re-docking process, it was necessary, initially, to select a protein–protein complex from the interaction network provided by the STRING tool. Priority was given to choosing known complexes with comfort from curated databases and experimentally determined. Therefore, molecular docking experiments were performed using the ClusPro 2.0 server (<https://cluspro.org>) (accessed on 20 January 2023), the best-performing server currently available for the CAPRI challenge [32]. The GPU option was selected because it uses more specific computer graphics units from the Massachusetts Green High-Performance Computing Center (MGHPC). The best complexes generated by molecular docking studies were analyzed regarding interface energy and interaction between residues. This analysis sought to evaluate and understand how the proteins interact with each other, observing the predominant interaction pose and the minimum energy value.

2.16. Statistical Analysis

Data were shown as a mean \pm standard deviation (SD) and the groups were compared with each other by Analysis of Variance (ANOVA) followed by Bonferroni's posttest. Significant differences were considered with an interval of confidence of 95% ($p < 0.05$). GraphPad Prism 5.01 (San Francisco, CA, USA) software was used for data analysis and graph design.

3. Results

3.1. Differential Gene Expression in Gastric Tumor Meta-Dataset

We constructed a meta-dataset for transcriptome analysis to assess the gene expression profile of gastric cancer tissue versus normal gastric tissue. After batch correction among datasets (Figure 1A), the differentially expressed genes were demonstrated in a volcano plot, representing the significance of the adjusted p -value and fold change (Figure 1B). Thus, the top ten genes with the highest and lowest values of fold change (log), whose p -values were significant ($p < 0.05$), were organized, as shown in Table 1. The highest gene expression levels in the gastric tumor dataset were observed for *AJUBA* (1.44×10^{14}), *GPNMB* (1.11×10^{14}) and *CD80* (1.09×10^{14}). Otherwise, the lowest expression levels were observed for the *FBXL13* (-1.56×10^{14}), *PDILT* (-1.41×10^{14}) and *CCDC69* (-1.28×10^{14}) genes. Those up- and downregulated genes were chosen because our focus was to develop a methodology effective for identifying gene markers in GC development. If we compare control and cancer cells, the top three up- and downregulated genes were most associated with cancer development (upregulated genes) or not (downregulated genes) (Table 1). Therefore, it is feasible to think that the genes overexpressed in cancer cells are important for cancer development. Based on that, they are good targets for developing new target-directed drugs.

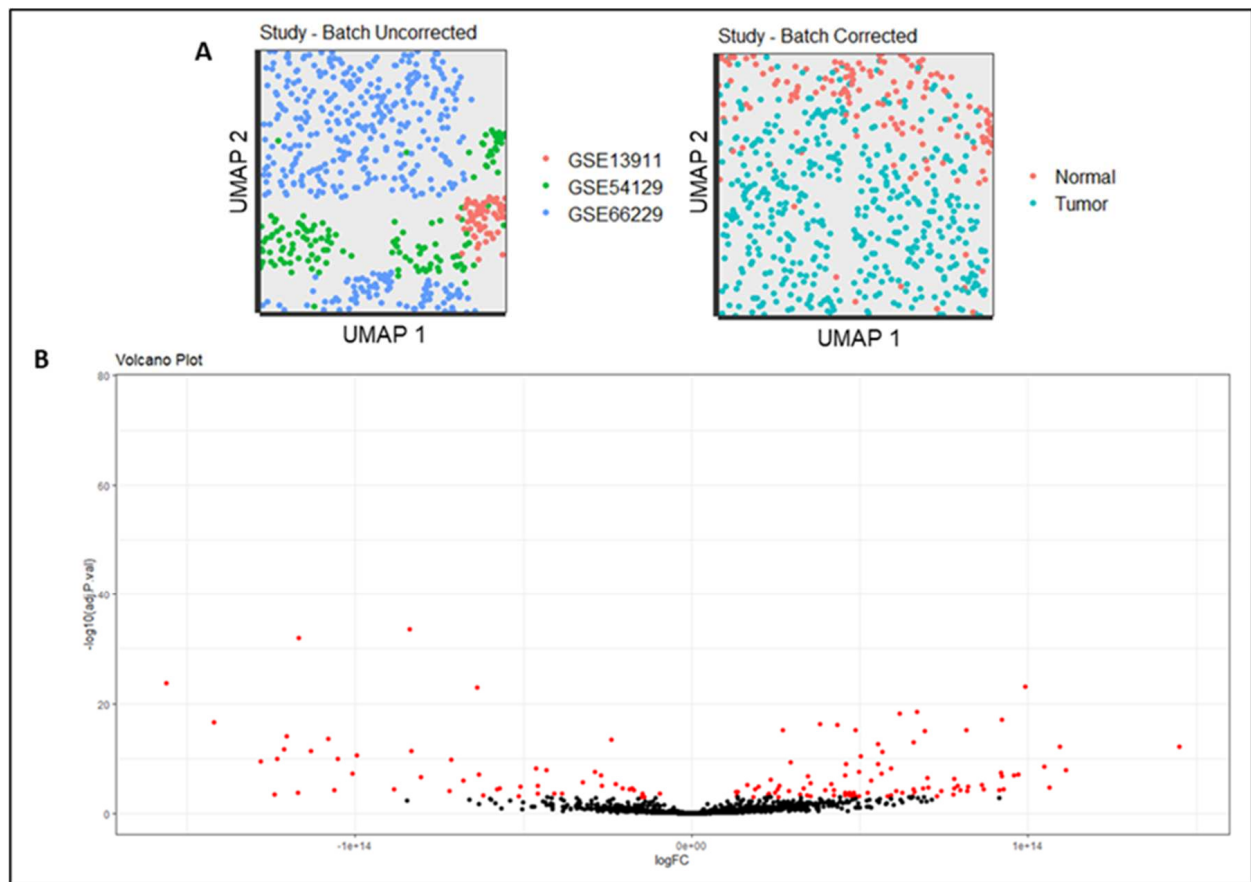


Figure 1. (A) Batch effect corrected among the studies. (B) Volcano plot of differentially expressed genes (DEGs) in gastric tumors. Red dots represent significant expressed genes.

Table 1. Top 10 up- and downregulated genes in gastric tumors.

Differentially Expressed Genes							
Upregulated				Downregulated			
Gene Symbol	LogFC	t	Adjusted <i>p</i> -Value	Gene Symbol	LogFC	t	Adjusted <i>p</i> -Value
<i>AJUBA</i>	1.44×10^{14}	7.80	7.78×10^{13}	<i>FBXL13</i>	-1.56×10^{14}	-11.18	2.01×10^{-24}
<i>GPNUMB</i>	1.11×10^{14}	6.20	1.53×10^8	<i>PDILT</i>	-1.14×10^{14}	-9.20	2.98×10^{-17}
<i>CD80</i>	1.09×10^{14}	7.84	5.74×10^{-13}	<i>CCDC69</i>	-1.28×10^{14}	-6.83	3.98×10^{-10}
<i>ANLN</i>	1.06×10^{14}	4.82	1.61×10^{-5}	<i>PDZK1IP1</i>	-1.24×10^{14}	-4.03	4.02×10^{-14}
<i>ADGRG7</i>	1.06×10^{14}	4.75	2.22×10^{-5}	<i>SCIN</i>	-1.23×10^{14}	-7.05	1.02×10^{-10}
<i>BICD1</i>	1.04×10^{14}	6.47	3.44×10^{-9}	<i>ITIH5</i>	-1.21×10^{14}	-7.66	1.98×10^{-12}
<i>KNL1</i>	9.91×10^{14}	11.01	8.37×10^{-5}	<i>NKX2-3</i>	-1.20×10^{14}	-8.46	7.58×10^{-15}
<i>ABCD3</i>	9.71×10^{13}	5.89	8.40×10^{-8}	<i>ITGB1</i>	-1.17×10^{14}	-4.27	1.59×10^{-4}
<i>CENPL</i>	9.54×10^{13}	5.85	1.03×10^{-7}	<i>SIGLEC11</i>	1.16×10^{14}	-13.16	1.33×10^{-32}
<i>PGTS2</i>	9.26×10^{14}	4.60	4.17×10^{-5}	<i>PTCHD1</i>	-1.13×10^{14}	-7.52	5.07×10^{-12}

Legend: LogFC: fold change in logarithmic scale; t: Student's *t*-statistic; P.Value: *p*-value; Adj.P.Val.: adjusted *p*-value.

3.2. Gastric Tumor Group Involved in Multiple Cancer Progression Pathways

In addition to the analysis with R Studio (Table 1), the GSEA platform was also used to determine gene enrichment in gastric tumor samples [14]. For this, the GSEA provided graphs with the specifications of the 18 main hallmarks in the tumor and normal samples. GSEA assessed the functional differences by comparing gastric tumors versus normal gastric tissue. For instance, gastric tumors were positively correlated with several cancer

hallmarks (Figure 2). The most enriched pathways were the G2M checkpoint (NES = 2.22, $p = 0.00001$), spermatogenesis (NES = 2.00, $p = 0.00001$) and E2F targets (NES = 2.05, $p = 0.00001$). Therefore, an intensive regulatory role was observed for the development and progression of gastric tumors, exhibiting significant changes in pathways.

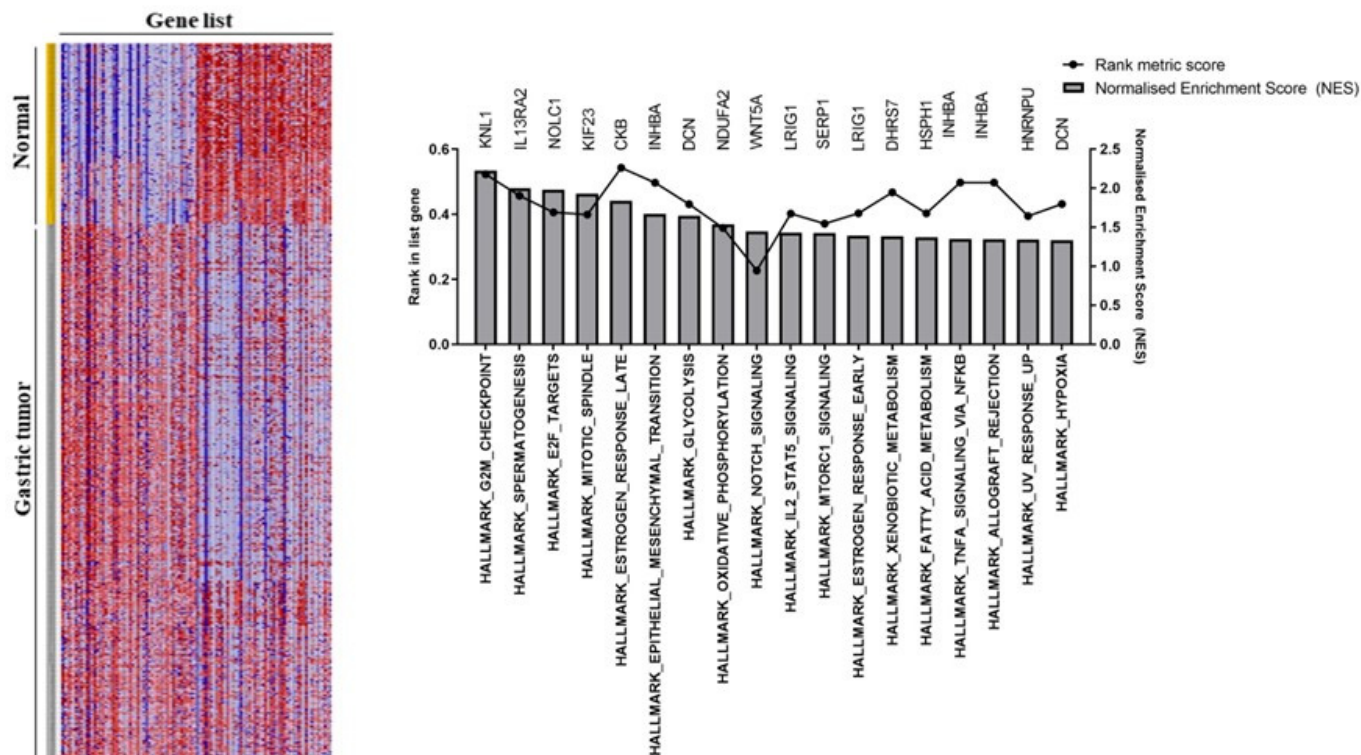


Figure 2. Differentially expressed genes were found using Gene Set Enrichment Analysis (GSEA).

3.3. Expression and Prognostic Value of Genes Involved in Gastric Cancer Progression

In the analysis of gene expression associated with prognosis, nine genes were selected. Three genes were overexpressed (*AJUBA*, *GPNMB* and *CD80*), three were underexpressed (*FBXL13*, *PDILT*, *CCDC69*) and three other genes were enriched (*KNL1*, *IL13RA* and *NOLC1*). Comparison between the mRNA expression levels of these genes in gastric cancer (identified as STAD) and in normal tissues revealed the following results with statistical significance ($p < 0.05$): overexpression of the *AJUBA*, *CD80*, *NOLC1* and *KNL1* genes and hypoexpression of the *CCDC69* gene in gastric cells (Figure 3). The results of the evaluation of whether the most relevant genes were associated with poor survival in gastric cancer patients are shown in Figure 4. Interestingly, the expression levels of seven genes were significantly correlated with the survival of patients with gastric cancer. Prognostic analysis using the Kaplan–Meier plotter revealed that the high expression of *AJUBA* (p -value = 6.1×10^{-6}), *CD80* (p -value = 1.1×10^{-8}), *CCDC69* (p -value = 3.3×10^{-3}), *KNL1* (p -value = 0.00034) and *NOLC1* (p -value = 6.9×10^{-3}) and the low expression of *GPNMB* (p -value = 0.0033) and *PDILT* (p -value = 0.031) were significantly correlated with poor prognosis in patients with gastric cancer. The overexpressed genes associated with a worse prognosis were selected for (1) the design of their primers and, subsequently, (2) undergoing polymerase chain reaction (PCR) for validation in a gastric cancer cell line model.

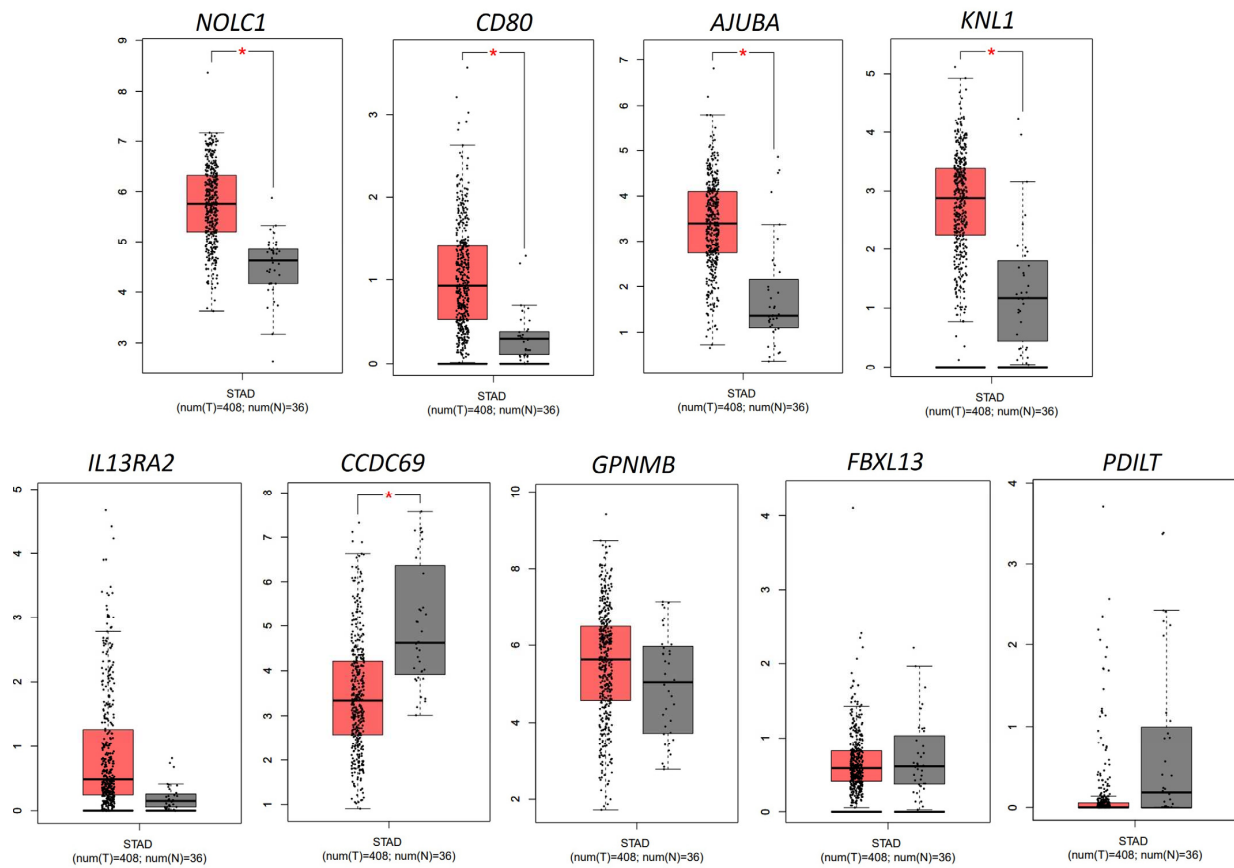


Figure 3. TCGA (RNA-seq) expression data for selected genes using Gene Expression Profiling Interactive Analysis (GEPIA). Bars indicate the difference between treatments. * $p < 0.01$ by one-way (ANOVA) followed by Bonferroni's test.

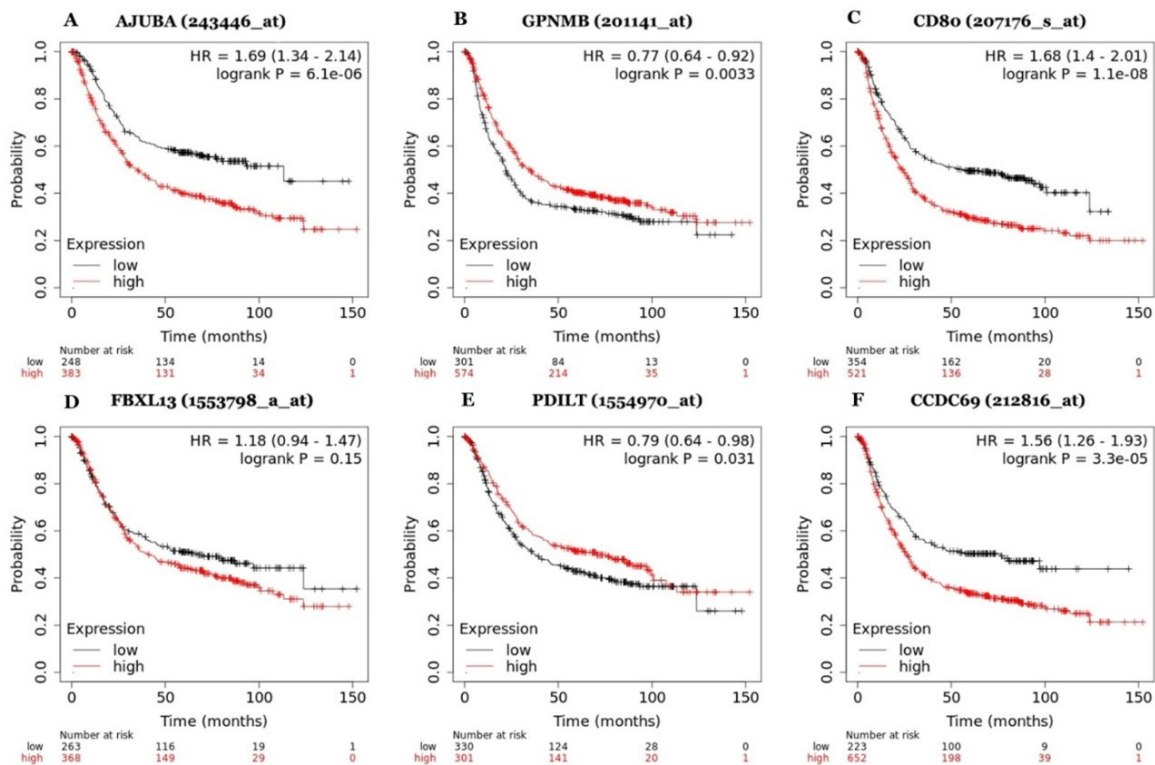


Figure 4. Cont.

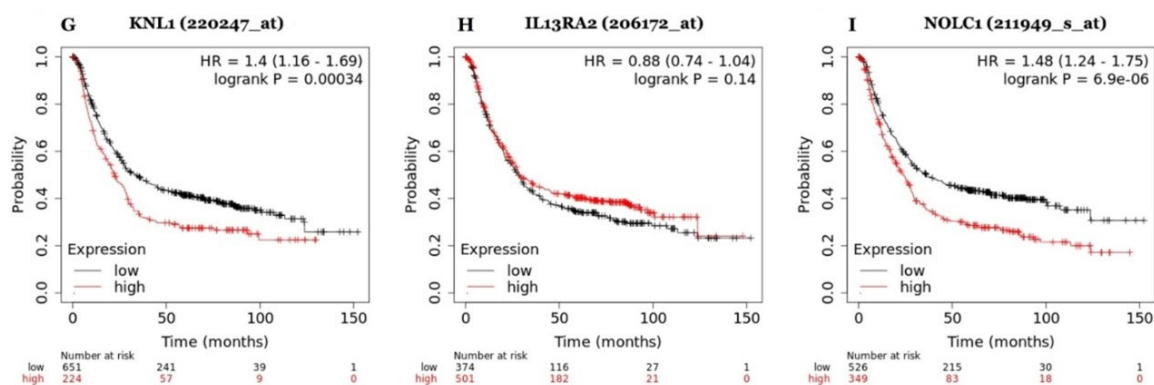


Figure 4. Survival analysis for the genes (A) *AJUBA*, (B) *GPNMB*, (C) *CD80*, (D) *FBXL13*, (E) *PDILT*, (F) *CCDC69*, (G) *KNL1*, (H) *IL13RA2* and (I) *NOLC1* using Kaplan–Meier plotter (KM plotter).

3.4. Validation of Relevant Genes in Gastric Tumor Cell Lines Compared to Normal Gastric Cell Lines

To validate and evaluate how these selected genes are expressed in gastric cancer in an in vitro model, we compared the relative gene expression levels of gastric cancer cell lines (ACP-02, ACP-03, AGP-01 and AGS) and a non-malignant gastric cell line (MNP-01). The results showed a significant reduction in *KNL1* gene expression in ACP-02 cells compared to MNP-01 (Figure 5A). In the case of ACP-03, *AJUBA*, *CD80*, *NOLC1* and *KNL1* were overexpressed when compared to MNP-01 (Figure 5B). For the AGP-01 cell line, *AJUBA* in AGP-01 presented an increased expression compared to MNP-01. In contrast, *KNL1* presented a reduced expression (Figure 5C). For the AGS cell line, *AJUBA* and *KNL1* genes presented higher expression compared to MNP-01 (Figure 5D).

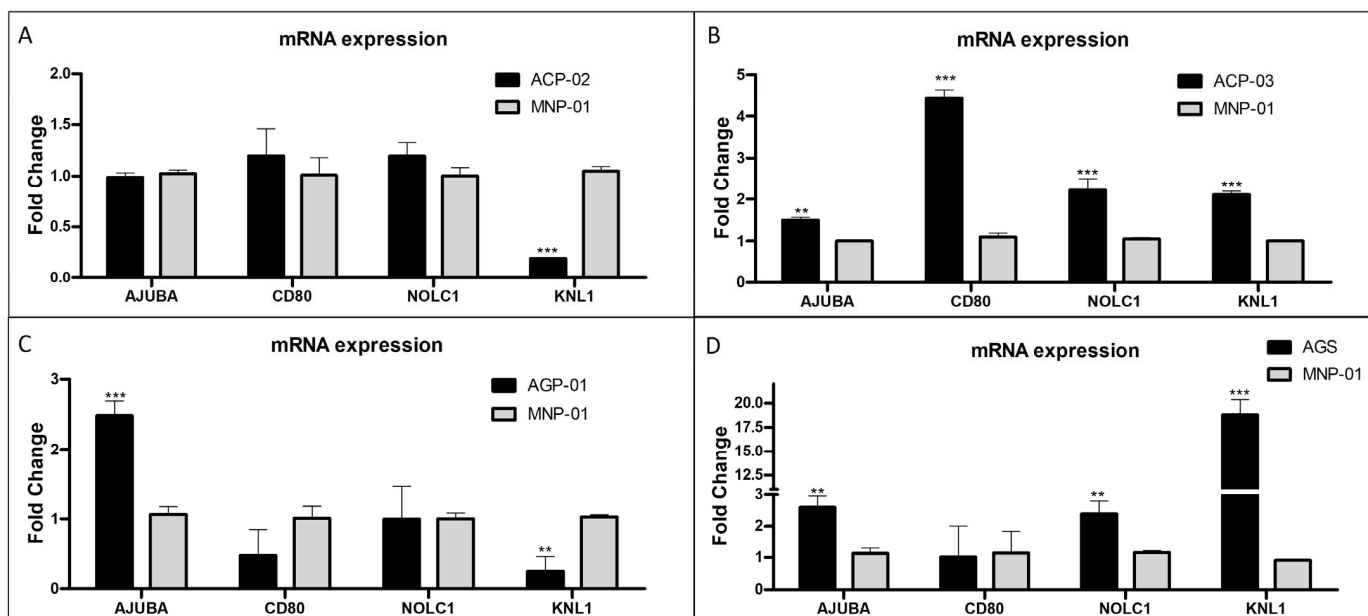


Figure 5. The relative expression level of *AJUBA*, *CD80*, *NOLC1* and *KNL1* genes in samples of gastric tumor cell lines (A) ACP-02, (B) ACP-03, (C) AGP-01 and (D) AGS is related to normal gastric cells, MNP-01. ** $p < 0.01$; *** $p < 0.001$ by one-way (ANOVA) followed by Bonferroni's test.

3.5. In Silico High-Throughput Virtual Screening

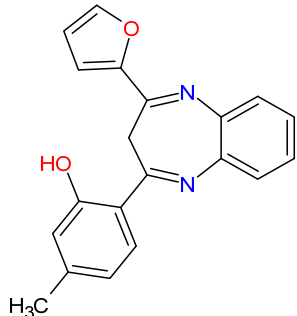
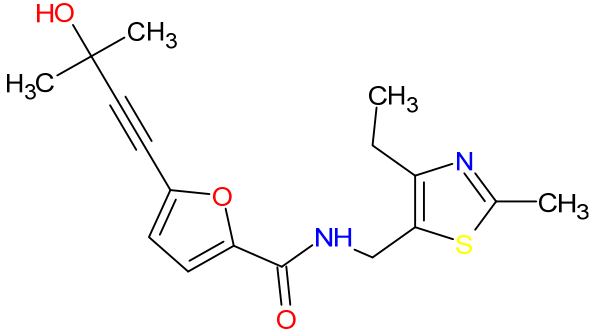
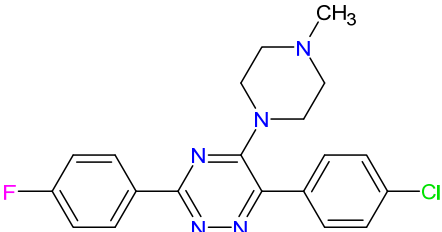
Using a structure-based approach to drug screening, an extensive collection of small molecules was investigated for their potential to interact with a designated target protein. In this investigation, a screening process involving 10,000 ligands from the MCULE library was conducted. The selection of target proteins was guided by overexpression data obtained

from gastric cancer cell lines, specifically focusing on genes such as *AJUBA*, *CD80* and *NOLC1*. The KNL1 protein was not selected for further analysis of SBVS because its mRNA expression by RT-qPCR showed upexpression in two lines of GC cells and downexpression in the other two lines of GC cells. Based on these controversial results, it was better to move forward only with three genes selected: *AJUBA*, *CD80* and *NOLC1*. Through virtual screening, the top 100 ligands were initially identified and subsequently refined to the top 10 based on VINA scores (Supplementary Tables S3–S5). These chosen ligands were further evaluated. The molecules found were suitable for subsequent analysis, considering their favorable interaction energies and toxicological characteristics.

3.6. Molecular Docking (MD) Validation

The in silico evaluation of the best hits at the end of each virtual screening, selecting a compound with the best prediction of pharmacological parameters for each protein target studied, was possible. The molecules were designated with Mcule IDs as MCULE-2386589557-0-6, MCULE-9178344200-0-1 and MCULE-5881513100-0-29. The best molecules were chosen based on (1) the best pose of interaction (a site important for protein activity), (2) the number of interactions, (3) the distance of bonds and (4) toxicity (Supplementary Tables S3–S5). The formula, chemical structure and molecular weight of these chosen compounds are shown in Table 2.

Table 2. The formulae for the three main compounds. Chemical structure and molecular weight were virtually tested against the protein targets *AJUBA*, *CD80* and *NOLC1*. ACD/ChemSketch (version 2020.2.1) was used to draw the 2D chemical structures of compounds.

Ligand ID	Target	Chemical Formula	Mol. Wt.	2D Structure
1. MCULE-2386589557-0-6	<i>AJUBA</i>	C ₂₀ H ₁₆ N ₂ O ₂	316.352	
2. MCULE-9178344200-0-1	<i>CD80</i>	C ₁₇ H ₂₀ N ₂ O ₃ S	332.419	
3. MCULE-5881513100-0-29	<i>NOLC1</i>	C ₂₀ H ₁₉ ClF ₂ N ₅	383.848	

Molecular docking analyses revealed that the compound MCULE-2386589557-0-6 presented a polar bond interaction with the Val⁴⁴³ and two pi-alkyl interactions with the Leu²³⁵ and Pro²³² residues of *AJUBA* (Figure 6A). MCULE-9178344200-0-1 formed two polar bonds with the Glu¹⁷⁷ and Asp²⁰⁵ residues, one Alkyl with Ile¹⁸⁵ and one pi-alkyl Leu¹⁸² with the *CD80* protein (Figure 6B). Regarding the compound MCULE-5881513100-0-29 and the *NOLC1* protein, a polar interaction with Arg³⁹⁰ and a pi-cation interaction with the residue Lys387 (Figure 6C) were identified.

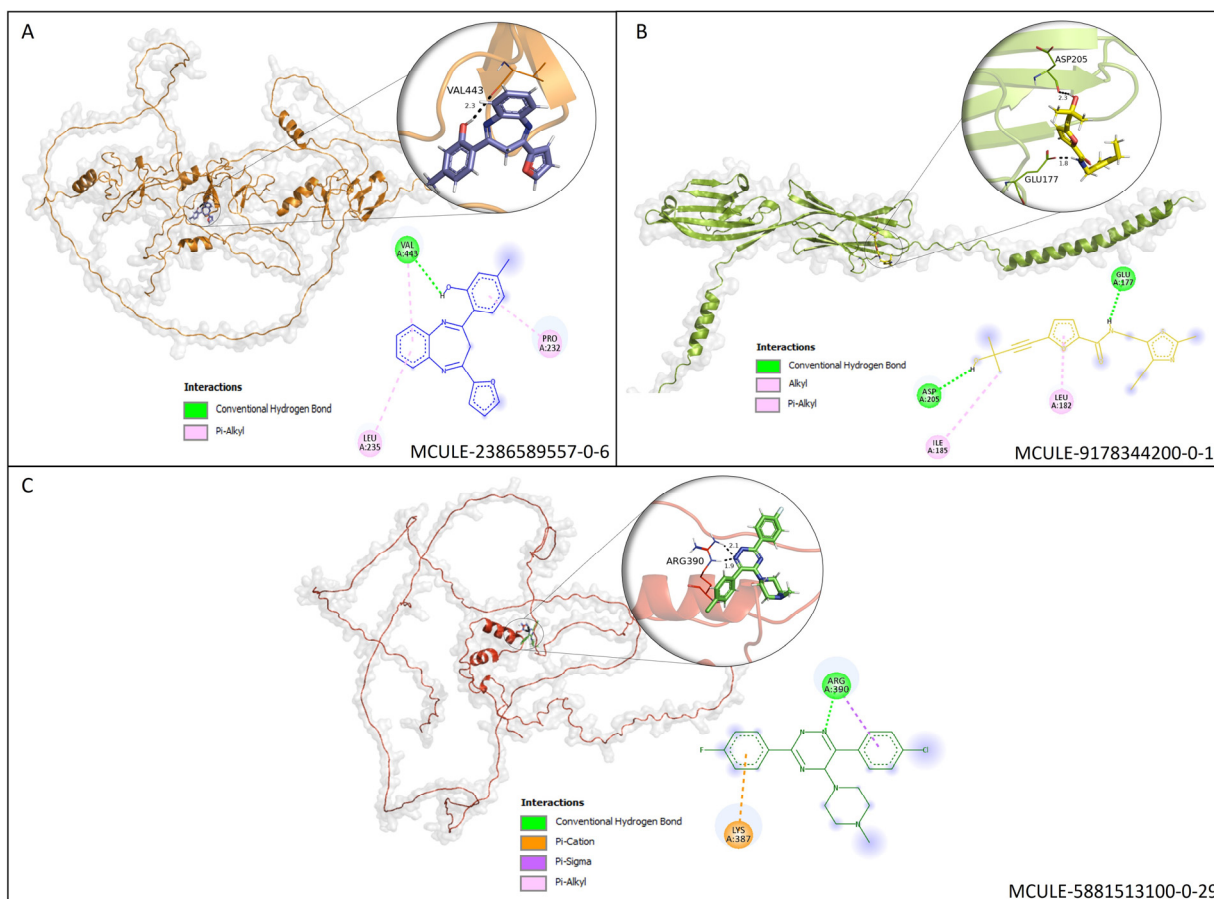


Figure 6. (A) Molecular docking analysis of the *AJUBA* protein and molecule MCULE-2386589557-0-6. (B) Molecular docking analysis of the *CD80* protein and molecule MCULE-9178344200-0-1. (C) Molecular docking analysis of the *NOLC1* protein and molecule MCULE-5881513100-0-29. Figure 6 shows the 2D and 3D analysis of the interaction. In the 3D representation, the three compounds are in stick format; proteins are represented in cartoon format, while the residues involved in hydrogen bonding are shown in line format. Black dotted lines represent hydrogen bonds; the bond length is expressed in the Angstrom (\AA) measurement unit. The 2D diagram shows the amino acid residues involved in the interactions between *AJUBA*, *CD80* and *NOLC1* proteins and the selected MCULE compound for each protein. The present type of interaction is represented by colors, which are identified by the legend in the figure.

Concerning docking scores for the best poses, Table 3 shows the minimum binding energy for each receptor–ligand complex evaluated and the prediction of the toxicity parameters LD50 value and acute oral toxicity, determined by the middle of the toxicity class. All three selected compounds show a prediction for toxicity class equal to or greater than IV and no prediction for toxicity endpoint models. It is essential to consider that on the toxicity scale, class I represents the compounds most likely to manifest acute oral toxicity, and class VI represents the compounds with higher safety scores.

Table 3. Result of docking scores. Using DockThor and Mcule toxicity analysis. Using the ProTox-II tool.

Protein–Ligand Complex		Docking Score		Predicted Toxicity	
Ligand ID	Target	DockThor	Mcule	LD50	Class
MCULE-2386589557-0-6	AJUBA	−8.4	−7.3	2500 mg/kg	V
MCULE-9178344200-0-1	CD80	−7.7	−5.6	600 mg/kg	IV
MCULE-5881513100-0-29	NOLC1	−7.2	−7.5	640 mg/kg	IV

3.7. In Silico Pharmacokinetics Prediction

Table 4 indicates the results related to the ADME in silico parameters of the three selected compounds: (1) MCULE-2386589557-0-6, (2) MCULE-9178344200-0-1 and (3) MCULE-5881513100-0-29. Pharmacokinetic data were obtained from the SwissADME platform and included information on molecular weight (PM), topological polar surface area (TPSA), lipophilicity coefficient (cLogP), solubility in aqueous media (LogS), gastrointestinal absorption (AGi), penetration of the blood–brain barrier (BBB) and data on P-glycoprotein (P-Gp) substrates.

Table 4. In silico prediction of ADME properties of compounds (1) MCULE-2386589557-0-6, (2) MCULE-9178344200-0-1 and (3) MCULE-5881513100-0-29 estimated by SwissADME.

ADME Property	(1)	(2)	(3)
Molecular weight	316.35	332.42	383.85
TPSA	58.09	103.60	45.15
cLogP	3.81	2.73	3.72
LogS	−4.75	−3.49	−4.73
GI absorption	High	High	High
BBB permeant	Yes	No	Yes
P-gp substrate	No	No	Yes

As shown in Table 4, the compound with the highest coefficient of lipophilicity is MCULE-2386589557-0-6 (cLogP = 3.81). Consequently, this compound has a lower solubility value in aqueous media (LogS = −4.75). All analyzed compounds presented satisfactory TPSA. This parameter is used in medicinal chemistry to describe the ability of a molecule to permeate cells and physiological barriers [29]. This data comprise the basis for discussing possible pharmacokinetic properties and the analysis of experimental assays since drug transport is required to reach the site of pharmacological action.

All compounds analyzed showed high absorption via the gastrointestinal tract (Table 4). Regarding penetration through the blood–brain barrier, only compounds (1) MCULE-2386589557-0-6 and (3) MCULE-5881513100-0-29 showed permeability capacity. The compound (3) MCULE-5881513100-0-29 was classified as a P-glycoprotein (P-Gp) substrate. Expressed in cell membranes, P-Gp acts as an efflux pump of some substances, especially xenobiotics, from the interior of cells.

3.8. Protein–Protein Interaction Network

By analyzing the network of protein–protein interactions (PPIs), it was possible to evaluate the pathways of our targets (Figure 7); somehow, the molecules chosen to interfere with those pathways (Figure 8). The analysis performed on the STRING database (Figure 7) revealed that AJUBA, CD80 and NOLC1 are involved in a complex pathway with many other proteins. Based on those analyses, one protein for each target was selected following the score provided by STRING to perform a re-docking analysis to assess our molecules' interference in PPI interaction molecules. For AJUBA (Figure 8, Panel 1), the protein selected was CTNBN1; for CD80 (Figure 8, Panel 1), the protein selected was CTLA4; and for NOLC1 (Figure 8, Panel 1), the protein selected was NHP2. In the re-docking analysis, the control was the interaction between the proteins without our molecules (Figure 8, Panel 2). After the re-docking analysis of our targets complexed with each proposed molecule and the

proteins selected, it was clear that interaction happens in a different site compared to the control (Figure 8, Panel 3). These results strongly suggest that the PPI is affected by the presence of molecules selected, which could indicate an interference in the pathway.

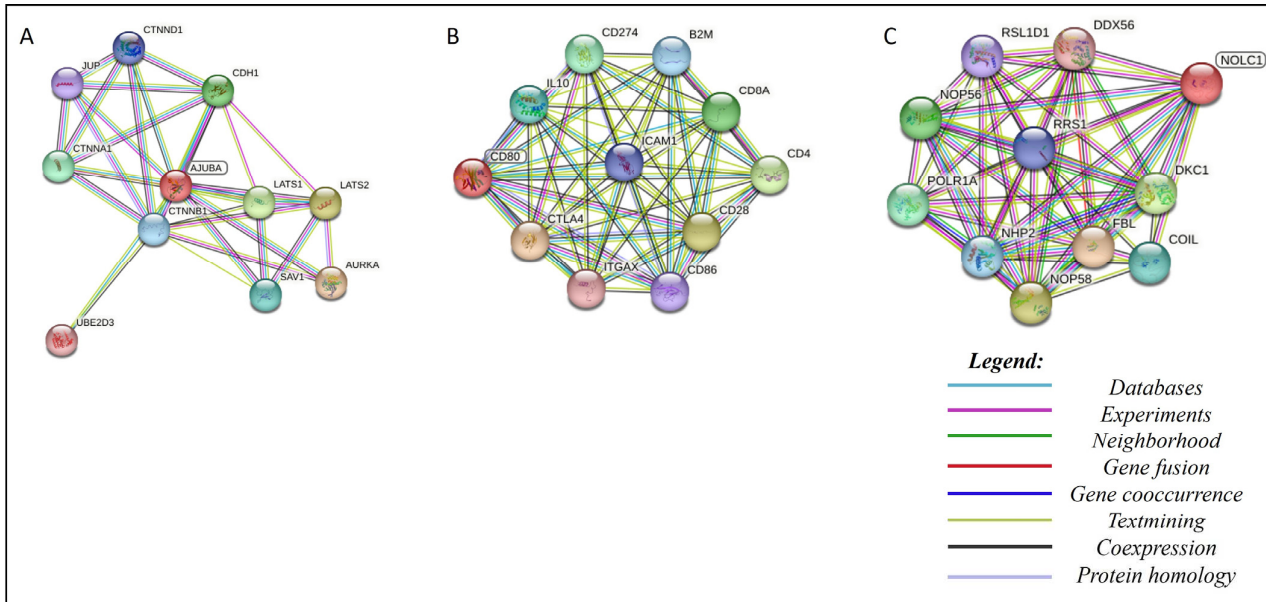


Figure 7. Graphic representation of the network of protein interactions for proteins (A) *AJUBA*, (B) *CD80* and (C) *NOLC1*, identified using STRING v11.5. Each node represents a protein, and each edge represents an interaction. Colored lines between the proteins indicate the various types of interaction evidence.

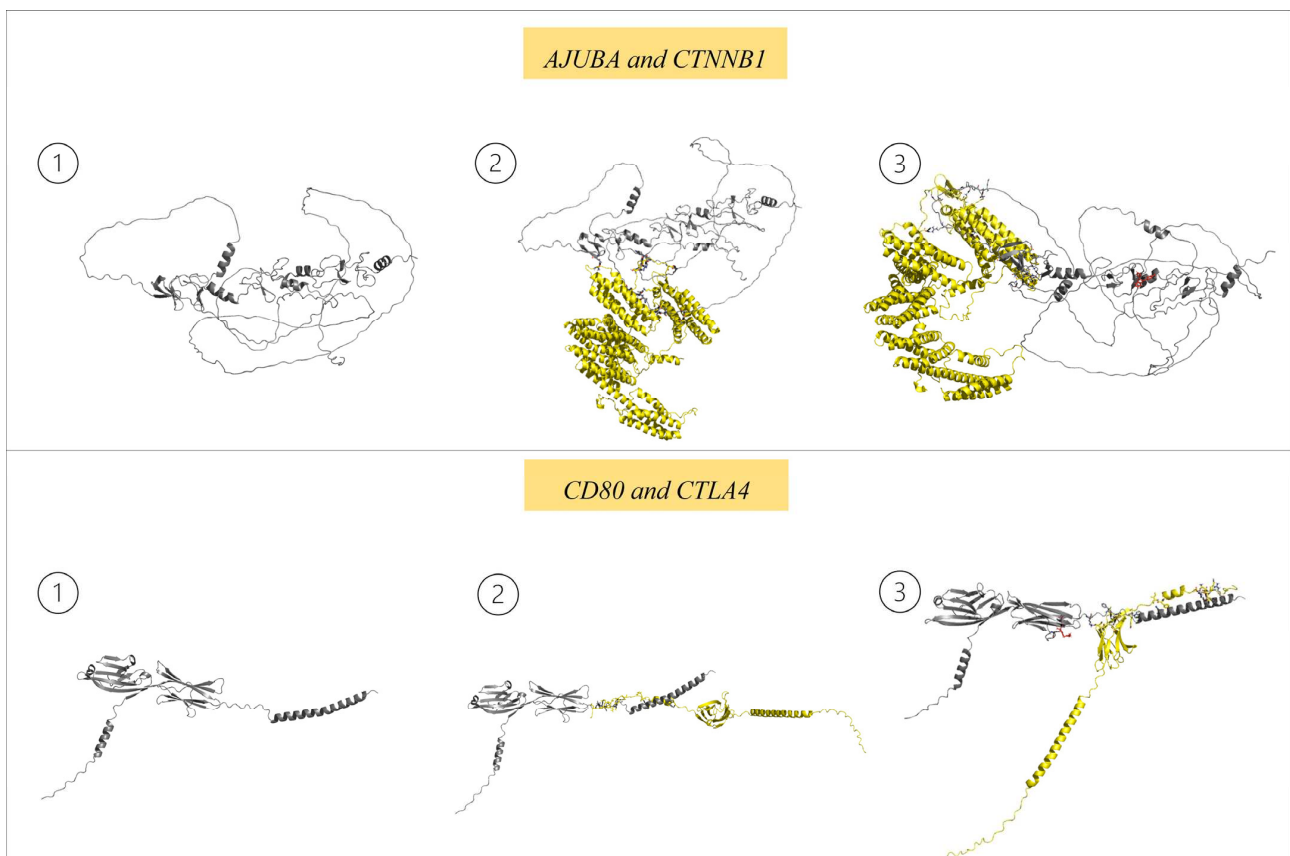


Figure 8. Cont.

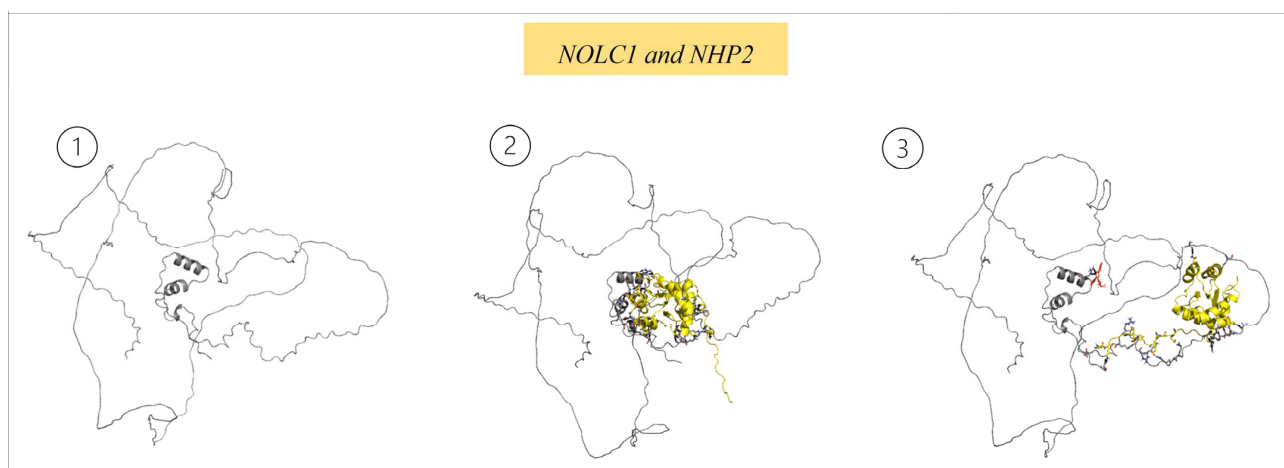


Figure 8. ① Protein; ② interaction between the targeted protein and the protein in the respective pathway selected on STRING; ③ analysis of complex formed by the molecule and targeted protein with the protein in the respective pathway.

4. Discussion

Despite advances in science and the various therapeutic options currently available for controlling gastric cancer, the prognosis of patients affected by it remains unfavorable. In this context, chemotherapy resistance and the serious adverse effects of conventional pharmacological treatments represent a major obstacle to the successful treatment of gastric cancer.

Drug resistance is a phenomenon that results from a variety of pharmacokinetic and molecular changes. It refers to the ability of microorganisms or cancer cells to resist the effects of a normally effective drug against them. Although many types of cancer are initially susceptible to chemotherapy, with prolonged use, the development of resistance to chemotherapy drugs is observed through different mechanisms, such as inactivation or reduction in drug activation; changing drug targets; drug efflux; DNA damage, repair and metabolic changes; inhibition of cell death; epithelial–mesenchymal transition and metastasis; heterogeneity of cancer cells; and epigenetic modifications, with the possibility of combining any of these mechanisms [33].

As a new type of approach, targeted therapies play an important role in the treatment of gastric cancer by interfering with gene expression or target proteins that play or regulate critical roles in tumor growth or progression, providing the new generation of chemotherapy drugs for the treatment of cancer with greater selectivity and efficacy and reduced toxicity [34]. Genomic and genetic studies provide valuable information about genomic changes in tumor samples compared to normal tissue samples. These studies provide important tools for understanding key information about tumor initiation, progression and metastasis [35]. As shown in the present study, evaluating the transcriptional profile in gastric tumor samples is a strong strategy for identifying new molecular targets.

In searching for drug targets and discovering new drug candidates, computer-aided drug design (CADD) methodologies stand out as a powerful and promising technology for faster, cheaper and more effective drug design in drug research [36]. Furthermore, they provide an absolute starting point for drug target discovery. Faced with the high cost and time required for research and development of drugs in the oncology area, computational models represent an efficient alternative since they are capable of predicting physical–chemical, pharmacokinetic, pharmacodynamic and toxicological parameters from a given molecular structure, as well as optimizing the *in vitro* test step [36].

The results obtained so far in obtaining new drugs through *in silico* studies are well known. For example, there is the development of the drug captopril, the first angiotensin-converting enzyme (ACE) inhibitor and one of the first successful drugs produced using computational tools to optimize drug planning in the 1980s [37]. Following this study,

structure-based drug development exhibited a significant impact on drug design with an increasing number of applications, and a rapid growth of computational tools for drug discovery, including anticancer therapies, was observed.

Structure-based virtual screening (SBVS) is a robust technique that allows rapid identification of biologically active compounds, providing an efficient and cost-effective alternative to high-throughput experimental screenings. This technique allows the prediction of the best mode of interaction between two molecules to form a stable complex. It uses scoring functions to estimate the strength of a non-covalent interaction between a ligand and molecular target. Different successful examples of SBVS applications are reported in the literature, evidencing the versatility, high performance and great utility of SBVS in drug discovery programs. In this study, the SBVS technique enabled the identification of synthetic molecules with great potential to inhibit target proteins relevant to carcinogenesis and the establishment of gastric cancer. The ligands with the best classification, considering the minimum energy of binding to the target, had their ADMET properties evaluated and underwent a molecular docking validation protocol.

Analyzing ADMET properties is an important step in drug design development. ADMET refers to the processes of absorption (A), distribution (D), metabolism (M), excretion (E) and toxicity (T) still in the early stages of the drug discovery process. This step drastically reduces the fraction of failure related to pharmacokinetics in the clinical phases and the toxic effects associated with drugs [28].

Faced with the need to develop new therapeutic options to improve the effectiveness of gastric cancer treatment and patient survival statistics, targeted therapies stand out as instruments with great potential for therapeutic success. In this context, the present study points to the *AJUBA*, *CD80* and *NOLC1* proteins as potential candidates for targeted therapy in the treatment of GC.

The *AJUBA* protein has been implicated in the development of several human cancers. It is known that this protein participates in the assembly of countless protein complexes and is involved in several cellular biological processes, such as the repression of gene transcription, cell–cell adhesion, mitosis, differentiation, proliferation and cell migration [38]. Previous studies have shown that the *AJUBA* protein promotes colorectal cancer cell growth by suppressing the JAK1/STAT1/IFIT2 network and activating N-cadherin expression through interaction with Twist in colorectal cancer cells [39,40]. However, its expression pattern and biological significance in gastric cancer are still not fully elucidated.

In the present study, analysis of the microarray metadata revealed that *AJUBA* gene expression was higher in gastric cancer samples than in normal tissues. By comparing the relative expression levels of this gene in samples of gastric tumor cell lines (ACP-02, ACP-03, AGP-01 and AGS) and normal gastric cells (MNP-01) using qRT-PCR, the results confirmed a significant increase in the *AJUBA* gene expression level in AGP-01 and AGS cell lines. Data from the survival analysis obtained using the Kaplan–Meier plotter database revealed that the increase in *AJUBA* expression is closely associated with a reduction in the overall survival rates of patients affected by GC.

Dommann et al. [41] developed a study that analyzed the transcriptome of SW480 human colon cancer cell lines by RNA sequencing and confirmed the sequencing data with biological assays. In this analysis, it was possible to conclude that cells devoid of *AJUBA* were less proliferative, more sensitive to irradiation, migrated less and were less efficient in forming colonies. Furthermore, loss of *AJUBA* expression decreased tumor burden in a murine model of colorectal metastasis to the liver [41].

From these data, it is assumed that the inhibition of the *AJUBA* protein in patients with gastric cancer can reproduce the phenomena observed in the work of Dommann et al. [41]. Thus, compounds that inhibit this target may represent a new therapeutic alternative for GC.

CD80 plays an important role in T-cell activation, exerting a dual effect on tumor immunity: it binds to CD28 to provide a costimulatory signal for T-cell activation, and it binds to CTLA-4, resulting in an immunosuppressive effect. It is understood that the

binding of *CD80* with CTLA-4, a receptor that acts as an important negative regulator of T-cell responses, is favorable for carcinogenesis because cancer cells commonly use the immunosuppressive function of regulatory T cells to avoid immunological attacks [42–44].

Based on this understanding, a monoclonal antibody against CTLA-4 (ipilimumab) was approved by the Food and Drug Administration (FDA) for the treatment of melanoma [45]. Ipilimumab blocks the co-inhibitory signal induced by CTLA-4 binding with *CD80* to enable CTL-mediated antitumor immunity [44].

Considering the positive results of blockade of the co-inhibitory signal induced by the binding of CTLA-4 with *CD80* for patients with melanoma, it is believed that it is important to obtain a greater understanding of expression data and the function of *CD80* in gastric cancer, as well as to characterize the existing molecular interaction between the CTLA-4 and *CD80* proteins.

The analysis of the protein interaction network developed in the present study using the STRING v11.5 tool made it possible to evaluate the protein–protein interaction network. Among the results of our study, it was revealed through a molecular docking assay that the molecular binding between the CTLA-4 and *CD80* proteins is altered after the anchoring of the MCULE-9178344200-0-1 compound to the *CD80* protein (Figure 6). Alteration of the molecular binding between the two proteins may result in the functional change of this interaction and, consequently, promote the blockade of the co-inhibitory signal induced by the binding of CTLA-4 with *CD80*.

Concerning *CD80* expression and function data in gastric cancer, the results of our study revealed an increase in the expression level of the *CD80* gene in samples of gastric cancer tumors compared to normal tissues in the microarray metadata analysis, as well as in real-time PCR detection, which revealed a significant increase in the expression level of the *CD80* gene in the ACP-03 cell line. Survival analysis data obtained using the Kaplan–Meier plotter database revealed that increased *CD80* expression is associated with reduced overall survival rates of patients affected by GC. These results show the protein and the *CD80* gene as potential successful therapeutic targets for the control of GC.

On the other hand, in a study by Feng et al. [44], the determination of *CD80* mRNA levels in gastric adenocarcinoma tissues and adjacent normal tissues by RT-qPCR was performed. As a result, it was seen that *CD80* is downregulated in gastric cancer tissues in 15 out of 20 patients compared to normal gastric tissue. Specifically, 70% of gastric tumor tissues demonstrated reduced *CD80* expression [44]. Thus, it is important to consider that the *CD80* gene is differentially expressed in gastric adenocarcinoma cell lines.

The nucleolar and coiled-body phosphoprotein 1 (*NOLC1*) protein is responsible for various cellular life activities, including ribosome biosynthesis, DNA replication, transcription regulation, RNA processing, cell cycle regulation, apoptosis and cell regeneration [46]. Our results demonstrated that gene expression was higher in samples of gastric cancer tumors than in normal tissues (Figure 2), which was confirmed by RT-qPCR for the GC cell lines ACP-03 and AGS (Figure 4). Data obtained using the Kaplan–Meier plotter database revealed that patients affected by GC with overexpression of *NOLC1* have shorter overall survival than those with low expression of *NOLC1* (Figure 3). Additionally, the gene enrichment analysis suggests the participation of the *NOLC1* gene as an important regulator for the development and progression of gastric tumors.

In a study carried out by Kong et al. [47], the role of *NOLC1* in esophageal cancer (ESCA) was determined, and its gene expression in ESCA tissues and cell lines was evaluated by qRT-PCR, immunohistochemistry or Western blotting. Among the results, overexpression of *NOLC1* was observed in ESCA tissues and ESCA cell lines (EC9706, Eca109, TE-13, Kyse170, T.TN) compared to adjacent normal tissues and normal esophageal cell lines. *NOLC1* overexpression was markedly associated with larger tumor size, lymph node metastases and advanced TNM stage.

The results of the correlation between *NOLC1* gene expression and overall survival using Kaplan–Meier plotter for patients with esophageal cancer coincided with the data obtained for patients with gastric cancer, evaluated in our study. So, *NOLC1* overexpression

was also associated with reduced overall survival rates for patients with ESCA. *NOLC1* knockdown, in turn, inhibited proliferation, migration, invasion and cyclin B1 expression and promoted apoptosis and cleaved-caspase-3 expression of two ESCA cell lines [47]. The in-depth study of data on *NOLC1* gene expression and its role in carcinogenesis shows that the protein encoded by this gene is a promising therapeutic target.

Cell life is a result of the interaction and coordinated activity of many proteins working at the same time. Different proteins from different pathways work together to provide a meaningful biological process essential to cell development [47–49]. In cancer, protein–protein interaction is essential to form complexes, allowing uncontrolled cellular division, development, growth and tumor promotion. Recently, cancer, neurodegenerative diseases and even infections have been determined to be a result of aberrant protein–protein interactions [49]. In cancer, aberrant proteins interact with other proteins, establishing the initial stages of cancer [48,49]. Based on that, protein–protein interaction analysis has become an alternative target for developing new anticancer compounds [48]. Based on that, a protein–protein interaction analysis of the targets used in this study was performed (Figure 6). The protein–protein interaction analysis revealed that all targets involved in this work are pivotal in their pathways.

For example, the *AJUBA* protein revealed an interaction with the proteins CTNNB1 and β -catenin (Figure 6A). CTNNB1 regulates cellular adhesion and gene transcription during mitotic fuse establishment [50]. The β -catenin protein is a component of the centrosome during the interphase [50]. Bahmanyar et al. [50] suggested that aberrant interactions between the *AJUBA* protein and CTNNB1 and β -catenin lead to uncontrolled cellular division and, thus, cancer development. Our results revealed that the molecule MCULE-2386589557-0-6 interacts with *AJUBA*, leading to a misplaced interaction between *AJUBA* and CTNNB1, interfering in this pathway and probably preventing its role in cancer establishment.

It is important to notice that although our analysis has provided a pipeline to find potential genes that could be used as targets for new anticancer molecules, it is relevant to look to the other side. Our pipeline also provides an analysis of the genes that could be selected as biomarkers of GC prognosis (Figure 4). Despite being either upregulated or downregulated in GC cell lines, genes such as *AJUBA*, *GPNMB*, *CD80*, *PDILT*, *CCDC69*, *KNL1* and *NOLC1* were shown by our results as indicative of a low survival rate for patients (Figure 4). The data revealed that our pipeline has the potential to be employed in both types of studies related to cancer.

5. Conclusions

Although tumor markers for different types of cancer have been rapidly discovered in recent years, there is still a lack of specific and sensitive tumor markers for GC management. Combining a systematic collection of public microarray data with a comparative meta-profile approach provided a suitable platform for identifying tumor markers. This activation of pathways shows that these genes are important in carcinogenesis and are probably the result of the convergence of several transforming processes in various cellular contexts. Furthermore, the significant differential expression of these genes implies that they may be useful as therapeutic targets and biomarkers.

Targeted therapies stand out as instruments with great potential for therapeutic success. Our results point to the *AJUBA*, *CD80* and *NOLC1* proteins as candidates for targeted therapy in treating GC. Using a virtual screening approach, a molecular docking study was performed for proteins encoded by genes that play important roles in cellular functions for carcinogenesis.

This study contributed to identifying three compounds with favorable pharmacokinetic, pharmacodynamic and toxicological properties that showed promising results in the molecular docking assay against protein targets, providing information that may help these compounds become potential chemotherapeutics in the clinical therapy of GC. Ad-

ditional in vivo or in vitro studies may be required to confirm the anticancer activity of these compounds.

Supplementary Materials: The following supporting information can be downloaded at: <https://www.mdpi.com/article/10.3390/pharmaceutics15092303/s1>, Table S1: List of studies for the construction of the meta-data; Table S2: List of RNAm, NCBI Reference Sequences and Primer sequences (forward and reverse complement) for the PCR. Table S3: List of top 10 ligands identified by screening MCULE's purchasable library using AutoDock Vina for the *AJUBA* target, organized in descending order of minimum energy value. Results obtained for prediction of toxicity class, toxicity endpoint models, docking score by DockThor server and final punctuation. Table S4: List of top 10 ligands identified by screening MCULE's purchasable library using AutoDock Vina for the *CD80* target, organized in descending order of minimum energy value. Results obtained for prediction of toxicity class, toxicity endpoint models, docking score by DockThor server and final punctuation. Table S5: List of top 10 ligands identified by screening MCULE's purchasable library using AutoDock Vina for the *NOLC1* target, organized in descending order of minimum energy value. Results obtained for prediction of toxicity class, toxicity endpoint models, docking score by DockThor server and final punctuation. Figure S1: Enrichment plots of genes were analyzed using Gene Set Enrichment Analysis (GSEA).

Author Contributions: All authors made substantial contributions. The conception and design of the study and acquisition of data, analysis, and interpretation were performed by D.M.S.B., O.G.L., F.P.M., E.L.d.S., M.E.A.d.M., R.M.R.B., R.C.M. and P.F.N.S. R analysis was carried out by D.M.S.B., O.G.L., F.P.M. and P.F.N.S. In vitro analysis was carried out by E.L.d.S., M.E.A.d.M., R.M.R.B. and R.C.M. Writing or revising the article was done by D.M.S.B., F.P.M. and P.F.N.S. Final approval and submission P.F.N.S. All authors have read and agreed to the published version of the manuscript.

Funding: This work was supported by the National Council for Scientific and Technological Development (CNPq) with a research grant to Rommel Mario Rodrigues Burbano (403493/2021-8) and research productivity grants to Raquel Carvalho Montenegro (305459/2019-8) and Pedro Filho Noronha Souza (305003/2022-4). Felipe Pantoja Mesquita thanks CNPq for the provision of a post-doctoral grant (PDJ program, number 151388/2022-9). Raquel Carvalho Montenegro also thanks Red Latinoamericana de Implementación y Validación de guías clínicas Farmacogenómicas (RELI-VAF) for supporting this work. The APC was funded by Pró-Reitoria de Pesquisa e Pós-Graduação (PROPESP) from the Federal University of Pará (UFPA). We also thank the Office of Coordination for the Improvement of Higher Education Personnel (CAPES).

Institutional Review Board Statement: Not applicable.

Informed Consent Statement: Not applicable.

Data Availability Statement: Data are available under reasonable requirements.

Acknowledgments: The authors thank the Brazilian Agencies CNPq, CAPES, FUNCAP and the Federal University of Ceara for fellowships and financial support. The authors thank the multiuser unit of the Drug Research and Development Center (NPDM) of the Federal University of Ceara for technical support.

Conflicts of Interest: The authors declare no conflict of interest.

References

1. Smyth, E.C.; Nilsson, M.; Grabsch, H.I.; van Grieken, N.C.; Lordick, F. Gastric Cancer. *Lancet* **2020**, *396*, 635–648. [[CrossRef](#)] [[PubMed](#)]
2. Sung, H.; Ferlay, J.; Siegel, R.L.; Laversanne, M.; Soerjomataram, I.; Jemal, A.; Bray, F. Global Cancer Statistics 2020: GLOBOCAN Estimates of Incidence and Mortality Worldwide for 36 Cancers in 185 Countries. *CA Cancer J. Clin.* **2021**, *71*, 209–249. [[CrossRef](#)] [[PubMed](#)]
3. Liu, Y.; Ao, X.; Wang, Y.; Li, X.; Wang, J. Long Non-Coding RNA in Gastric Cancer: Mechanisms and Clinical Implications for Drug Resistance. *Front. Oncol.* **2022**, *12*, 841411. [[CrossRef](#)] [[PubMed](#)]
4. *INCA Estimativa 2023: Incidência de Câncer No Brasil*; Instituto Nacional de Câncer: Brasília, Brazil, 2022; ISBN 9786588517093.
5. Lauren, P. The two histological main types of gastric carcinoma: Diffuse and so-called intestinal-type carcinoma. an attempt at a histo-clinical classification. *Acta Pathol. Microbiol. Scand.* **1965**, *64*, 31–49. [[CrossRef](#)] [[PubMed](#)]

6. Sasako, M.; Sakuramoto, S.; Katai, H.; Kinoshita, T.; Furukawa, H.; Yamaguchi, T.; Nashimoto, A.; Fujii, M.; Nakajima, T.; Ohashi, Y. Five-Year Outcomes of a Randomized Phase III Trial Comparing Adjuvant Chemotherapy with S-1 versus Surgery Alone in Stage II or III Gastric Cancer. *J. Clin. Oncol.* **2011**, *29*, 4387–4393. [[CrossRef](#)]
7. Leichman, L.; Silberman, H.; Leichman, C.G.; Spears, C.P.; Ray, M.; Muggia, F.M.; Kiyabu, M.; Radin, R.; Laine, L.; Stain, S.; et al. Preoperative Systemic Chemotherapy Followed by Adjuvant Postoperative Intraperitoneal Therapy for Gastric Cancer: A University of Southern California Pilot Program. *J. Clin. Oncol.* **1992**, *10*, 1933–1942. [[CrossRef](#)]
8. Ajani, J.A.; Mansfield, P.F.; Lynch, P.M.; Pisters, P.W.; Feig, B.; Dumas, P.; Evans, D.B.; Rajiman, I.; Hargraves, K.; Curley, S.; et al. Enhanced Staging and All Chemotherapy Preoperatively in Patients with Potentially Resectable Gastric Carcinoma. *J. Clin. Oncol.* **1999**, *17*, 2403–2411. [[CrossRef](#)]
9. Guan, W.L.; He, Y.; Xu, R.H. Gastric Cancer Treatment: Recent Progress and Future Perspectives. *J. Hematol. Oncol.* **2023**, *16*, 57. [[CrossRef](#)]
10. Joshi, S.S.; Badgwell, B.D. Current Treatment and Recent Progress in Gastric Cancer. *CA Cancer J. Clin.* **2021**, *71*, 264–279. [[CrossRef](#)]
11. Miller, Z.; Kim, K.S.; Lee, D.M.; Kasam, V.; Baek, S.E.; Lee, K.H.; Zhang, Y.Y.; Ao, L.; Carmony, K.; Lee, N.R.; et al. Proteasome Inhibitors with Pyrazole Scaffolds from Structure-Based Virtual Screening. *J. Med. Chem.* **2015**, *58*, 2036–2041. [[CrossRef](#)]
12. Rohr, M.; Beardsley, J.; Nakkina, S.P.; Zhu, X.; Aljabban, J.; Hadley, D.; Altomare, D. A Merged Microarray Meta-Dataset for Transcriptionally Profiling Colorectal Neoplasm Formation and Progression. *Sci. Data* **2021**, *8*, 214. [[CrossRef](#)]
13. Liberzon, A.; Subramanian, A.; Pinchback, R.; Thorvaldsdóttir, H.; Tamayo, P.; Mesirov, J.P. Molecular Signatures Database (MSigDB) 3.0. *Bioinformatics* **2011**, *27*, 1739–1740. [[CrossRef](#)]
14. Subramanian, A.; Tamayo, P.; Mootha, V.K.; Mukherjee, S.; Ebert, B.L.; Gillette, M.A.; Paulovich, A.; Pomeroy, S.L.; Golub, T.R.; Lander, E.S.; et al. Gene Set Enrichment Analysis: A Knowledge-Based Approach for Interpreting Genome-Wide Expression Profiles. *Proc. Natl. Acad. Sci. USA* **2005**, *102*, 15545–15550. [[CrossRef](#)] [[PubMed](#)]
15. Györfy, B. Discovery and Ranking of the Most Robust Prognostic Biomarkers in Serous Ovarian Cancer. *GeroScience* **2023**, *45*, 1889–1898. [[CrossRef](#)]
16. Maués, J.H.D.S.; Ribeiro, H.F.; Pinto, G.R.; de Oliveira Lopes, L.; Lamarao, L.M.; Pessoa, C.M.F.; de Fátima Aquino Moreira-Nunes, C.; de Carvalho, R.M.; Assumpção, P.P.; Rey, J.A. Gastric Cancer Cell Lines Have Different MYC-Regulated Expression Patterns but Share a Common Core of Altered Genes. *Can. J. Gastroenterol. Hepatol.* **2018**, *2018*, 5804376. [[CrossRef](#)] [[PubMed](#)]
17. Riquelme, I.; Tapia, O.; Espinoza, J.A.; Leal, P.; Buchegger, K.; Sandoval, A.; Bizama, C.; Araya, J.C.; Peek, R.M.; Roa, J.C. The Gene Expression Status of the PI3K/AKT/MTOR Pathway in Gastric Cancer Tissues and Cell Lines. *Pathol. Oncol. Res.* **2016**, *22*, 797–805. [[CrossRef](#)]
18. Mesquita, F.P.; Lucena da Silva, E.; Souza, P.F.N.; Lima, L.B.; Amaral, J.L.; Zuercher, W.; Albuquerque, L.M.; Rabenhorst, S.H.B.; Moreira-Nunes, C.A.; Amaral de Moraes, M.E.; et al. Kinase Inhibitor Screening Reveals Aurora-a Kinase Is a Potential Therapeutic and Prognostic Biomarker of Gastric Cancer. *J. Cell. Biochem.* **2021**, *122*, 1376–1388. [[CrossRef](#)] [[PubMed](#)]
19. Bustin, S.A.; Beaulieu, J.-F.; Huggett, J.; Jaggi, R.; Kibenge, F.S.B.; Olsvik, P.A.; Penning, L.C.; Toegel, S. MIQE Precise: Practical Implementation of Minimum Standard Guidelines for Fluorescence-Based Quantitative Real-Time PCR Experiments. *BMC Mol. Biol.* **2010**, *11*, 74. [[CrossRef](#)]
20. Varadi, M.; Anyango, S.; Deshpande, M.; Nair, S.; Natassia, C.; Yordanova, G.; Yuan, D.; Stroe, O.; Wood, G.; Laydon, A.; et al. AlphaFold Protein Structure Database: Massively Expanding the Structural Coverage of Protein-Sequence Space with High-Accuracy Models. *Nucleic Acids Res.* **2022**, *50*, D439–D444. [[CrossRef](#)]
21. Jumper, J.; Evans, R.; Pritzel, A.; Green, T.; Figurnov, M.; Ronneberger, O.; Tunyasuvunakool, K.; Bates, R.; Žídek, A.; Potapenko, A.; et al. Highly Accurate Protein Structure Prediction with AlphaFold. *Nature* **2021**, *596*, 583–589. [[CrossRef](#)]
22. DeLano, W.L.; Lam, J. PyMOL: A Communications Tool for Computational Models. In *Abstracts of Papers of the American Chemical Society*; AMER CHEMICAL SOC: Washington, DC, USA, 2005.
23. Kiss, R.; Sandor, M.; Szalai, F.A. <http://Mcule.com>: A Public Web Service for Drug Discovery. *J. Cheminform.* **2012**, *4*, 2012. [[CrossRef](#)]
24. Muteeb, G.; Rehman, M.T.; AlAjmi, M.F.; Aatif, M.; Farhan, M.; Shafi, S. Identification of a Potential Inhibitor (MCULE-8777613195-0-12) of New Delhi Metallo- β -Lactamase-1 (NDM-1) Using In Silico and In Vitro Approaches. *Molecules* **2022**, *27*, 5930. [[CrossRef](#)]
25. Lipinski, C.A.; Lombardo, F.; Dominy, B.W.; Feeney, P.J. Experimental and Computational Approaches to Estimate Solubility and Permeability in Drug Discovery and Development Settings. *Adv. Drug Deliv. Rev.* **2012**, *64*, 4–17. [[CrossRef](#)]
26. Lipinski, C.A. Drug-like Properties and the Causes of Poor Solubility and Poor Permeability. *J. Pharmacol. Toxicol. Methods* **2000**, *44*, 235–249. [[CrossRef](#)] [[PubMed](#)]
27. Banerjee, P.; Eckert, A.O.; Schrey, A.K.; Preissner, R. ProTox-II: A Webserver for the Prediction of Toxicity of Chemicals. *Nucleic Acids Res.* **2018**, *46*, W257–W263. [[CrossRef](#)]
28. Daina, A.; Zoete, V. A BOILED-Egg To Predict Gastrointestinal Absorption and Brain Penetration of Small Molecules. *ChemMed-Chem* **2016**, *11*, 1117–1121. [[CrossRef](#)]
29. Daina, A.; Michielin, O.; Zoete, V. SwissADME: A Free Web Tool to Evaluate Pharmacokinetics, Drug-Likeness and Medicinal Chemistry Friendliness of Small Molecules. *Sci. Rep.* **2017**, *7*, 42717. [[CrossRef](#)]

30. De Magalhães, C.S.; Almeida, D.M.; Barbosa, H.J.C.; Dardenne, L.E. A Dynamic Niching Genetic Algorithm Strategy for Docking Highly Flexible Ligands. *Inf. Sci.* **2014**, *289*, 206–224. [[CrossRef](#)]
31. Guedes, I.A.; Barreto, A.M.S.; Marinho, D.; Krempser, E.; Kuenemann, M.A.; Sperandio, O.; Dardenne, L.E.; Miteva, M.A. New Machine Learning and Physics-Based Scoring Functions for Drug Discovery. *Sci. Rep.* **2021**, *11*, 3198. [[CrossRef](#)]
32. Inbar, Y.; Schneidman-Duhovny, D.; Halperin, I.; Oron, A.; Nussinov, R.; Wolfson, H.J. Approaching the CAPRI Challenge with an Efficient Geometry-Based Docking. *Proteins Struct. Funct. Bioinform.* **2005**, *60*, 217–223. [[CrossRef](#)]
33. Housman, G.; Byler, S.; Heerboth, S.; Lapinska, K.; Longacre, M.; Snyder, N.; Sarkar, S. Drug Resistance in Cancer: An Overview. *Cancers* **2014**, *6*, 1769–1792. [[CrossRef](#)] [[PubMed](#)]
34. Borriello, A.; Caldarelli, I.; Basile, M.A.; Bencivenga, D.; Tramontano, A.; Perrotta, S.; della Ragione, F.; Oliva, A. The Tyrosine Kinase Inhibitor Dasatinib Induces a Marked Adipogenic Differentiation of Human Multipotent Mesenchymal Stromal Cells. *PLoS ONE* **2011**, *6*, e28555. [[CrossRef](#)] [[PubMed](#)]
35. Yi, Y.; Xu, T.; Tan, Y.; Lv, W.; Zhao, C.; Wu, M.; Wu, Y.; Zhang, Q. CCDC69 Is a Prognostic Marker of Breast Cancer and Correlates with Tumor Immune Cell Infiltration. *Front. Surg.* **2022**, *9*, 879921. [[CrossRef](#)] [[PubMed](#)]
36. Prieto-Martínez, F.D.; López-López, E.; Eurídice Juárez-Mercado, K.; Medina-Franco, J.L. Computational Drug Design Methods—Current and Future Perspectives. In *Silico Drug Design: Repurposing Techniques and Methodologies*; Elsevier: Amsterdam, The Netherlands, 2019; pp. 19–44. [[CrossRef](#)]
37. Anthony, L.F.W.; Kanding, B.; Selvan, R. Carbontracker: Tracking and Predicting the Carbon Footprint of Training Deep Learning Models. *arXiv* **2020**, arXiv:2007.03051.
38. Song, Y.; Ye, L.; Tan, Y.; Tong, H.; Lv, Z.; Wan, X.; Li, Y. Therapeutic Exosomes Loaded with SERPINA5 Attenuated Endometrial Cancer Cell Migration via the Integrin B1/FAK Signaling Pathway. *Cell. Oncol.* **2022**, *45*, 861–872. [[CrossRef](#)]
39. Wu, H.; Cui, M.; Li, C.; Li, H.; Dai, Y.; Cui, K.; Li, Z. Kaempferol Reverses Aerobic Glycolysis via MiR-339-5p-Mediated PKM Alternative Splicing in Colon Cancer Cells. *J. Agric. Food Chem.* **2021**, *69*, 3060–3068. [[CrossRef](#)]
40. Jia, H.; Song, L.; Cong, Q.; Wang, J.; Xu, H.; Chu, Y.; Li, Q.; Zhang, Y.; Zou, X.; Zhang, C. The LIM Protein *AJUBA* Promotes Colorectal Cancer Cell Survival through Suppression of JAK1/STAT1/IFIT2 Network. *Oncogene* **2017**, *36*, 2655–2666. [[CrossRef](#)]
41. Dommann, N.; Sánchez-Taltavull, D.; Eggs, L.; Birrer, F.; Brodie, T.; Salm, L.; Baier, F.A.; Medova, M.; Humbert, M.; Tschan, M.P. The LIM Protein *AJUBA* Augments Tumor Metastasis in Colon Cancer. *Cancers* **2020**, *12*, 1913. [[CrossRef](#)]
42. Li, J.; Yang, Y.; Inoue, H.; Mori, M.; Akiyoshi, T. The Expression of Costimulatory Molecules *CD80* and *CD86* in Human Carcinoma Cell Lines: Its Regulation by Interferon Gamma and Interleukin-10. *Cancer Immunol. Immunother.* **1996**, *43*, 213–219. [[CrossRef](#)]
43. Horn, L.A.; Long, T.M.; Atkinson, R.; Clements, V.; Ostrand-Rosenberg, S. Soluble *CD80* Protein Delays Tumor Growth and Promotes Tumor-Infiltrating Lymphocytes. *Cancer Immunol. Res.* **2018**, *6*, 59–68. [[CrossRef](#)]
44. Feng, X.Y.; Lu, L.; Wang, K.F.; Zhu, B.Y.; Wen, X.Z.; Peng, R.Q.; Ding, Y.; Li, D.D.; Li, J.J.; Li, Y.; et al. Low Expression of *CD80* Predicts for Poor Prognosis in Patients with Gastric Adenocarcinoma. *Future Oncol.* **2019**, *15*, 473–483. [[CrossRef](#)] [[PubMed](#)]
45. Peggs, K.S.; Quezada, S.A. Ipilimumab: Attenuation of an Inhibitory Immune Checkpoint Improves Survival in Metastatic Melanoma. *Expert Rev. Anticancer Ther.* **2010**, *10*, 1697–1701. [[CrossRef](#)] [[PubMed](#)]
46. Zhai, F.; Wang, J.; Luo, X.; Ye, M.; Jin, X. Roles of *NOLC1* in Cancers and Viral Infection. *J. Cancer Res. Clin. Oncol.* **2023**, *149*, 10593–10608. [[CrossRef](#)] [[PubMed](#)]
47. Kong, F.; Shang, Y.; Diao, X.; Huang, J.; Liu, H. Knockdown of *NOLC1* Inhibits PI3K-AKT Pathway to Improve the Poor Prognosis of Esophageal Carcinoma. *J. Oncol.* **2021**, *2021*, 9944132. [[CrossRef](#)]
48. L Garner, A.; D Janda, K. Protein-Protein Interactions and Cancer: Targeting the Central Dogma. *Curr. Top. Med. Chem.* **2010**, *11*, 258–280. [[CrossRef](#)]
49. Lu, H.; Zhou, Q.; He, J.; Jiang, Z.; Peng, C.; Tong, R.; Shi, J. Recent Advances in the Development of Protein-Protein Interactions Modulators: Mechanisms and Clinical Trials. *Signal Transduct. Target. Ther.* **2020**, *5*, 213. [[CrossRef](#)]
50. Bahmanyar, S.; Kaplan, D.D.; DeLuca, J.G.; Giddings, T.H.; O’Toole, E.T.; Winey, M.; Salmon, E.D.; Casey, P.J.; Nelson, W.J.; Barth, A.I.M. β -Catenin Is a Nek2 Substrate Involved in Centrosome Separation. *Genes Dev.* **2008**, *22*, 91–105. [[CrossRef](#)]

Disclaimer/Publisher’s Note: The statements, opinions and data contained in all publications are solely those of the individual author(s) and contributor(s) and not of MDPI and/or the editor(s). MDPI and/or the editor(s) disclaim responsibility for any injury to people or property resulting from any ideas, methods, instructions or products referred to in the content.

CAPÍTULO III

Antimicrobial synthetic peptide alters morphological, ultrastructural and nanomechanical properties in metastatic gastric cancer cells

**Artigo a ser submetido na Revista *The British Journal of Cancer*
(Fator de Impacto 10.5, Qualis A1)**

Daiane Maria da Silva Brito

1 **Antimicrobial synthetic peptide alters morphological, ultrastructural and**
2 **nanomechanical properties in metastatic gastric cancer cells**

3
4 Daiane M. S. Brito ^{1,2}, Felipe P. Mesquita ², Emerson L. da Silva ², Francisco L. de
5 Oliveira ², Ana B. da Lima ², Maria E. A. de Moraes ², Raquel C. Montenegro ^{2,3},
6 Luciana M. R. Alencar ⁴ and Pedro F. N. Souza ^{1,2}

7
8 ¹Pharmacogenetics Laboratory, Drug Research and Development Center (NPDM), Federal University of
9 Ceará, Fortaleza, CE, 60430-275, Brazil.

10 ²Department of Biochemistry and Molecular Biology, Federal University of Ceará, Fortaleza, Brazil.

11 ³Red Latinoamericana de Implementación y Validación de guías clínicas Farmacogenómicas (*RELIVAF*).

12 ⁴Laboratory of Biophysics and Nanosystems, Physics Department, Federal University of Maranhão, São
13 Luís 65020070, Brazil

14
15 * **Correspondent authors:**

16 Pedro F. N. Souza (pedrofilhobio@gmail.com - P.F.N.S)

17 Address: Laboratory of Pharmacogenetics, Drug Research and Development Center (NPDM),
18 Federal University of Ceará, Street Cel. Nunes de Melo, 1000 – Rodolfo Teófilo, Fortaleza, Ceará,
19 Brazil. Phone: +55 (85) 3366-8033.

20 **ORCID:**

21 0000-0003-2524-4434 (P.F.N.S)

22

23

24

25

26

27

28 **Abstract**

29 Gastric cancer (GC) resistance to chemotherapy is a huge problem worldwide. One option
30 could be repositioning antimicrobial peptides to overcome that problem. Here, we aimed
31 to reposit synthetic antimicrobial peptides (SAMPs) against GC. After screening against
32 several lines of GC, the SAMP RcAlb-PepI presented the best selective index (SI) toward
33 the AGP-01 metastatic cell line of GC. The mechanisms of action revealed increased
34 membrane permeabilization, pore formation and loss of internal content, leading to death.
35 Atomic force microscopy (AFM) analysis revealed that RcAlb-PepI-treated AGP-01 cells
36 showed damage to the membrane, leading to loss of internal content, alteration in
37 ultrastructure and nanomechanical properties, and vibrational signature. Additionally,
38 RcAlb-PepI is also able to inhibit the migration of AGP-01. *In silico* analysis predicted
39 that RcAlb-PepI could interact with the AJUBA and NOLC1 proteins, both highly
40 accumulated in AGP-01 cells compared to control MNP-01, leading to conformational
41 changes in 3D structure, suggesting inhibition of their activity. *In vitro* and *in vivo* studies
42 revealed that RcAlb-PepI is not toxic to non-cancerous human cells, zebrafish embryos,
43 and larvae, even at concentrations 20-fold higher than IC₅₀. Thus, PepGAT and PepKAA
44 have great potential to be candidates as anticancer molecules.

45

46 **Keywords:** Anticancer synthetic peptides; repositioning of antimicrobial peptides;
47 synthetic peptides; mechanisms of action by AFM.

48 **1. Introduction**

49 Gastric cancer (GC) ranks fifth, representing 5.6% of cases. Although a worldwide
50 decrease in incidence and mortality rates has been observed in recent decades, the recent
51 statistics from the Globocan project (2020)¹ classified GC as the fourth leading cause of
52 cancer-related mortality worldwide, with 768,000 deaths in 2020. Therefore, GC is one
53 of the problems with the world's greatest socioeconomic and public health impact².

54 The conventional treatment of GC is based on the therapeutic triad of surgery,
55 chemotherapy, and radiotherapy. Treatment options are selected primarily based on the
56 stage of the disease, the presence of biomarkers, and the patient's condition³.
57 Chemotherapy aims to stimulate cell death mechanisms, which can be triggered by direct
58 or indirect damage to DNA, resulting in the deregulation of tumor replication by
59 genotoxic agents. These agents can be endogenous, such as reactive oxygen species
60 (ROS), and exogenous, such as UV light, ionizing radiation (IR), and chemotherapeutic
61 agents^{4,5}.

62 Cancer can develop resistance to virtually all types of therapies, such as radiation
63 therapy, chemotherapy, and even targeted therapies⁶. Searching for molecules that explore
64 new therapeutic targets is urgent to cope with chemoresistance. Since cancer cells have
65 developed resistance to the mechanisms used by most cytotoxic drugs and molecularly
66 targeted therapies currently available⁷. Repositioning synthetic antimicrobial peptides
67 (SAMPs) is a promising option in this context. In addition to their antimicrobial activity,
68 it is known in the literature that SAMPs can exhibit immunomodulatory, antibiofilm and
69 anticancer properties. This variety of functions has brought great research interest to
70 understanding the mechanisms and different aspects of the anticancer potential of
71 SAMPs^{8,9}.

72 SAMPs represent an alternative therapeutic intervention in the treatment of GC
73 because they are strategically designed to have low levels of toxicity, multifaceted
74 performance, and high selectivity⁸⁻¹⁰. Based on this, the present study investigated the
75 repositioning potential of SAMPs to induce cytotoxicity, interfere with cancer cell
76 processes, and provide insights into the mechanism of action behind their anticancer
77 activity.

78

79 **2. Methodology**

80

81 **2.1. Ethical Statement**

82 All experiments with zebrafish were endorsed by the Ethics Committee in the Use
83 of Animals of the Federal University of Paraiba, with authorization documented by
84 protocol no. 4460140920. The methods of handling animals followed the guidelines and
85 regulations of the ARRIVE guidelines.

86

87 **2.2. Synthetic Peptides**

88 The synthetic peptides used in this study were *Mo*-CBP₃-PepI (CPAIQRCC), *Mo*-
89 CBP₃-PepII (NIQPPCRCC), and *Mo*-CBP₃-PepIII (AIQRCC) designed from the plant
90 protein *Mo*-CBP₃ by Oliveira et al. ¹¹, and *Rc*Alb-PepI (AKLIPTIAL), *Rc*Alb-PepII
91 (SLRGCC), and *Rc*Alb-PepIII (AKLIPTIA) designed from the plant protein *Rc*-2*S*-*Alb*
92 by Dias et al. ¹². All peptides were synthesized by SynPeptide Co. Ltd.
93 (<http://www.synpeptide.com/custom.asp?id=1>) from China. All synthetic peptides
94 possess at least 95% purity, confirmed by reverse-phase high-performance liquid
95 chromatography (HPLC) and mass spectrometry (MS) analysis.

96

97 **2.3 Bioinformatics analysis**

98

99 *2.3.1 Anticancer and Toxicity Prediction*

100 Before *in vitro* analysis, all synthetic peptides were run into servers to predict
101 possible anticancer potential, biological properties, and toxicity. For anticancer potential,
102 the online server AntiCP tool is freely accessible
103 (https://webs.iitd.edu.in/raghava/anticp/multi_pep.php).¹³ DNA bind prediction of
104 peptides using the online server DNA bind (<https://dnabind.szilab.org/>)¹⁴. LD50 and
105 toxicity predictions were calculated using the online tool Protox-II tool ([https://tox-](https://tox-new.charite.de/prottox_II/)
106 [new.charite.de/prottox_II/](https://tox-new.charite.de/prottox_II/))¹⁵.

107 The toxicity of peptides was predicted using the ProTox-II, a freely available
108 online server (https://tox-new.charite.de/prottox_II/, accessed in July 2023)¹⁵. The toxicity
109 prediction considers molecular similarities with other molecules and pharmacophore
110 groups. ProTox-II employs machine learning models to predict toxicity endpoints such as
111 acute toxicity, hepatotoxicity, cytotoxicity, carcinogenicity, immunotoxicity and
112 mutagenicity. In addition, based on algorithms present in the ProTox-II's database is
113 possible to predict the LD50 of compounds¹⁵.

114

115 *2.3.2 Molecular docking (MD) assays of peptides against targets in cancer gastric*

116 Before going through *in vitro* analysis against gastric cancer cells, all peptides
117 were assayed toward targets of GC. Our research group recently described the new targets
118 for GC, such as AJUBA, CD80 and NOLC1 proteins¹⁶. Although peptides are small
119 molecules, they are of protein class. Based on that, the best server to perform MD analysis
120 was ClusPro 2.0 (<https://cluspro.org/>)¹⁷, the best-performing server for protein-protein

121 docking currently available by the Critical Assessment of Prediction of Interactions
122 (CAPRI) challenge¹⁷.

123 The MD assays in the ClusPro were done using the Graphic Processing Unit
124 (GPU) option that accesses the more powerful computer for graphics from the
125 Massachusetts Green High-Performance Computing Center (MGHPC). The MD results
126 were evaluated based on the number of repetitions of the same pose of interaction,
127 interface energy, and residue interactions. The BIOVIA Discovery Studio Visualizer
128 (version 21.1.0.20298) and the PyMol molecular graphics systems (version 2.5.4,
129 Schrödinger, LLC, San Diego, CA, USA)¹⁸ generated the graphics about interactions.

130

131 **2.4. Cell Culture and Cytotoxicity by Alamar Blue Assay**

132

133 The gastric cancer cell line AGP-01 was obtained from the malignant ascitic fluid
134 of primary metastatic intestinal-type tumors. The ACP-02 and ACP-03 cell lines were
135 established from Brazilian patients with diffuse-type and primary intestinal-type tumors,
136 respectively. The non-malignant gastric cell lineage MNP-01 was previously established
137 from normal gastric mucosa and was used as a cell-type-specific control¹⁹. All cells were
138 cultured in Dulbecco's modified Eagle's medium (DMEM; Gibco®), supplemented with
139 10% (v/v) fetal bovine serum (Gibco®), 1% (v/v) penicillin (100 U mL⁻¹) and
140 streptomycin (100 mg mL⁻¹) (Invitrogen®), in a humidified atmosphere with 5% CO₂ at
141 37 °C. Cell confluence was observed under a conventional microscope.

142 The cytotoxicity of the synthetic peptides was determined against gastric tumor
143 cell lines (ACP-02, ACP-03, and AGP-01) and normal gastric cells (MNP-01). The cell
144 lines were seeded (3×10^3 cells/well) in a 96-well plate and incubated in an oven with a
145 5% CO₂ atmosphere at 37 °C, being cultivated for 24 h. Then, treatment was carried out

146 with the peptides in a serial dilution curve (100 to 400 $\mu\text{g mL}^{-1}$) for 72 h. Afterward, the
147 fluorescent compound Alamar Blue (0.2 mg mL^{-1}) (MERCK $\text{\textcircled{R}}$) was added for an
148 incubation period of 3 h. Therefore, the fluorescence intensity was measured using a
149 spectrophotometer (Beckman Coulter Microplate Reader DTX 880) and the 50%
150 inhibition concentration of cell line growth (IC_{50}) was measured. From the results
151 obtained, it was possible to define which synthetic peptides and cell lines will be used for
152 the next experiments.

153 **2.5. Membrane Damage induced by peptides**

154 The effect of synthetic peptides on the membrane permeability of GC cells was
155 evaluated by the propidium iodide (PI) uptake assay described by Oliveira et al.¹¹.
156 Therefore, the GC cell lines were seeded (3×10^3 cells/well) in a 96-well plate and
157 incubated for 24 hours. Then, the cells were treated with peptides at IC_{50} concentration
158 for 24 hours. A non-toxic concentration of DMSO (0.01%) was used as a negative control.
159 After incubation, the samples were washed three times with 0.15 M NaCl (centrifuged
160 $5000 \times g$ 5 min at $4 \text{ }^\circ\text{C}$), incubated with PI at $1 \text{ }\mu\text{M}$ for 30 minutes at room temperature
161 in the dark and analyzed in a Cytation 3 Cell Multimode Reader (Biotek $\text{\textcircled{R}}$) with an
162 excitation wavelength of 488 nm and an emission wavelength of 525 nm.

163 In the same experiment, cells were also incubated with $1 \text{ }\mu\text{M}$ fluorescein
164 isothiocyanate (FITC)-Dextran conjugate with a size of 6 kDa (Sigma Aldrich, SP,
165 Brazil), 30 min at $25 \text{ }^\circ\text{C}$ in the dark. As in the IP uptake assay, they were washed three
166 times with 0.15 M NaCl (centrifuged $5000 \times g$ 5 min at $4 \text{ }^\circ\text{C}$) and analyzed with an
167 excitation wavelength of 490 nm and an emission wavelength of 520 nm, following the
168 method described by Oliveira et al.¹¹.

169 **2.6. Induction of Reactive Oxygen Species (ROS)**

170 A fluorometric assay was performed to evaluate the generation of ROS induced
171 by peptides (H_2O_2) using DCFH-DA (2',7' dichlorofluorescein diacetate)¹². The samples
172 followed the same preparation described above. Finally, 10 μ M DCFH-DA was added
173 and cells were incubated for 20 min at 22 ± 2 °C in the dark. Then, the samples were
174 washed and observed in a Cytation 3 Cell Multimode Reader (Biotek®) with an
175 excitation wavelength of 535 nm and an emission wavelength of 617 nm.

176

177 **2.7. Atomic Force Microscopy (AFM) Analysis**

178 GC cell lines were cultured at 9×10^5 cells per well and seeded in 13 mm circular
179 glass coverslips in a 12-well plate. Then, the cells were treated with synthetic peptides or
180 a non-toxic concentration of DMSO (0.01%) for 24 h. Afterward, the cells were washed
181 with PBS and fixed with a 3.7% formaldehyde solution for 10 min. Then, cells were
182 washed twice with ultrapure water and air-dried for morphological imaging and
183 ultrastructural analysis. Two independent experiments were carried out.

184 AFM analysis was performed using an AFM Multimode 8 (Bruker, Santa Barbara,
185 CA, USA) in PeakForce Quantitative Nanomechanics (QNM) mode with 0.4 N/m
186 cantilever and 2 nm tip radio. The data was acquired under controlled conditions (23 °C
187 temperature and 44% humidity) with scan parameters of 0.5 Hz scan rate $2.5 \times 2.5 \mu\text{m}^2$
188 scan size. A total of 30 maps were analyzed for each group: (i) control cells treated with
189 DMSO at a non-toxic concentration and (ii) cells treated with peptide(s); in both groups,
190 the treatment time was 24 hours.

191 For the ultrastructural evaluation the statistical analysis of roughness was based
192 on the height of each pixel in the image, analyzed from the height map. The parameter

193 Rq refers to the mean square roughness, a parameter extremely sensitive to peaks and
194 hollows, being defined by Equation (1)²⁰:

$$195 \quad R_q = \sqrt{\frac{1}{N} \sum_{i=1}^N z_i^2}$$

196 where Z is each pixel height, and N is the total number of pixels, in our case, 65536 pixels.
197 Before calculating roughness values, no image pre-treatment was performed on the maps,
198 and the scan size was standardized. An area of 2.5 μm^2 in the center of each cell was
199 chosen. For area and volume data analysis, Gwyddion 2.60 software was used. The area
200 was calculated by triangulating the masked surface and volume as the integral of the
201 surface height over the masked cell area.

202 Nanomechanical analysis was done based on the force curves obtained from
203 measurements with AFM carrying much information about the physical nature of the
204 sample surface. Each curve portion has specific information, and precise mathematical
205 models were employed in their calculation²¹. The sample adhesion and Young's Modulus
206 were calculated from all force curves. The adhesion force between the probe and the
207 sample surface was obtained from retraction curves, considered at the minimum
208 cantilever deflection value. This value represents the AFM probe's resistance to leaving
209 the sample surface. AFM data analysis was done according to a single criterion and
210 assessed by ANOVA and Tukey's post-test, with significance as $p < 0.05$. Statistical
211 analyses and stiffness, adhesion and roughness graphs were done using Origin software.
212 Again, differences were considered significant when the p-value was < 0.05 .

213

214 **2.8. Raman spectroscopic analysis**

215 Raman spectra were acquired using a triple Raman spectrometer (Model T64000,
216 Horiba), run in single mode with slits set to a resolution of less than 2 cm^{-1} . The instrument

217 has a liquid N₂-cooled charge-coupled device (CCD) detector. The 532 nm green line of
218 a solid-state laser (LAS-532-100-HREV) operating at 14 mW was used for excitation. An
219 Olympus microscope was used with a 100x focal length objective to focus the light on
220 the sample. Within each spectral dispersion range, spectra were acquired on the surface
221 of the samples after nine acquisitions of 20s each. Data processing was carried out using
222 the LabSpec6 software. The narrow peaks caused by cosmic rays were sequentially
223 removed, and the fluorescence background variation and the glass substrate were
224 estimated using the fifth-order polynomial fit and subtracted.

225 **2.9. Wound healing assay**

226 The anti-migratory effect of the synthetic peptide was evaluated according to the
227 method described by¹⁹. GC cells were plated (2×10^5 cells/well) in a 12-well plate, and
228 after fixing the cells, scratches were made in each well with a sterile pipette tip. Then,
229 cells were treated with peptides at IC₅₀ for 24 hours, and photos were taken at different
230 time points (0 and 24 hours) to analyze cell migration using ImageJ software.

231 **2.10. Evaluation of Cytotoxicity to non-cancerous cells**

232 The cytotoxicity was measured by the reduction of MTT (3-(4,5-dimethyl-2-
233 thiozoly)-2,5-diphenyl-2H-tetrazolium bromide) to formazan²². The Rio de Janeiro Cell
234 Bank (BCRJ, Brazil) gently provided the cell lines L929 (murine fibroblasts, ATCC
235 number CCL-1), MRC-5 (human lung fibroblasts, ATCC number CCL-171), and HaCat
236 (human keratinocytes). The cell lines were grown in DMEM medium supplemented with
237 10% FBS, 2 mM of glutamine, 100 U/mL of penicillin, and 100 µg/mL of streptomycin
238 at 37 °C under 5% CO₂.

239 For the experiments, cells were plated in 96-well plates, HaCat (0.1×10^6
240 cells/mL) and L929 and MRC-5 cell lines (0.1×10^4 cells/mL). After 24 h, the tested
241 peptides (1 mg mL^{-1} in the culture medium) were added to each well, and the cells were

242 incubated for 72 h. Methyl methanesulfonate (MMS) (4×10^{-5} M) was used as the
243 positive control for cytotoxicity. After that, the plates were centrifuged, and the medium
244 was replaced with a fresh medium (150 μ L) containing 0.5 mg mL of MTT and incubated
245 for 3h. The MTT formazan product was dissolved in 150 μ L DMSO, and the absorbance
246 was measured using a multiplate reader (Spectra Count, Packard, Ontario, Canada) at 595
247 nm.

248 **2.11. Comet assay**

249 The concentration of peptides for comet assay was 1 mg mL⁻¹. DMSO-NaCl was
250 the negative control for damage and MMS (4×10^{-5} M) was the positive control for DNA
251 damage. The comet assay was performed as described²². After cell treatment for 24 h,
252 cells were washed with ice-cold PBS, trypsinized and resuspended to a complete medium.
253 After, 20 μ L of cells (0.7×10^5 cells mL) in 0.75% low-melting-point agarose was spread
254 onto a glass microscope slide previously treated with a 1% agarose layer. Slides were
255 incubated in ice-cold lysis solution (2.5 M NaCl, 0.01 M Tris, 0.1 M EDTA, 1% Triton
256 X-100, and 10% DMSO, pH 10.0) at 4 °C for at least 1 h to remove cell membranes,
257 leaving DNA molecules, in nucleoids format.

258 After that, the slides were placed in a horizontal electrophoresis unit that was
259 conducted for 20 min at 25 V (94 V/cm). All the above steps were performed in the dark
260 to prevent additional DNA damage. After electrophoresis, slides were neutralized (0.4 M
261 Tris, pH 7.5) and stained using 20 μ g mL⁻¹ of ethidium bromide. These cells were visually
262 scored according to tail length into five classes: (1) class 0: undamaged, without a tail;
263 (2) class 1: with a tail shorter than the diameter of the head nucleus; (3) class 2: with tail
264 length 1-2x the diameter of the head; (4) class 3: with a tail longer than 2x the diameter
265 of the head; and (5) class 4: comets with no heads. The damage index (DI) value was
266 assigned to each sample according to²².

267 **2.12. Morphological characterization of apoptotic cells**

268 The concentration of peptides used in this assay was the same as the others, 1 mg
269 mL⁻¹. DMSO-NaCl was the negative control for damage and MMS (4 x 10⁻⁵ M) was the
270 positive control for DNA damage. Peptides and control solutions were incubated as
271 described above. Then, cells with morphological characteristics of apoptosis were
272 evaluated after 24 h with the 1 µL acridine orange (AO, 100 µg/mL)/ethidium bromide
273 (EB, 100 µg/mL) in PBS. The apoptotic characteristics evaluated were peripheral
274 chromatin condensation, fragmented nucleus, small cell volume, and apoptotic bodies.
275 The percentage of apoptotic cells was then calculated according to²³.

276 **2.13. Zebrafish toxicity**

277 *2.13.1. Zebrafish embryos*

278 Zebrafish embryos with 1 HPF (hour post-fertilization) were provided by the
279 Production Unit for Alternative Model Organisms (UniPOM), Federal University of
280 Paraíba, João Pessoa, Brazil. The animals were kept in a recirculation-monitored system
281 at a controlled temperature (26 ± 1 °C) and photoperiod (14:10 light/dark cycle). Fish
282 were fed daily with commercial feed (Color Bits Tetra, Melle, Germany) and freeze-dried
283 spirulina (Fazenda Tamanduá, Patos, Brazil). Adult zebrafish (male-to-female ratio of
284 2:1) were transferred to a 7-L spawning tank with a bottom mesh for embryo collection.
285 Embryos were collected only on the day of the experiment and cultured embryonic
286 medium E3 (5.0 mM NaCl, 0.17 mM KCl, 0.33 mM CaCl, and 0.33 mM MgSO₄). Only
287 samples with a fertilization rate above 90% were used.

288

289 *2.13.1. Acute toxicity test*

290 According to the OECD Guideline number 236 in 96-well plates, the test was
291 conducted independently with peptides. Zebrafish embryos up to 3 hpf were exposed to

292 1 mg mL⁻¹ of peptides. For each test and control sample, 20 wells were filled with 0.3 mL
293 of solution and 1 embryo. Twenty embryos were treated only with the E3 medium (the
294 solvent control). Lethal and non-lethal effects were observed daily for 96 h. Embryos
295 presenting lethal aspects, such as the absence of heartbeat, coagulation, and no
296 detachment of the tail, were considered dead. The survival % (the number of live
297 organisms/total number of organisms x 100) per tested sample was determined based on
298 the lethal aspects counting. Observations were performed with a stereomicroscope
299 (Olympus SZX7, Japan) at 56 x magnification, and pictures were taken with a digital
300 camera (Moticam 5+, China). After 96 h, surviving larvae were euthanized with eugenol
301 and properly discarded.

302

303 **2.14. Statistical analysis**

304 The assays were performed in three independent experiments. The statistics were
305 expressed as the mean \pm standard deviation. The data were submitted to ANOVA,
306 followed by the Tukey test, using GraphPad Prisma 5.01, with a significance of $p < 0.05$.

307

308 **3. Results**

309

310 **3.1. Bioinformatics Analysis of Synthetic Peptides**

311 The analysis of the AntiCP server revealed that all synthetic peptides are predicted
312 to be anticancer molecules (Table 1). The analysis in the DNA bind server revealed that
313 all peptides can interact with DNA molecules (Table 1).

314

315 **Table 1.** Bioinformatic characterization and prediction of synthetic peptides

Biological properties	Mo-CBP3-PepI	Mo-CBP3-PepII	Mo-CBP3-PepIII	RcAlb-PepI	RcAlb-PepII	RcAlb-PepIII
Anticancer ^a	Yes	Yes	Yes	Yes	Yes	Yes
DNA interaction ^b	Yes	Yes	Yes	Yes	Yes	Yes
Toxicity class ^c	5	5	5	4	4	5
Predicted LD50 ^c	5000 mg/kg	5000 mg/kg	5000 mg/kg	2000 mg/kg	2000 mg/kg	5000 mg/kg
Hepatotoxicity ^c	No	No	No	No	No	No
Carcinogenicity ^c	No	No	No	No	No	No
Immunogenicity ^c	No	No	No	No	No	No
Mutagenicity ^c	No	No	No	No	No	No
Cytotoxicity ^c	No	No	No	No	No	No

316 ^a The anticancer potential of synthetic peptides was calculated using the AntiCP tool

317 (https://webs.iiitd.edu.in/raghava/anticp/multi_pep.php)¹³.

318 ^b DNA interaction prediction of synthetic peptides was calculated using the DNA bind tool (<https://dnabind.szilab.org/>)¹⁴.

319 ^c Prediction was done using the protox-II tool (https://tox-new.charite.de/protox_II/)¹⁵.

320 The toxic features of all peptides were done using the server Protox-II (Table 1).
321 In a score produced by the protox-II server, where 1 is the most toxic and 6 most the safe,
322 peptides *Mo*-CBP₃-PepI, *Mo*-CBP₃-PepII, *Mo*-CBP₃-PepIII, and RcAlb-PepIII presented
323 score in class 5 and RcAlb-PepI and RcAlb-PepII presented score in class 4 (Table 1).
324 The LD50 analysis predicted an LD50 value of 5000 mg/kg to *Mo*-CBP₃-PepI, *Mo*-CBP₃-
325 PepII, *Mo*-CBP₃-PepIII, and RcAlb-PepIII and 2000 mg/kg RcAlb-PepI and RcAlb-PepII
326 (Table 1).

327

328 **3.2. Cytotoxicity of peptides against gastric cancer lines**

329 As all peptides presented good results *in silico* analysis (Table 1), they were all
330 tested against the GC cell lines (Table 2). *Mo*-CBP₃-PepII and RcAlb-PepIII presented no
331 anticancer effect against the cell lines tested (Table 2). The peptides *Mo*-CBP₃-PepI, *Mo*-
332 CBP₃-PepIII, RcAlb-PepI, and RcAlb-PepII presented IC₅₀ for all GC (Table 2). The
333 lowest values of IC₅₀ presented by peptides came from RcAlb-PepI with an IC₅₀ value
334 of 53.87 $\mu\text{g mL}^{-1}$ and 57.00 $\mu\text{g mL}^{-1}$, respectively, against AGP-01 and ACP-03 (Table
335 2).

336 Despite the IC₅₀ values presented against GC cells, values of IC₅₀ were also
337 found against the non-cancerous cell MNP-01 (Table 1). The IC₅₀ values against MNP-
338 01 were 101.9 $\mu\text{g mL}^{-1}$, 125.1 $\mu\text{g mL}^{-1}$, 105.1 $\mu\text{g mL}^{-1}$, and 133.3 $\mu\text{g mL}^{-1}$, respectively,
339 for *Mo*-CBP₃-PepI, *Mo*-CBP₃-PepIII, RcAlb-PepI, and RcAlb-PepII (Table 2). As all
340 peptides presented an IC₅₀ against MNP-01 cells, a selective index (SI) (Table 2) was
341 calculated to choose the best peptide and GC cell line to move forward with the
342 mechanisms of action. The peptide with the best SI indicating selective to cancer cells
343 than healthy cells was presented by RcAlb-PepI against the metastatic cell line AGP-01
344 (Table 2), which was chosen to evaluate the mechanisms of action.

345 **Table 2** - Cytotoxicity of synthetic peptides against gastric tumor cell lines (ACP-02, ACP-03, and AGP-01) and normal gastric cells (MNP-01)

<i>Cell lines</i>	<i>IC₅₀ (μg/mL) and IC [95%]^a</i>				<i>Selective index^b</i>			
	Mo-CBP3-PepI	Mo-CBP3-PepIII	RcAlb-PepI	RcAlb-PepII	Mo-CBP3-PepI	Mo-CBP3-PepIII	RcAlb-PepI	RcAlb-PepII
<i>AGP-01</i>	77.55 (55.41 - 108.5)	88.18 (72.39 - 107.4)	53.87 (36.48 - 79.55)	107.9 (88.28 - 131.8)	1.31	1.41	1.95	1.21
<i>ACP-02</i>	146.6 (123.1 - 174.7)	119.8 (96.14 - 149.2)	68.98 (46.83 - 101.6)	75.48 (59.79 - 95.29)	0.69	1.04	1.52	1.76
<i>ACP-03</i>	89.06 (78.23 - 101.4)	83.44 (71.30 - 97.66)	57.00 (36.01 - 90.24)	87.80 (61.31 - 125.7)	1.14	1.49	1.84	1.51
<i>MNP-01</i>	101.9 (83.78 - 124.0)	125.1 (104.3 - 150.0)	105.2 (93.22 - 118.6)	133.3 (110.0 - 161.5)				

346

347

348

^a IC [95%]: 95% confidence interval, IC50: half-maximal inhibitory concentration.

349

^b Selective index was calculated as a simple ratio of IC50 of healthy and cancer cells²⁴.

350

351

352

353

354

355

356 **3.3. RcAlb-PepI induces membrane damage in AGP-01 cells**

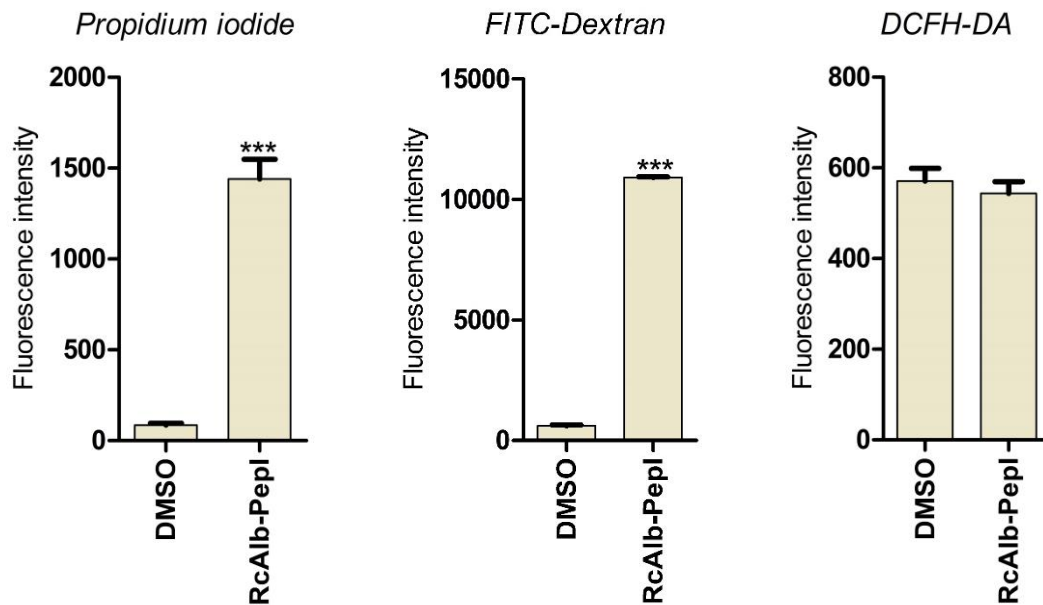
357

358 All the experiments of mechanisms of action of RcAlb-PepI against AGP-01 cell
359 were done at IC50 concentration presented in Table 1. The IP uptake assay revealed that
360 treatment with RcAlb-PepI led to an increase in the membrane permeability of AGP-01
361 cells, based on the PI uptake and consequently increase in fluorescence emission in the
362 treated cells compared to control cells, as seen in Figure 1. Alone, the PI uptake assay
363 does not confirm the pore formation.

364 Corroborating the results reported by PI uptake assay, RcAlb-PepI-treated AGP-
365 01 cells were incubated with the FITC-Dextran, with a size of 6-kDa (Fig. 1). The
366 fluorescence in AGP-01 treated cells revealed the movement of AGP-01 through the
367 membrane, indicating a pore formed with, at least, a size of 6-kDa. Control AGP-01
368 showed no fluorescence (Fig. 1).

369 In parallel, it was also decided to investigate the ability of RcAlb-PepI to induce
370 ROS accumulation in AGP-01 cells. As a result, AGP-01 cells treated with RcAlb-PepI
371 and a non-toxic concentration of DMSO did not accumulate high levels of ROS, with
372 similar fluorescence emission observed in both groups tested (Fig. 1).

373 The results obtained and described above provide us with important information
374 regarding the mechanism of RcAlb-PepI, making it possible to suggest that one of the
375 main mechanisms of action of this peptide refers to its potential to cause damage to cell
376 membranes and, consequently, cause cellular disorder in the cell's physical parameters.



378

379 **Figure 1.** The membrane permeabilization analysis by PI uptake assay, membrane pore
 380 formation by uptake of a 6-kDa Dextran-FITC, and ROS overaccumulation in AGP-01
 381 cells after treatment with RcAlb-PepI.

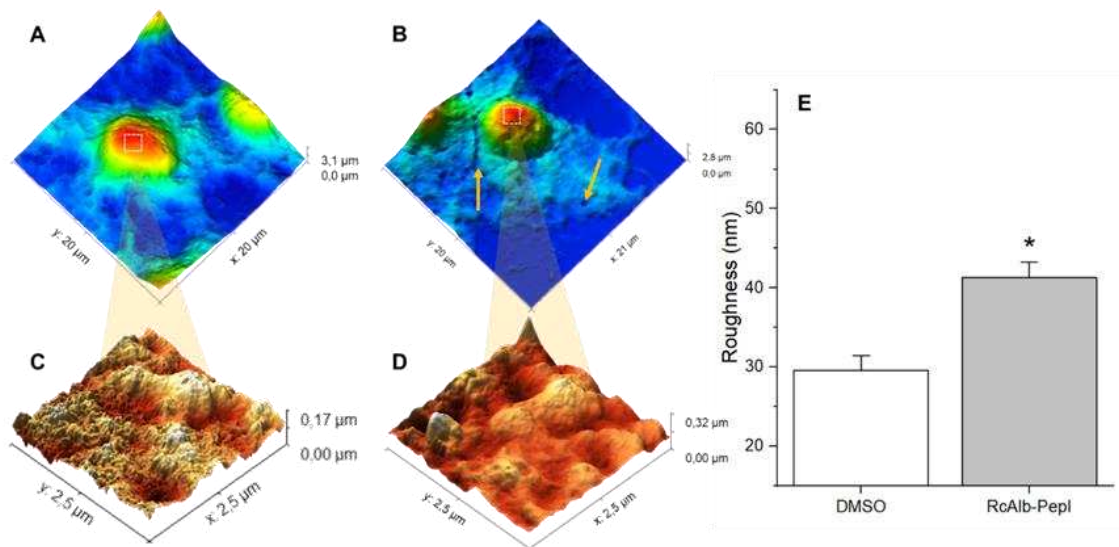
382

383 **3.4 RcAlb-PepI induces morphological, nanomechanical and ultrastructural** 384 **changes in AGP-01 cells**

385

386 To shed more light on the mechanism of action of RcAlb-PepI, AFM analysis was
 387 performed in AGP-01 cells treated with RcAlb-PepI to evaluate change in cell
 388 morphology, nanomechanical and ultrastructural aspects. AFM scan on control AGP-01
 389 cells revealed no damage to cell structure and morphology, with a good shape (Fig. 2A).
 390 No apparent damage in control AGP-01 cells was seen even in a 20 μm^2 scan (Fig. 2A).
 391 In contrast, RcAlb-PepI-treated AGP-01 AFM analysis revealed several damages to the
 392 morphology of AGP-01 cells, including an increase in roughness of treated cell compared
 393 to control (Fig. 2B). At a microscopic level, it is already possible to observe changes, such
 394 as pores and cracks, in the peripheral cell membrane (yellow arrows), possibly caused by
 395 the action of the RcAlb-PepI on the membrane of AGP-01 cells (Fig. 2B). Fig. 2C and D

396 show, respectively, a $2.5 \mu\text{m}^2$ zoom in the cell body region of each of the respective
397 images (A [AGP-01 control] and B [AGP-01 treated]), highlighting the nanoscopic
398 ultrastructural changes in the cell membrane caused by the action of the RcAlb-PepI.
399 Quantification of roughness (R_q) revealed an increase in roughness from 29.6 nm in
400 control cells to 41.3 nm in treated cells, indicating damage in the cell surface (Fig. 2E).

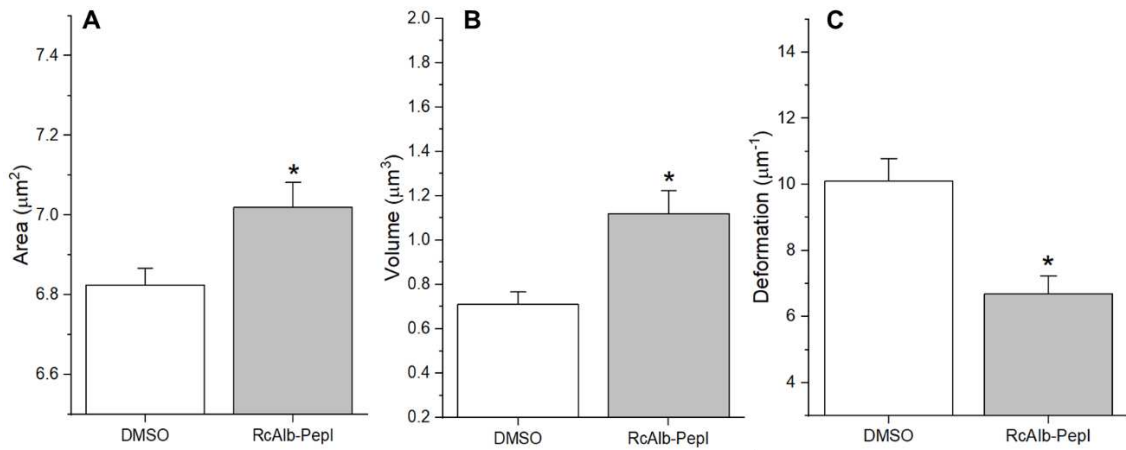


401

402 **Figure 2.** AFM analysis of AGP-01 cells control and treated with RcAlb-PepI. (A) 20
403 μm^2 scan of control AGP-01 cells. (B) $20 \mu\text{m}^2$ scan of AGP-01 cells treated with RcAlb-
404 PepI. Images (C) and (D) show, respectively, a $2.5 \mu\text{m}^2$ zoom in the cell body region of
405 each of the respective images (A and B). (E) Average R_q graph for all analyzed samples
406 from each group. Data are represented as mean \pm standard error. Statistically significant
407 differences by ANOVA followed by the Turkey post-test: * $p < 0.05$.

408

409 Ultrastructural analysis obtained by AFM revealed more interesting results (Fig.
410 3). The ultrastructural analysis of AGP-01 cell surface revealed that cells treated with
411 RcAlb-PepI have significant ($p < 0.05$) increase in area (Fig. 3A) and volume (Fig. 3B)
412 compared to control AGP-01 cells. The most interesting result of ultrastructure was about
413 the deformation of AGP-01 cells. After treatment with RcAlb-PepI, there was an evident
414 decrease in deformation of AGP-01 cells compared to the control treatment (Fig. 3C).

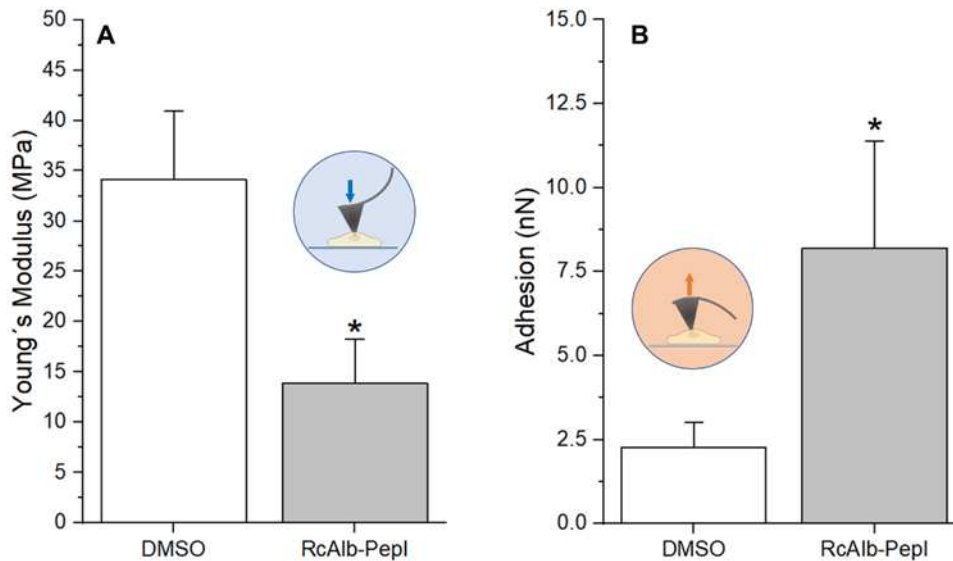


415

416 **Figure 3 – Ultrastructural parameters obtained by AFM maps.** (A) Surface area graph
 417 (measured by triangulation) of cell membranes from untreated and RcAlb-PepI-treated
 418 AGP-01 gastric cancer lines. (B) The volume plot was obtained by AFM standardized
 419 map ($2.5 \mu\text{m}^2$), calculated as the integral of the surface height of each map over the map
 420 area. The average volume values were calculated for the respective groups. (C) The cell
 421 deformation graph is calculated from the geometric parameters of the cell. The average
 422 deformation values were calculated for the respective groups. Data are represented as
 423 mean \pm standard error. Statistically significant differences by ANOVA followed by the
 424 Turkey post-test: * $p < 0.05$.

425

426 Nanomechanical data obtained by AFM analysis revealed contrasting but
 427 important results (Fig. 4). The nanomechanical analysis revealed a reduction in Young's
 428 modulus (YM) value, which indicates changes in the cytoskeleton, in AGP-01 cells after
 429 treatment with RcAlb-PepI compared to control cells (Fig. 4A). In contrast, the adhesion
 430 ability of AGP-01 increases after treatment with RcAlb-PepI compared to control AGP-
 431 01 cells (Fig. 4B).



432

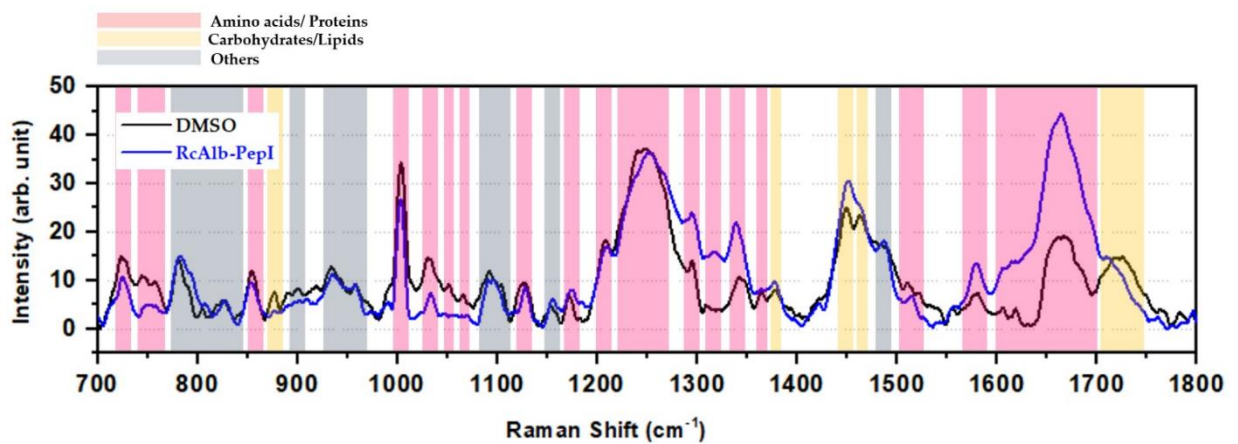
433 **Figure 4 – Nanomechanical parameters obtained from AFM maps. (A)** Young's
 434 modulus (YM) plot of control and RcAlb-PepI-treated AGP-01 cells. The representative
 435 figure in the inset shows the behavior of the probe during MY measurements
 436 (indentation). **(B)** Graph of adhesion forces between the AFM probe and the cell membrane
 437 surface. The average adhesion force values for the control and RcAlb-PepI-treated AGP-01. The
 438 representative figure in the inset shows the behavior of the probe during the adhesion
 439 measurements (retraction cycle). Data are represented as mean \pm standard deviation. Statistically
 440 significant differences by ANOVA followed by the Turkey post-test: * $p < 0.05$.

441

442 3.5 RcAlb-PepI alters the vibrational signature of AGP-01 cells

443 The Raman spectroscopic analysis revealed several changes in the surface of
 444 AGP-01 cells treated with RcAlb-PepI (Fig. 5 and Table 3). In the spectra (Fig. 5), it is
 445 possible to identify vibrational modes of the fundamental biochemical components that
 446 make up these cellular structures: lipids, proteins and nucleic acids. In the spectral region
 447 from 700 to 770 cm^{-1} , we notice vibrational modes related to proteins such as the
 448 Tyrosine, Phenylalanine and Tryptophan modes. The presence of Amide bands, the 1347
 449 cm^{-1} mode, attributed to amide III, the 1554 cm^{-1} mode, related to Amide II and the 1667
 450 cm^{-1} mode, which is attributed to Amide I, which are composed of atoms of carbon,
 451 oxygen and nitrogen (CONH), plays a crucial role in the formation of proteins by forming
 452 crucial bonds that confer structural rigidity and also provides information about the
 453 organization of secondary structure in actin filaments.

454 Furthermore, bands corresponding to lipids were identified (877 cm⁻¹, 1377 cm⁻¹,
 455 1449 cm⁻¹, 1462 cm⁻¹ and 1726 cm⁻¹), indicating the treatment with RcAlb-PepI led to a
 456 change in lipids pattern in membranes. These modes reflect the composition, organization
 457 and structure of lipids in samples. The wavelength for each of the bases is listed in Table
 458 3.
 459



460 **Figure 5 – Vibrational Signature of AGP-01 cells.** The Raman spectra of AGP-01 cells
 461 control- (black line) and RcAlb-PepI-treated (blue line).
 462

463 **Tabela 1.** Atribuições de cada modo do espectro Raman

464

Wavenumber (cm ⁻¹)	Amino acid/ Protein	Lipid/ Carbohydrate	Other
724	C – S protein CH ₂ rocking, Adenine		
744	Tryptophan		
780			Cytosine/Uracil
805			Uracil
826			Phosphodiester
854	Tyrosine		
877		C – C – N sym. str.	
900	Adenine		
934			C – C backbone
958			Carotenoids

1003	Phenylalanine		
1031	Phenylalanine		
1053	C – O stre., C – N str.		
1066	Proline		
1092			Phosphodioxy
1128	C – N str.		
1153			Carotenoids
1172	Tyrosine		
1208	Tryptophan/ Phenylalanine		
1247	Amide III		
1295	CH ₂ def.		
1342	CH def.		
1364	Tryptophan		
1377		δ CH ₃ sym.	
1449		C – H vib.	
1462		CH ₂ / CH ₃ def.	
1489			Collagen
1512			Cytosine
1554	Amide II		
1581	C – C str.		
1606	Tyrosine		
1618	Tryptophan		
1667	Amida I		
1726		Triacylglycerols	

465

466 Abbreviation: str. = stretching, sym. = symmetric, asym. = asymmetric, def = deformation

467

468 **3.6 RcAlb-PepI reduces the migration of AGP-01**

469 A wound healing assay was performed to evaluate the antimigratory effect of

470 RcAlb-PepI. However, previously, it was necessary to evaluate if the IC₅₀ concentration

471 (53.87 $\mu\text{g mL}^{-1}$) of the RcAlb-PepI peptide presents inhibitory activity on AGP-01 cells

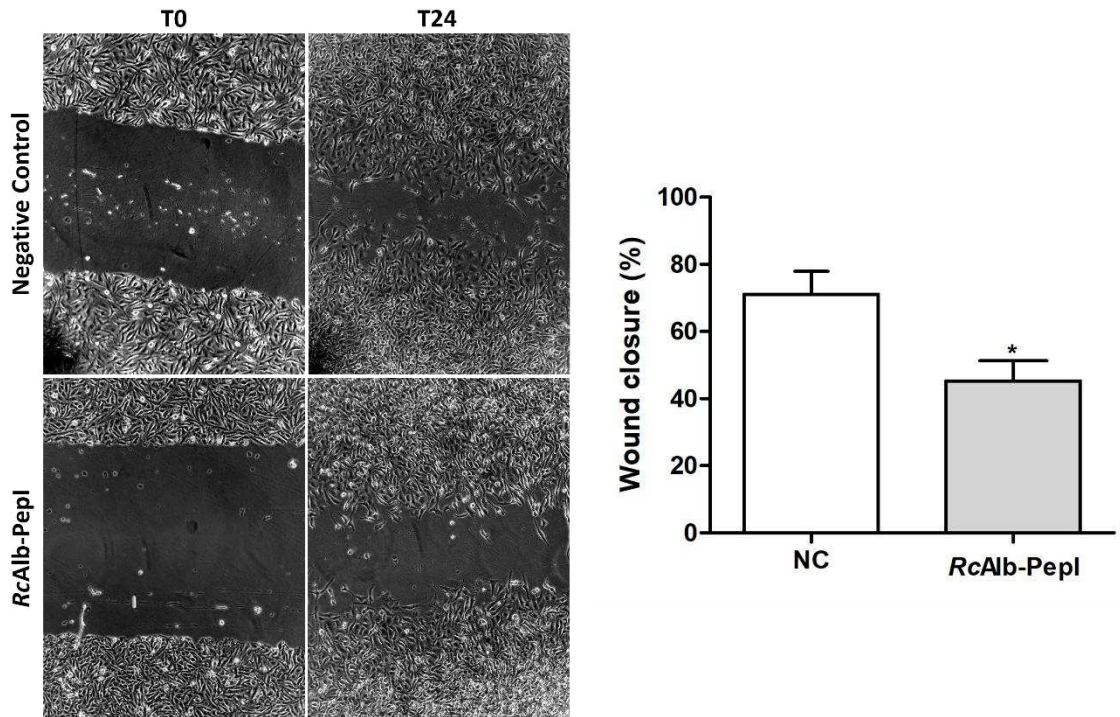
472 within 24 hours, which constitutes the treatment time used in the cell migration assay

473 (Supplementary Figure 1). As seen in Supplementary Figure 1, this concentration does

474 not inhibit cells within 24 hours. Therefore, the wound healing assay can be performed

475 using this concentration of RcAlb-PepI.

476 The wound healing assay results indicate that, after a 24-hour incubation, RcAlb-
477 PepI demonstrated 45% wound closure, compared to 71% achieved by the control group.
478 Therefore, RcAlb-PepI inhibited 26% of the wound closure (migration) of AGP-01 cells
479 (Fig. 6).



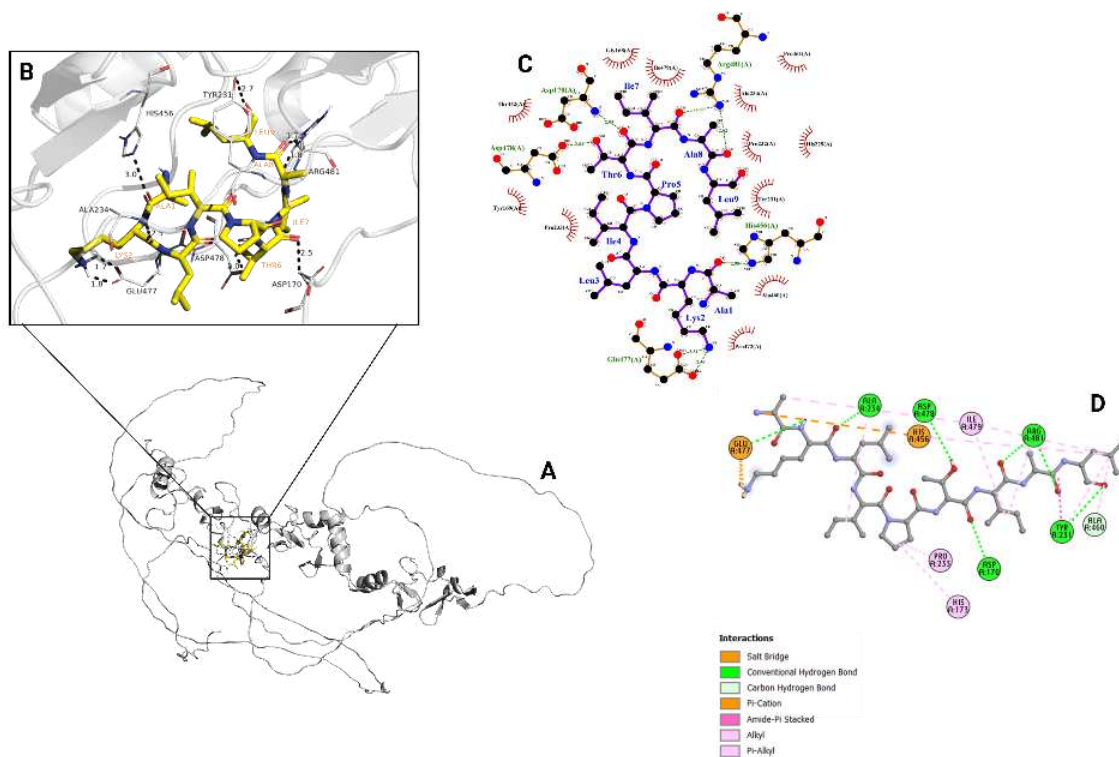
480

481 **Figure 6 – Migration assay of AGP-01 cells.** Wound healing graph according to the
482 percentage of wound closure related to cell migration. Large, scratched areas indicate
483 migratory inhibition. Wound healing images showing migration inhibition activity of
484 RcAlb-PepI. AGP-01 was incubated with DMSO at a non-toxic concentration, the
485 negative control n as related in the methodology.

486 3.7. Molecular Docking Assay

487 Recently, our research developed a pipeline to find new druggable targets in GC
488 ¹⁶. The genes overexpressed in AGP-01 cell lines were Ajuba and NOLC1. Therefore,
489 RcAlb-PepI was assayed by MD analysis to evaluate if it could interact with those targets.
490 In the MD analysis of the AJUBA protein complex and the RcAlb-PepI peptide, it was
491 obtained an RMSD of 0.694 Å, indicating the RcAlb-PepI caused changes in the 3D
492 structure of AJUBA protein (Fig. 7A). Yet, it was possible to identify the presence of polar
493 interactions such as conventional hydrogen bonds with residues Asp⁴⁷⁸, Arg⁴⁸¹, Asp¹⁷⁰,
494 Ala²³⁴ and Tyr²³¹ (Fig. 7B), in addition to hydrogen interactions that also performed Pi-
495 Alkyl type interactions, two interactions with the Glu⁴⁷⁷ residue, one being a conventional
496 bond and the other a salt bridge, the His⁴⁵⁶ residue also performing salt bridge and alkyl
497 type interactions, the residues Pro²³³, His¹⁷³ and Ile⁴⁷⁹ performed apolar interactions of
498 the Alkyl type. Visualizing a Carbon Hydrogen type covalent bond with residue Ala460
499 was possible. It was possible to identify hydrophobic contacts with residues Thr⁴⁴²,
500 Gly¹⁶⁸, Pro¹⁶¹, Pro²³², His²²⁹, Pro⁴⁷² and Tyr¹⁶⁹ (Fig. 7C and D).

501 In the complex formed by the NOLC1 protein and the RcAlb-PepI peptide, we
502 obtain the value of RMSD 0.805 Å, also indicating a change in the 3D structure of
503 NOLC1 protein (Fig. 8A). It was possible to visualize conventional hydrogen interactions
504 with residues Asn³⁶¹ and Glu³⁵³ (Fig. 8B), which in addition to this interaction carried out
505 salt bridge type bonds as well as residues Asp³⁵⁵ and Glu⁴¹⁸, we identified nonpolar Alkyl-
506 type interactions with residues Ile³⁵², Val³⁴⁷, Val³⁵⁴ and Val³⁵⁸. We visualized hydrophobic
507 contacts with residue Asp³⁶⁰ (Fig. 8C and D).



508

509

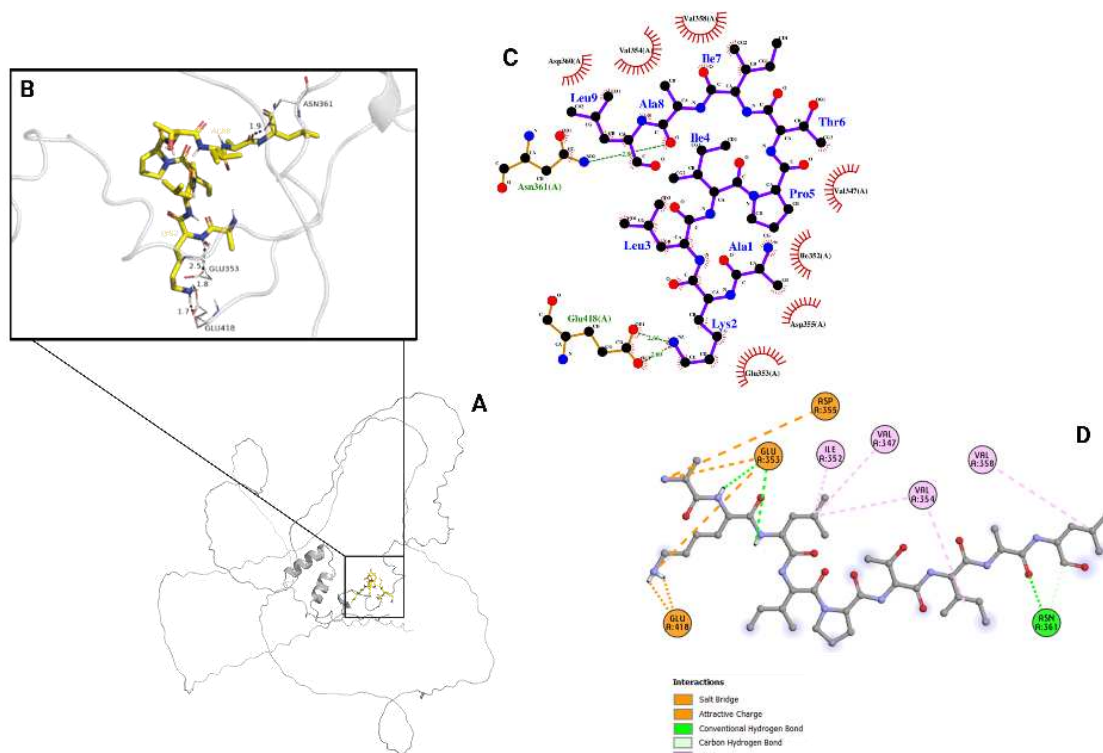
510 **Figure 7. Molecular docking analysis between AJUBA and RcAlb-PepI.** (A) the
 511 AJUBA protein in cartoon format in gray and the RcAlb-PepI peptide in stick format
 512 in yellow. (B) zoomed image in a 3D format showing the interactions that support the
 513 Peptide-Protein complex, the amino acid residues, and the distance in angstrom of the
 514 interaction bridges. (C) Image generated by the LigPlot+ software for 2D visualization of
 515 the hydrophobic interactions between the peptide and the protein. (D) 2D image produced
 516 using the Discovery Studio Visualizer software where it is possible to identify the
 517 interactions of the Peptide-Protein complex and the types of bonds.

518

519

520

521



522
 523
 524
 525
 526
 527
 528
 529
 530
 531
 532

Figure 8. Molecular docking analysis between NOLC1 and RcAlb-PepI. (A) the NOLC1 protein in cartoon format in gray and the RcAlb-PepI peptide in stick format in yellow. (B) zoomed image in 3D shows the interactions that support the Peptide-Protein complex, the amino acid residues, and the distance in the angstrom of the interaction bridges. (C) Image generated by the LigPlot+ software for 2D visualization of the hydrophobic interactions between the peptide and the protein. (D) 2D image produced using the Discovery Studio Visualizer software where it is possible to identify the interactions of the Peptide-Protein complex and the types of bonds.

533 3.8 RcAlb-PepI is not toxic to healthy cells and zebra-fish

534 Seeking a possible clinical application for RcAlb-PepI, their toxicity to human
 535 cells was assessed (Figure 9). Additionally, it was experimented to evaluate if RcAlb-
 536 PepI, even at a concentration 20 times (1 mg mL^{-1}) higher than IC_{50} , could cause damage
 537 to the DNA of human cells by comet assay (Fig. 9A-C). Three cell lines: L929 fibroblast
 538 (Fig. 9A) cells from mice and two human lines – human fetal lung fibroblast (MRC-5-
 539 line, Fig. 9B) and human keratinocytes (HaCaT line, Fig. 9C). RcAlb-PepI did not cause
 540 any DNA damage (Figure 9A-C). On the other hand, the MMS ($4 \times 10^{-5} \text{ M}$) agent caused
 541 severe damage to the DNA from all cell lines (Figure 9A-C).

542 At the same concentration of RcAlb-PepI, it was analyzed to see if the peptide
543 induces apoptosis in the same cell lines (Fig. 9D-F). As expected, the cells treated with
544 RcAlb-PepI showed no signal of apoptosis of any kind (Fig. 9D-F), compared to cells
545 incubated with MMS at 4×10^{-5} M, which small cell volume, peripheral condensation of
546 chromatin, apoptotic bodies, and fragmented nucleus all characteristic of apoptosis
547 (Figure 9D-E).

548 Regarding the *in vivo* toxicity, the model used was a zebra-fish embryo (Fig. 10).
549 Zebrafish larvae and embryos presented a survival rate of $\geq 95\%$ after exposure to 1 mg
550 mL^{-1} of the RcAlb-PepI for 96 h (Fig. 10A). After 96 h of treatment, morphological
551 analysis revealed no alterations (nonlethal effects) in the embryos exposed to the control
552 (Figure 10B-D) and RcAlb-PepI (Figure 10E-G).

553
554
555
556
557
558
559
560
561
562
563
564
565
566
567
568
569
570
571
572
573
574
575
576
577
578
579
580
581
582
583
584

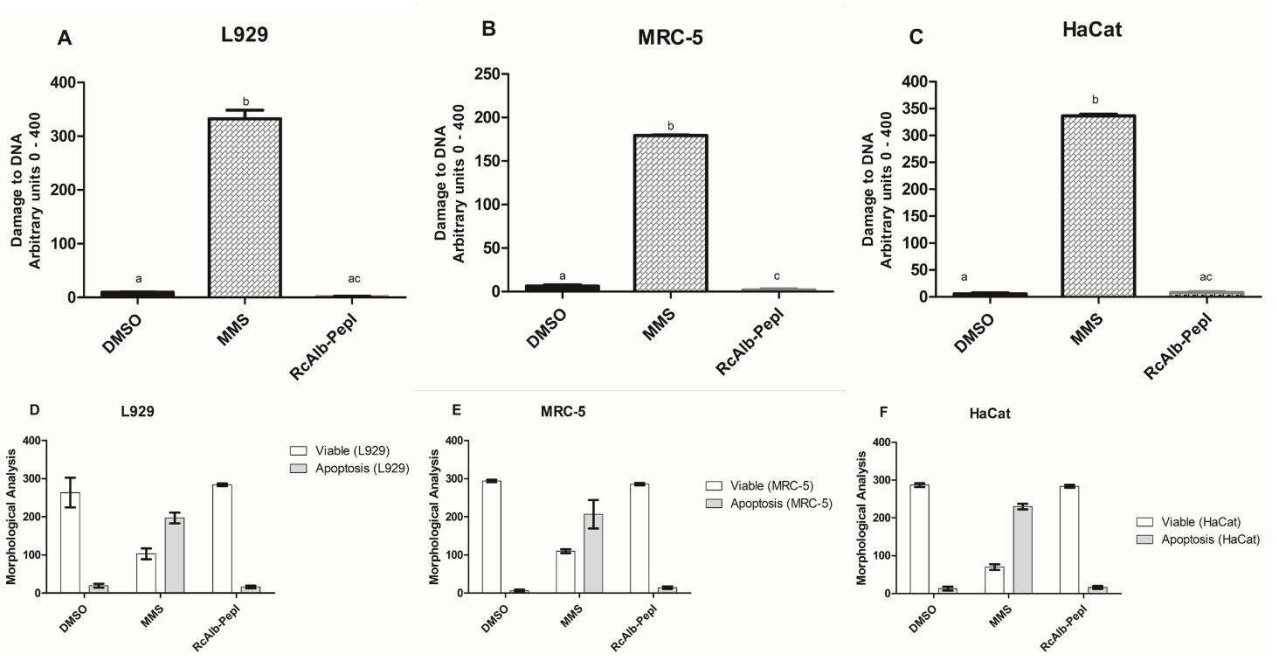
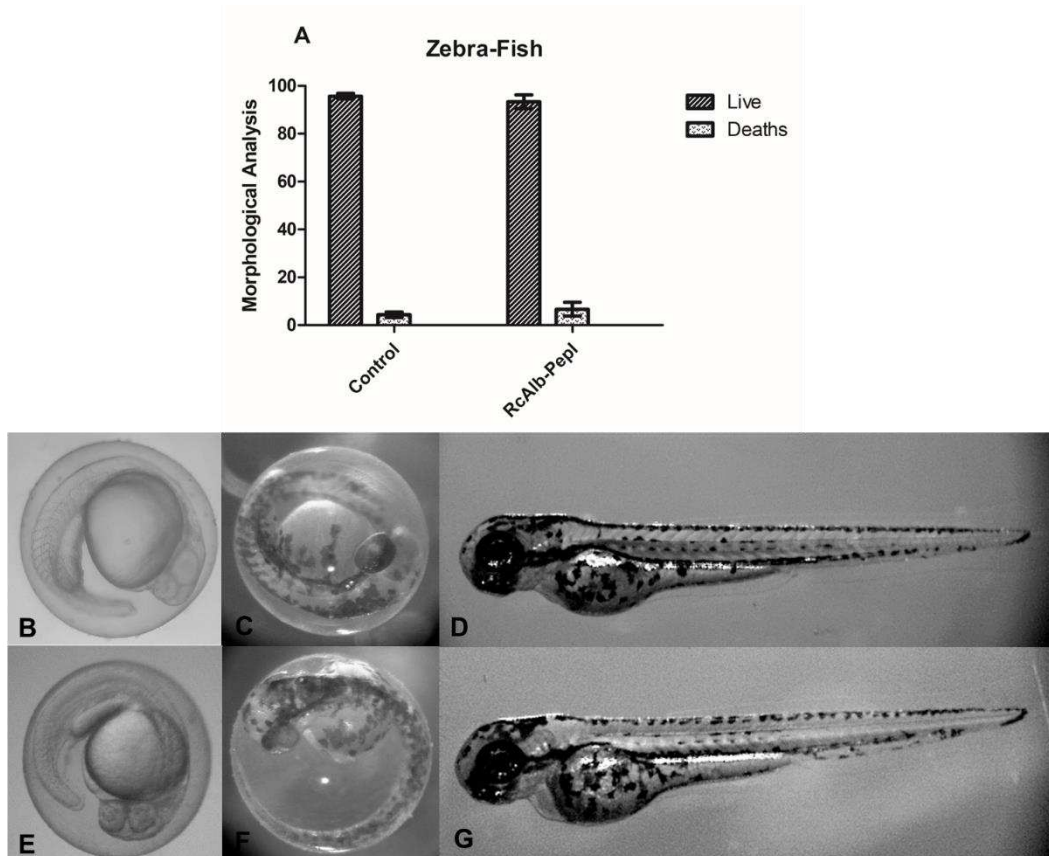


Figure 9. Toxicity of RcAlb-PepI to human cell lines. (A) L929, (B) MRC-5, and (C) HaCat lines incubated with RcAlb-PepI at a concentration of 1 mg mL testing damage to DNA by comet assay. In (D), (E), and (F) is the analysis induction of apoptosis in cell lines after incubation with RcAlb-PepI as described. Methyl methanesulphonate (MMS; 4×10^{-5} M) was the positive control for cell toxicity and healthy cells as the negative control for toxicity. Data are shown as mean \pm standard deviation of three independent experiments. *** $P < 0.001$.

585

586

587



588

589 **Figure 10. In vivo toxicity of *RcAlb-PepI* to Zebrafish embryos.** (A) the survival rate
590 (%) of zebrafish embryos and larvae after incubation with *RcAlb-PepI* (1 mg mL⁻¹) and
591 control (E3 medium) for 96 h. (B-D) represents the exposition to control medium E3 and
592 (E-G) to *RcAlb-PepI* for 96 h. Data are shown as mean ± standard deviation of three
593 independent experiments.

594

595 4. Discussion

596 Gastric cancer represents a significant public health challenge, being classified as
597 the fifth most common malignancy and the fourth leading cause of cancer-related
598 mortality worldwide²⁵. In 2020, the year in which GLOBOCAN released the latest
599 estimates, 1,089,103 new cases and 768,793 deaths from gastric cancer. These data,
600 together with the projected 62% increase in the global burden of gastric cancer by 2040
601 highlight the urgent need for advances in treatment to combat gastric cancer²⁶⁻²⁸.

602 Standard treatment for gastric cancer (GC) generally involves a multidisciplinary
603 approach that combines surgery, chemotherapy, and radiotherapy. Some therapeutic
604 regimens are well described in the literature and are widely used in the pharmacological
605 treatment of GC. Cytotoxic therapies include the FLOT regimen (5-fluorouracil,
606 leucovorin, oxaliplatin and taxane), the ECF regimen (epirubicin, cisplatin and
607 fluorouracil), FOLFOX (5-fluorouracil, leucovorin and oxaliplatin), infusion of cisplatin
608 (CF) and mono drug regimen with irinotecan^{29,30}. Substantial advances have been
609 achieved with anti-HER2 therapeutic agents²⁹, including trastuzumab, a humanized
610 monoclonal antibody that targets the extracellular domain 4 of HER2, which is the
611 standard choice for patients with advanced GC^{31,32}.

612 Although treatment for GC has gradually improved in recent decades, the
613 prognosis for most patients remains challenging. For example, a therapeutic regimen
614 involving docetaxel, cisplatin and 5-fluorouracil demonstrated a response of around 37%,
615 with a survival rate of 9.2 months. Furthermore, cytotoxic therapies are increasingly
616 restricted due to problems such as chemoresistance, low selectivity and, consequently,
617 high toxicity. In a phase III study, the superiority of triple therapy with
618 docetaxel/cisplatin/5-fluorouracil (DCF) revealed this combination was not
619 recommended in Asian guidelines due to its high toxicity^{19,33,34}.

620 To overcome these challenges, searching and developing new agents with
621 potential against GC that present low toxicity for healthy cells and patients is urgently
622 necessary. Another option is drug repositioning. Drug repositioning is an important
623 approach because it could reduce the time of drug application in addition to contributing
624 to produced drugs with low toxicity⁸. In this context, repositioning antimicrobial peptides
625 (AMPs) against cancer has been an alternative approach researchers use to combat cancer
626 resistance to chemotherapy^{8,35,36}.

627 Natural AMPs are low molecular weight defense compounds found in all living
628 organisms. Peptides have emerged as an alternative therapeutic because of their ability to
629 interact with constituents of the cell membrane¹⁰. However, due to the low resistance to
630 proteolysis, short half-life, and toxicity to the host, AMPs have faced problems during
631 clinical trials. Furthermore, high costs are associated with AMP purification, which limits
632 its use³⁷.

633 Based on that, synthetic antimicrobial peptides (SAMPs), strategically developed
634 to ensure high efficacy and low toxicity, emerged as a promising option to be repositioned
635 for cancer treatment^{8,9}. Advances in chemical synthesis have made synthetic peptides
636 viable for application. Additionally, there are other positive characteristics associated with
637 SAMPs, such as the low probability of developing resistance to anticancer peptides, as
638 these compounds are not limited to a single mechanism of action^{38,39} and the activation
639 of an antitumor immune response⁴⁰.

640 The SAMPs tested here are multifunctional peptides with activity against bacteria,
641 fungi, yeast, nematodes, and viruses^{9,41-43}. These were designed to achieve properties
642 essential for antimicrobial activity: low molecular mass, positive charge, and high
643 hydrophobicity⁹. They have also been tested against human red blood cells with no
644 toxicity^{11,12}. Here, before being tested against GC cell lines, the peptides were analyzed
645 by bioinformatics for the anticancer potential (Table 1). All were predicted as anticancer
646 peptides and then tested against GC cell lines to analyze the IC50 (Table 2). Out of six,
647 four peptides presented an IC50 to all GC cell lines tested (Table 2). Besides all the great
648 results, the SI²⁴ was employed to choose the best peptide for further analysis (Table 2).
649 The SI is calculated as a ratio of IC50 molecules for healthy and cancer cells. Molecules
650 with SI values higher than 1 possess great selectivity against cancer cells⁴⁴⁻⁴⁷. Except for
651 *Mo*-CBP3-PepI, which presented an SI value of 0.61 against GC line ACP-02, all peptides

652 presented SI >1 (Table 2), indicating higher selectivity to cancer cells than normal cells
653 (in our case is MNP-01). RcAlb-PepI was the peptide with the best SI value (1.95) against
654 the metastatic GC line, AGP-01 (Table 2), which is an interesting result. For example, the
655 SI value of RcAlb-PepI is 5.7-fold higher than the SI of bortezomib²⁴. Bortezomib is an
656 anticancer drug used to treat multiple myeloma^{48,49}. The results of SI highlight the
657 selective of RcAlb-PepI against AGP-01 cells.

658 RcAlb-PepI is a synthetic antimicrobial peptide designed based on the sequence
659 of Rc-2S-Alb¹², a 2S albumin purified from *Ricinus communis* seed cake⁵⁰. RcAlb-PepI
660 is a cell-penetrating peptide that can interact with plasmatic membranes and induce pore
661 formation with antibacterial, antifungal, and antiviral activities^{9,12,22,37}. The RcAlb-PepI
662 peptide exhibited a potent cytotoxic effect on all gastric cancer cell lines studied (Table
663 1), specifically and selectively toward the AGP-01 cell line (derived from primary
664 metastatic tumors of the intestinal type). Therefore, based on the data found, RcAlb-PepI
665 demonstrated efficacy in inhibiting the growth of gastric cancer cells and exhibited
666 selectivity in its cytotoxic effect, as higher concentrations are required to affect healthy
667 cells.

668 The ability to differentiate between cancer and healthy cells is crucial for potential
669 therapeutic agents, as it minimizes toxic effects on normal tissues⁵¹⁻⁵³. This phenomenon
670 suggests that the peptide may have a specific target or mechanism of action specific to
671 malignant cells. In this case, the selectivity observed is probably due to the difference in
672 membrane composition and charge in cancerous cells compared to healthy ones⁵⁴⁻⁵⁶. The
673 membrane of cancer cells presents a higher concentration of phosphatidylserine exposed
674 to the outside layer⁵¹⁻⁵³. The higher concentration of phosphatidylserine led to a negative
675 charge in the external portion of the membrane of cancer cells. This negative charge
676 increases your susceptibility to AMPs. RcAlb-PepI is a positively charged (+1) peptide¹²,

677 favoring its ionic attraction to cancer cell membranes. RcAlb-PepI was designed to be an
678 antimicrobial peptide. Based on the information that microbial membranes have lipids
679 with negatively charged exposed in the outer membrane, an arginine residue was inserted
680 to provide a liquid positive charge to RcAlb-PepI to provide a primary ionic attraction.
681 Additionally, apolar/hydrophobic amino acid residues were added for apolar/hydrophobic
682 interaction with the membrane core, allowing RcAlb-PepI to insert itself into the
683 membrane¹².

684 The experiment of PI uptake provides some information about the ability of
685 RcAlb-PepI to induce pore formation on the membrane of AGP-01 cells (Fig. 1).
686 However, PI has a small molecular weight of 668.4 Da, converting to nm is about 0.1 nm.
687 This is a very tiny pore, and it has been reported that cells could recover from it⁵⁷. An
688 additional experiment using FITC-Dextran with a size of 6-kDa (Fig. 1) strongly suggests
689 that RcAlb-PepI induces pore formation on the membrane of AGP-01 cells. To allow the
690 movement of FITC-Dextran through the membrane, the pore should have a size of at least
691 1.0 nm, considered a huge pore, where cells cannot recover⁵⁷. It has already been reported
692 that RcAlb-PepI could induce pores with a size of 6-kDa³⁷.

693 RcAlb-PepI has a molecular mass of 939.17 Da, so how is it possible to induce
694 the formation of a size with a size of 6-kDa? There is one feature of antimicrobial peptides
695 called self-association⁵⁸, where peptides could interact between them to induce huge
696 pores in the membrane⁵⁸. AFM analysis revealed that another peptide from the same
697 family of RcAlb-PepI, called RcAlb-PepIII, has the ability to interact between (RcAlb-
698 PepIII:RcAlb-PepIII complex) them to form a big structure during antihelminthic
699 activity⁵⁹.

700 AFM analysis corroborates the idea of pore formation on the membrane of AGP-
701 01 cells caused by RcAlb-PepI (Fig. 2B – yellow arrows). Additionally, to our knowledge,

702 this is the first study to point out the pore formation in cancer cells by atomic force
703 microscopy analysis. AFM analysis revealed many interesting results of the effects of
704 RcAlb-PepI on the AGP-01 cells. For example, AFM analysis revealed that the treatment
705 with RcAlb-PepI increases the roughness of the membrane from AGP-01 cells compared
706 to control cells. The increase in membrane roughness ultimately results from alterations
707 in the membrane's mechanical properties, which facilitates the pore formation in the
708 membrane⁶⁰⁻⁶³. Lara-Cruz et al.⁶⁰ reported by AFM that gold nanoparticles induce pore
709 formation on the membrane of breast cancer by inducing the roughness of the cell
710 membrane⁶⁰. This result is very similar to the one presented by RcAlb-PepI (Fig. 2).

711 The increase in roughness indicates alterations in the plasma membrane, which is
712 possible by contact of molecules with the cellular membrane⁶⁰. Based on that, it is feasible
713 to suggest that RcAlb-PepI interacts with a membrane of AGP-01 cells, leading to change
714 that ultimately increases membrane roughness and pore formation. Lara-Cruz et al.⁶⁰,
715 based on AFM analysis, strongly suggest a positive correlation between an increase in
716 roughness and pore formation, leading to the internalization of gold nanoparticles inside
717 cancer cells. Here, we show that RcAlb-PepI induced the formation of a pore with a size
718 of 6-kDa Fig. 1. Based on the information that RcAlb-PepI has a size of 939.17 Da¹², it
719 is feasible to hypothesize that RcAlb-PepI could move through the pore formed in the
720 membrane and find the intracellular target, which is possible to be DNA molecules once
721 bioinformatics analysis predicted that RcAlb-PepI could interact with DNA molecules
722 (Table 1).

723 Another result that reinforces the idea of pore formation caused by RcAlb-PepI
724 on the membrane of AGP-01 cells is driven by the increase in roughness is the fact that
725 RcAlb-PepI did not induce ROS overcalculation on AGP-01 cells. There are two ways of
726 inducing pore formation in cells: ROS-dependent or ROS-independent¹². Altogether, the

727 data suggest that the pore formation induced by RcAlb-PepI is ROS-independent once it
728 is related to an increase in the roughness of the membrane (Fig. 2). It is important to notice
729 that, by attacking the cellular membrane, RcAlb-PepI makes difficult the development of
730 resistance by cancer cells. In contrast to other drugs that affect one protein or biochemical
731 pathway, which is easy for cancer cells to change, targeting membrane makes it hard to
732 acquire resistance. The cell membrane is highly conserved in all cells through the
733 evolution course, and its change could be highly dangerous and have a high energy cost
734 to the cell⁶⁴.

735 AFM analysis brought more interesting results. Ultrastructural analysis revealed
736 that the area and volume of RcAlb-PepI-treated AGP cells are higher than control-treated
737 cells (Fig. 3A and B). Cell volume regulation is important to metastatic cancer cell
738 migration⁶⁵. During migration, metastatic cancer cells increase the transporter protein
739 expression on the membrane to control the osmotic potential to favor migration and, thus,
740 invasion⁶⁵. Controlling the water flow through the membrane is important to driving
741 forces for the migration process. Any dysregulation in this process could interfere with
742 this process and thus affect and even inhibit the migration of this process⁶⁵. Under osmotic
743 dysregulation, the migration process of cells is affected⁶⁵. The increase in the volume and
744 consequent surface (Fig. 3A and B) of AGP-01 after treatment with RcAlb-PepI could be
745 a result of osmolarity stress caused by the pores formed on the membrane leading to an
746 influx of water leading to cell swelling of AGP-01 cells⁶⁵. Here, AFM ultrastructural
747 analysis revealed that RcAlb-PepI interferes in the dynamic of AGP-01 volume
748 suggesting this is a mechanism to inhibit cell migration.

749 As discussed above, AGP-01 is a metastatic cell form of GC. Normally, metastatic
750 cancer cells have a high deformation rate that allows the movement through tiny gaps in
751 tissues during migration and invasion⁶⁶⁻⁶⁸. Based on that, over the years, there has been

752 an increase in interest in the mechanical behavior of cancer cells, mainly metastatic
753 ones^{67,68}. For example, Remmerbach et al.⁶⁸ proposed employing mechanical
754 phenotyping to diagnose oral squamous carcinomas.

755 Here, AFM analysis revealed that RcAlb-PepI reduces the deformation rate of
756 AGP-01 cells compared to control (Fig. 3C). Deformation is positively correlated with
757 cell flexibility required to move through space between tissues⁶⁶⁻⁶⁸. Therefore, by
758 reducing the deformation rate in AGP-01 cells, RcAlb-PepI also reduces its flexibility,
759 turning the AGP-01 cell into a rigid cell, like non-cancerous cells, making its movement
760 and invasion difficult. Besides that, deformation is also important to cancer cells evade
761 from immune system and resistance to chemotherapy drugs⁶⁹.

762 Young's modulus is another result that corroborates the changes in the deformation
763 of AGP-01 cells. RcAlb-PepI also reduced the Young's modulus of AGP-01 cells
764 compared to the control (Fig. 4A). Both the deformation rate and Young's modulus are
765 important to maintain the flexibility of metastatic cancer cells movement and invasion of
766 tissue⁶⁶. Hu et al.⁶⁶, studying the physical properties of cancer cells, reported a positive
767 correlation between deformation rate and Young's modulus, and those parameters are high
768 in metastatic cancer cells compared to non-metastatic cancer cells⁶⁶. Therefore, a positive
769 correlation was found in AGP-01-treated RcAlb-PepI, in which the deformation rate and
770 Young's modulus decreased (Figs. 3C and 4A).

771 It is well-known that the cytoskeleton in cancer cells presents a different behavior
772 than healthy cells, for example, deformation. These differences are even more prominent
773 between non-metastatic and metastatic cancer cells. The cytoskeleton assumes an
774 abnormal conformation in cancer cells to sustain cell deformation⁶⁹⁻⁷¹. The reduction in
775 the Young's modulus in AGP-01 after contact with RcAlb-PepI suggests and
776 disorganization of the cytoskeleton induced by the peptide, resulting in the deformation

777 rate of AGP-01, which ultimately affects AGP-01 movement (Fig. 6) and probable
778 invasion.

779 A nanomechanical property evaluated by AFM was the adhesion of AGP-01 cells
780 after treatment with RcAlb-PepI (Fig. 4B). The treatment of AGP-01 with RcAlb-PepI
781 increased its adhesion 3-fold compared to control. The adhesion dynamic in cancer cells
782 differs from healthy cells⁷². For metastatic cells, adhesion dynamics are important for
783 cells to evade the initial tissue where the cancer was established and invade and adhere to
784 the extracellular matrix from a new tissue, thus metastasis^{72,73}. By increasing the adhesion
785 of AGP-01, RcAlb-PepI may inhibit AGP-01 cells from spreading to other tissues, thus
786 preventing metastasis.

787 The Raman spectroscopic analysis provided the vibrational signature of AGP-01
788 cells treated and non-treated with RcAlb-PepI (Fig. 5 – Table 3). The treatment with
789 RcAlb-PepI changes the vibrational signature of AGP-01 cells. The differences in the
790 vibrational signature of AGP-01 treated revealed mainly alteration components, such as
791 proteins and lipids in the cell membrane^{74–76}. It is noticed alterations in the tryptophan
792 (744 cm^{-1}), tyrosine (850 cm^{-1}), phenylalanine (1003 and 1031 cm^{-1}) proline (1066 cm^{-1}),
793 and L-tyrosine (1200 nm^{-1}) (Fig. 5 and Table 3). These modifications in the signature of
794 AGP-01 cells after treatment with RcAlb-PepI suggest modifications in the pattern of
795 glycoproteins in the membrane of AGP-01^{75,76}. The data also suggest the presence of
796 deformation in the signature of treated cells around 1295 and 1342 cm^{-1} , which is related
797 to proteins in the membrane^{74,76}.

798 Yet a signature modification related to polysaccharides (877 cm^{-1}) lipids (1305
799 cm^{-1} and 1450 cm^{-1}) is also seen. These modifications in the lipids indicate that peptides
800 are acting by altering the lipid organization in the membrane, altering its dynamics. The
801 information on the changes in the protein and lipids signatures in the membrane of AGP-

802 01 cells treated with the peptide provides a clue about how the RcAlb-PepI induces pore
803 formation (Figs. 1 and 2B), alters the surface increases the roughness of AGP-01 cells
804 (Fig. 2C and E) and alter the ultrastructure e nanomechanics of AGP-01 cells (Figs. 3 and
805 4).

806 All the information seen in the ultrastructural and nanomechanical analysis was
807 corroborated by the migration assay (Fig. 6). RcAlb-PepI inhibited the migration of AGP-
808 01 cells. This result agrees with all analyses discussed above. The migration is an
809 important part of establishing metastasis^{77,78}. The migration process is important for
810 metastatic cancer cells to move from the initial cancer establishment to a potential new
811 site to initiate metastasis⁷⁷. By inhibiting the migration process RcAlb-PepI reduced the
812 probability of AGP-01 cell move and establish metastasis.

813 Looking for new potential targets, RcAlb-PepI was submitted to MD assays
814 against proteins from gastric cancer (Figs. 7 and 8). Recently, our research group reported
815 by bioinformatic analysis new genes that are hyperexpressed in gastric cancer (Brito et
816 al., 2023). AJUBA and NOLC1 were confirmed by RT-qPCR being expressed in AGP-01
817 cells compared to MNP-01 cells¹⁶. The AJUBA protein is involved in processes such as
818 protein assembling, regulation of gene expression, migration, cell adhesion, proliferation,
819 and differentiation⁷⁹. The other one, NOLC1 (nucleolar and coiled-body phosphoprotein
820 1), involves several nuclear processes such as DNA replication, RNA synthesis, and cell
821 cycle regulation⁸⁰.

822 The most important result was that interacting with both proteins (Fig. 7 and 8),
823 RcAlb-PepI induced conformational change in the 3D structure of these proteins, as
824 noticed by changes in the RMSD value. As it is known, changes in the 3D structure alter
825 (mostly inhibit) the protein activity. AJUBA and NOLC1 are both highly expressed in
826 AGP-01 cells than in MNP-01 cells¹⁶. As such, it is feasible to suggest both play an

827 essential role in AGP-01 growth. By inhibiting both, their function will not be available
828 to AGP-01, making its establishment hard. For example, by interacting with the AJUBA
829 protein, RcAlb-PepI could affect cell migration, which was confirmed by migration assay
830 (Fig. 6). By interacting with NOLC1, RcAlb-PepI could interfere in the process involved
831 in cell cycle arrest by which could drive AGP-01 cells to apoptosis.

832 There are no doubts about the anticancer action of RcAlb-PepI against AGP-01;
833 this action probably occurs in multiple ways. One critical point for considering RcAlb-
834 PepI as a potential molecule against cancer is the absence of toxicity. Bioinformatics
835 analysis predicted that RcAlb-PepI is non-toxic with an LD50 of 2000 mg kg⁻¹ (Table 1).
836 Dias et al., 2020 reported that RcAlb-PepI was not toxic to human erythrocytes. To get
837 more information about the potential safety of RcAlb-PepI was tested *in silico* (Table 1),
838 *in vitro* (Fig. 9). *In vivo* (Fig. 10). *In vitro* tests against human cells showed that RcAlb-
839 PepI, even at concentration (1 mg mL⁻¹) 20x times higher than IC50 was not toxic to
840 fibroblast and keratinocytes (Fig. 9). *In vivo* analysis on showed that RcAlb-PepI is not
841 toxic embryos and larvae of zebra-fish corroborating the absence of toxicity even at
842 higher concentration.

843

844 **5. Conclusions**

845 Our results showed that RcAlb-PepI possesses an anticancer potential against a
846 metastatic line of gastric cancer. RcAlb-PepI acts by multiple mechanisms of action that
847 induce pores on the membrane of cells to alter the ultrastructure and nanomechanical
848 properties that ultimately inhibit cell migration. *In vivo* and *in vitro* studies showed that
849 RcAlb-PepI presents no toxicity to healthy human cells, embryos and larvae of zebrafish.
850 Altogether, the results suggest the potential of RcAlb-PepI as anticancer molecules to
851 develop potential new drugs.

852 **Funding and Acknowledgments**

853 This work was supported by the National Council for Scientific and Technological
854 Development (CNPq) for a research grant to Felipe P. Mesquita (Process number:
855 421392/2023-1), for a research productivity grant to Raquel C. Montenegro (Process
856 number: 305459/2019-8), Pedro F. N. Souza (Process number: 305003/2022-4), Raquel
857 C. Montenegro also thanks Red Latinoamericana de Implementación y Validación de
858 guías clínicas Farmacogenómicas (RELIVAF) for supporting this work. We also thank
859 the Office of Coordination for the Improvement of Higher Education Personnel (CAPES)
860 and the Cearense Foundation to Support Scientific and Technological Development
861 (FUNCAP) for grants given to students.

862

863 **Conflict of interest**

864 All authors declare no conflict of interest.

865

866 **Data availability**

867 The datasets analyzed during the current study are available under request of the
868 corresponding author.

869 **References**

- 870 1. GLOBOCAN 2020: New Global Cancer Data | UICC. Available at:
871 <https://www.uicc.org/news/globocan-2020-new-global-cancer-data>. (Accessed:
872 9th February 2024)
- 873 2. Sung, H. *et al.* Global Cancer Statistics 2020: GLOBOCAN Estimates of Incidence
874 and Mortality Worldwide for 36 Cancers in 185 Countries. *CA. Cancer J. Clin.* **71**,
875 209–249 (2021).
- 876 3. Sexton, R. E., Al Hallak, M. N., Diab, M. & Azmi, A. S. Gastric cancer: a

- 877 comprehensive review of current and future treatment strategies. *Cancer*
878 *Metastasis Rev. 2020 394* **39**, 1179–1203 (2020).
- 879 4. Teng, Y. *et al.* Ultraviolet Radiation and Basal Cell Carcinoma: An Environmental
880 Perspective. *Front. public Heal.* **9**, (2021).
- 881 5. Borges da Silva, E. *et al.* Micronucleus assay for predicting side effects of
882 radiotherapy for cervical cancer. *Biotech. Histochem.* **96**, 60–66 (2021).
- 883 6. Vasan, N., Baselga, J. & Hyman, D. M. A view on drug resistance in cancer.
884 *Nature* **575**, 299–309 (2019).
- 885 7. Derbal, Y. The Adaptive Complexity of Cancer. *Biomed Res. Int.* **2018**, (2018).
- 886 8. de Almeida Gomes, I. *et al.* Recalculating the Route: Repositioning Antimicrobial
887 Peptides for Cancer Treatment. *Chem. Biodivers.* **202301840**, (2023).
- 888 9. Souza, P. F. N. *et al.* Synthetic antimicrobial peptides: From choice of the best
889 sequences to action mechanisms. *Biochimie* **175**, 132–145 (2020).
- 890 10. Liscano, Y. *et al.* Peptides with Dual Antimicrobial–Anticancer Activity:
891 Strategies to Overcome Peptide Limitations and Rational Design of Anticancer
892 Peptides. *Mol. 2020, Vol. 25, Page 4245* **25**, 4245 (2020).
- 893 11. Oliveira, J. T. A. *et al.* Mo-CBP3-PepI, Mo-CBP3-PepII, and Mo-CBP3-PepIII are
894 synthetic antimicrobial peptides active against human pathogens by stimulating
895 ROS generation and increasing plasma membrane permeability. *Biochimie* **157**,
896 10–21 (2019).
- 897 12. Dias, L. P. *et al.* RcAlb-PepII, a synthetic small peptide bioinspired in the 2S
898 albumin from the seed cake of *Ricinus communis*, is a potent antimicrobial agent
899 against *Klebsiella pneumoniae* and *Candida parapsilosis*. *Biochim. Biophys. Acta*
900 *- Biomembr.* **1862**, 183092 (2020).
- 901 13. Tyagi, A. *et al.* In Silico Models for Designing and Discovering Novel Anticancer

- 902 Peptides. *Sci. Reports 2013 31* **3**, 1–8 (2013).
- 903 14. Szilágyi, A. & Skolnick, J. Efficient prediction of nucleic acid binding function
904 from low-resolution protein structures. *J. Mol. Biol.* **358**, 922–933 (2006).
- 905 15. Banerjee, P., Eckert, A. O., Schrey, A. K. & Preissner, R. ProTox-II: a webserver
906 for the prediction of toxicity of chemicals. *Nucleic Acids Res.* **46**, W257–W263
907 (2018).
- 908 16. Brito, D. M. S. *et al.* A Shortcut from Genome to Drug: The Employment of
909 Bioinformatic Tools to Find New Targets for Gastric Cancer Treatment.
910 *Pharmaceutics* **15**, (2023).
- 911 17. Desta, I. T., Porter, K. A., Xia, B., Kozakov, D. & Vajda, S. Performance and Its
912 Limits in Rigid Body Protein-Protein Docking. *Structure* **28**, 1071-1081.e3 (2020).
- 913 18. Lill, M. A. & Danielson, M. L. Computer-aided drug design platform using
914 PyMOL. *J. Comput. Aided. Mol. Des.* **25**, 13–19 (2011).
- 915 19. Mesquita, F. P. *et al.* Kinase inhibitor screening reveals aurora-a kinase is a
916 potential therapeutic and prognostic biomarker of gastric cancer. *J. Cell. Biochem.*
917 **122**, 1376–1388 (2021).
- 918 20. Myers, N. O. Characterization of surface roughness. *Wear* **5**, 182–189 (1962).
- 919 21. Cappella, B. & Dietler, G. Force-distance curves by atomic force microscopy. *Surf.*
920 *Sci. Rep.* **34**, 1–104 (1999).
- 921 22. Souza, P. F. N. *et al.* Neutralizing Effect of Synthetic Peptides toward SARS-
922 CoV - 2. (2022). doi:10.1021/acsomega.2c02203
- 923 23. McGahon, A. J. *et al.* Chapter 9 The End of the (Cell) Line: Methods for the Study
924 of Apoptosis in Vitro. *Methods Cell Biol.* **46**, 153–185 (1995).
- 925 24. Lica, J. J. *et al.* Effective drug concentration and selectivity depends on fraction of
926 primitive cells. *Int. J. Mol. Sci.* **22**, (2021).

- 927 25. Morgan, E. *et al.* The current and future incidence and mortality of gastric cancer
928 in 185 countries, 2020–40: A population-based modelling study.
929 *EClinicalMedicine* **47**, (2022).
- 930 26. Pan, S., Thrift, A. P., Akhdar, G. & El-Serag, H. B. Gastric Cancer Risk in Patients
931 with Long-Term Use of Proton Pump Inhibitors: A Systematic Review and Meta-
932 Analysis of Observational and Interventional Studies. *Dig. Dis. Sci.* **68**, 3732–3744
933 (2023).
- 934 27. Thrift, A. P. & El-Serag, H. B. Burden of gastric cancer. *Clin. Gastroenterol.*
935 *Hepatol.* **18**, 534–542 (2020).
- 936 28. Liu, K. S., Raza, S. A., El-Serag, H. B. & Thrift, A. P. Recent trends in the
937 incidence of gastric cancer in the United States. *J. Clin. Gastroenterol.* **58**, 39–45
938 (2024).
- 939 29. Wagner, A. D. *et al.* EORTC-1203-GITCG-the “INNOVATION”-trial: Effect of
940 chemotherapy alone versus chemotherapy plus trastuzumab, versus chemotherapy
941 plus trastuzumab plus pertuzumab, in the perioperative treatment of HER2
942 positive, gastric and gastroesophageal junction adenoc. *BMC Cancer* **19**, 1–9
943 (2019).
- 944 30. Carlomagno, C. *et al.* Adjuvant FOLFOX-4 in patients with radically resected
945 gastric cancer: Tolerability and prognostic factors. *Exp. Ther. Med.* **1**, 611–617
946 (2010).
- 947 31. Li, W. *et al.* HER2-targeted advanced metastatic gastric/gastroesophageal junction
948 adenocarcinoma: treatment landscape and future perspectives. *Biomark. Res.* **10**,
949 1–20 (2022).
- 950 32. Zhu, Y., Zhu, X., Wei, X., Tang, C. & Zhang, W. HER2-targeted therapies in
951 gastric cancer. *Biochim. Biophys. Acta - Rev. Cancer* **1876**, 188549 (2021).

- 952 33. Sexton, R. E., Al Hallak, M. N., Diab, M. & Azmi, A. S. Gastric cancer: a
953 comprehensive review of current and future treatment strategies. *Cancer*
954 *Metastasis Rev.* **39**, 1179–1203 (2020).
- 955 34. Sato, Y. *et al.* Overview of Chemotherapy for Gastric Cancer. *J. Clin. Med.* **12**, 1–
956 15 (2023).
- 957 35. Cho, Y. H. *et al.* 5-FU promotes stemness of colorectal cancer via p53-mediated
958 WNT/ β -catenin pathway activation. *Nat. Commun.* **2020 111 11**, 1–13 (2020).
- 959 36. Hempel-Bruder, C. *et al.* Colorectal cancer testing rates after implementation of an
960 organised screening programme in Vaud, Switzerland. *Swiss Med. Wkly.* **153**,
961 (2023).
- 962 37. Lima, P. G. *et al.* Synthetic antimicrobial peptides control *Penicillium digitatum*
963 infection in orange fruits. *Food Res. Int.* **147**, (2021).
- 964 38. Aguiar, T. K. B. *et al.* Behind the Curtain : In Silico and In Vitro Experiments
965 Brought to Light New Insights into the Anticryptococcal Action of Synthetic
966 Peptides. 1–18 (2023).
- 967 39. Aguiar, T. K. B. *et al.* No Chance to Survive: Mo-CBP3-PepII Synthetic Peptide
968 Acts on *Cryptococcus neoformans* by Multiple Mechanisms of Action. *Antibiotics*
969 **12**, 378 (2023).
- 970 40. Berge, G. *et al.* Therapeutic vaccination against a murine lymphoma by
971 intratumoral injection of a cationic anticancer peptide. *Cancer Immunol.*
972 *Immunother.* **59**, 1285–1294 (2010).
- 973 41. Lima, P. G. *et al.* Anticandidal activity of synthetic peptides: Mechanism of action
974 revealed by scanning electron and fluorescence microscopies and synergism effect
975 with nystatin. *J. Pept. Sci.* 1–13 (2020). doi:10.1002/psc.3249
- 976 42. Dias, L. P. *et al.* RcAlb-PepII, a synthetic small peptide bioinspired in the 2S

- 977 albumin from the seed cake of *Ricinus communis*, is a potent antimicrobial agent
978 against *Klebsiella pneumoniae* and *Candida parapsilosis*. *Biochim. Biophys. Acta*
979 *- Biomembr.* **1862**, 183092 (2020).
- 980 43. Id, O., Gomes, R., Guimar, S., Id, O. & Article, O. *Antidermatophytic Activity of*
981 *Synthetic Peptides: Action mechanisms and clinical application as adjuvants to*
982 *enhance the activity and decrease the toxicity of Griseofulvin.* **4434**,
- 983 44. Peña-Morán, O. A., Villarreal, M. L., Álvarez-Berber, L., Meneses-Acosta, A. &
984 Rodríguez-López, V. Cytotoxicity, post-treatment recovery, and selectivity
985 analysis of naturally occurring podophyllotoxins from *Bursera fagaroides* var.
986 *fagaroides* on breast cancer cell lines. *Molecules* **21**, 1013 (2016).
- 987 45. Oliveira, P. F. de *et al.* Cytotoxicity screening of essential oils in cancer cell lines.
988 *Rev. Bras. Farmacogn.* **25**, 183–188 (2015).
- 989 46. Badisa, R. B. *et al.* Selective cytotoxic activities of two novel synthetic drugs on
990 human breast carcinoma MCF-7 cells. *Anticancer Res.* **29**, 2993–2996 (2009).
- 991 47. Kaminsky, R., Schmid, C. & Brun, R. An "in vitro selectivity index" for evaluation
992 of cytotoxicity of antitrypanosomal compounds. *In Vitro Toxicol.* **9**, 315–324
993 (1996).
- 994 48. Mortenson, M. M., Schlieman, M. G., Virudachalam, S. & Bold, R. J. Effects of
995 the proteasome inhibitor bortezomib alone and in combination with chemotherapy
996 in the A549 non-small-cell lung cancer cell line. *Cancer Chemother. Pharmacol.*
997 **54**, 343–353 (2004).
- 998 49. Yoo, Y. D. *et al.* Glioma-derived cancer stem cells are hypersensitive to
999 proteasomal inhibition. *EMBO Rep.* **18**, 150–168 (2017).
- 1000 50. Souza, P. F. N. *et al.* A 2S albumin from the seed cake of *ricinus communis* inhibits
1001 trypsin and has strong antibacterial activity against human pathogenic bacteria. *J.*

- 1002 *Nat. Prod.* **79**, (2016).
- 1003 51. Chen, B. *et al.* Targeting Negative Surface Charges of Cancer Cells by
1004 Multifunctional Nanoprobes. *Theranostics* **6**, 1887–1898 (2016).
- 1005 52. Lira, R. B. *et al.* To Close or to Collapse: The Role of Charges on Membrane
1006 Stability upon Pore Formation. *Adv. Sci.* **8**, 2004068 (2021).
- 1007 53. Moleón Baca, J. A., Ontiveros Ortega, A., Aránega Jiménez, A. & Granados
1008 Principal, S. Cells electric charge analyses define specific properties for cancer
1009 cells activity. *Bioelectrochemistry* **144**, 108028 (2022).
- 1010 54. Kaushik, A. C. *et al.* A-CaMP: a tool for anticancer and antimicrobial peptide
1011 generation. *J. Biomol. Struct. Dyn.* **39**, 285–293 (2021).
- 1012 55. Tan, J., Tay, J., Hedrick, J. & Yang, Y. Y. Synthetic macromolecules as
1013 therapeutics that overcome resistance in cancer and microbial infection.
1014 *Biomaterials* **252**, (2020).
- 1015 56. Vitale, I. *et al.* Targeting Cancer Heterogeneity with Immune Responses Driven
1016 by Oncolytic Peptides. *Trends in cancer* **7**, 557–572 (2021).
- 1017 57. Etxaniz, A., González-Bullón, D., Martín, C. & Ostolaza, H. Membrane Repair
1018 Mechanisms against Permeabilization by Pore-Forming Toxins. *Toxins 2018, Vol.*
1019 *10, Page 234* **10**, 234 (2018).
- 1020 58. Lima, P. G., Oliveira, J. T. A., Amaral, J. L., Freitas, C. D. T. & Souza, P. F. N.
1021 Synthetic antimicrobial peptides: Characteristics, design, and potential as
1022 alternative molecules to overcome microbial resistance. *Life Sci.* **278**, 119647
1023 (2021).
- 1024 59. Soares, A. M. S. *et al.* New insights into anthelmintic mechanisms of action of a
1025 synthetic peptide: An ultrastructural and nanomechanical approach. *Polymers*
1026 *(Basel)*. **13**, (2021).

- 1027 60. Lara-Cruz, C., Jiménez-Salazar, J. E., Ramón-Gallegos, E., Damian-Matsumura,
1028 P. & Batina, N. Increasing roughness of the human breast cancer cell membrane
1029 through incorporation of gold nanoparticles. *Int. J. Nanomedicine* **11**, 5149–5161
1030 (2016).
- 1031 61. Hong, S. *et al.* Interaction of poly (amidoamine) dendrimers with supported lipid
1032 bilayers and cells: hole formation and the relation to transport. *Bioconjug. Chem.*
1033 **15**, 774–782 (2004).
- 1034 62. Shukla, R. *et al.* Biocompatibility of gold nanoparticles and their endocytotic fate
1035 inside the cellular compartment: a microscopic overview. *Langmuir* **21**, 10644–
1036 10654 (2005).
- 1037 63. Vasir, J. K. & Labhasetwar, V. Quantification of the force of nanoparticle-cell
1038 membrane interactions and its influence on intracellular trafficking of
1039 nanoparticles. *Biomaterials* **29**, 4244–4252 (2008).
- 1040 64. Baxter, A. A., Lay, F. T., Poon, I. K. H., Kvensakul, M. & Hulett, M. D. Tumor
1041 cell membrane-targeting cationic antimicrobial peptides: novel insights into
1042 mechanisms of action and therapeutic prospects. *Cell. Mol. Life Sci.* **74**, 3809–
1043 3825 (2017).
- 1044 65. Morishita, K., Watanabe, K. & Ichijo, H. Cell volume regulation in cancer cell
1045 migration driven by osmotic water flow. *Cancer Sci.* **110**, 2337–2347 (2019).
- 1046 66. Hu, S. *et al.* Revealing elasticity of largely deformed cells flowing along confining
1047 microchannels. *RSC Adv.* **8**, 1030–1038 (2018).
- 1048 67. Coughlin, M. F. *et al.* Cytoskeletal stiffness, friction, and fluidity of cancer cell
1049 lines with different metastatic potential. *Clin. Exp. Metastasis* **30**, 237–250 (2013).
- 1050 68. Remmerbach, T. W. *et al.* Oral cancer diagnosis by mechanical phenotyping.
1051 *Cancer Res.* **69**, 1728–1732 (2009).

- 1052 69. An, L., Ji, F., Zhao, E., Liu, Y. & Liu, Y. Measuring cell deformation by
1053 microfluidics. *Front. Bioeng. Biotechnol.* **11**, 1–16 (2023).
- 1054 70. Ong, M. S. *et al.* Cytoskeletal proteins in cancer and intracellular stress: A
1055 therapeutic perspective. *Cancers (Basel)*. **12**, 1–24 (2020).
- 1056 71. Vogel, J. P. *et al.* Genome sequencing and analysis of the model grass
1057 *Brachypodium distachyon*. *Nature* **463**, 763–768 (2010).
- 1058 72. Yayan, J., Franke, K.-J., Berger, M., Windisch, W. & Rasche, K. Adhesion,
1059 metastasis, and inhibition of cancer cells: a comprehensive review. *Mol. Biol. Rep.*
1060 **51**, 165 (2024).
- 1061 73. Janiszewska, M., Primi, M. C. & Izzard, T. Cell adhesion in cancer: Beyond the
1062 migration of single cells. *J. Biol. Chem.* **295**, 2495–2505 (2020).
- 1063 74. Lakshmi, R. J. *et al.* Tissue Raman Spectroscopy for the Study of Radiation
1064 Damage: Brain Irradiation of Mice. [https://doi.org/10.1667/0033-](https://doi.org/10.1667/0033-7587(2002)157[0175:TRSFTS]2.0.CO;2)
1065 [7587\(2002\)157\[0175:TRSFTS\]2.0.CO;2](https://doi.org/10.1667/0033-7587(2002)157[0175:TRSFTS]2.0.CO;2) **157**, 175–182 (2002).
- 1066 75. Movasaghi, Z., Rehman, S. & Rehman, I. U. Raman Spectroscopy of Biological
1067 Tissues. *Appl. Spectrosc. Rev.* **42**, 493–541 (2007).
- 1068 76. Cells, S. H. N. & Lepore, M. Multivariate Analysis of Difference Raman Spectra
1069 of the Irradiated Nucleus and Cytoplasm Region of.
- 1070 77. Novikov, N. M., Zolotaryova, S. Y., Gautreau, A. M. & Denisov, E. V. Mutational
1071 drivers of cancer cell migration and invasion. *Br. J. Cancer* **124**, 102–114 (2021).
- 1072 78. Van Zijl, F., Krupitza, G. & Mikulits, W. Initial steps of metastasis: cell invasion
1073 and endothelial transmigration. *Mutat. Res.* **728**, 23–34 (2011).
- 1074 79. Song, Y. *et al.* Therapeutic exosomes loaded with SERPINA5 attenuated
1075 endometrial cancer cell migration via the integrin β 1/FAK signaling pathway. *Cell.*
1076 *Oncol.* **45**, 861–872 (2022).

1077 80. Zhai, F., Wang, J., Luo, X., Ye, M. & Jin, X. Roles of NOLC1 in cancers and viral
1078 infection. *J. Cancer Res. Clin. Oncol.* (2023). doi:10.1007/S00432-023-04934-5
1079
1080

CAPÍTULO IV

ANEXO I

Produção Científica durante o período do Mestrado

Daiane Maria da Silva Brito

Artigos Publicados

Artigo I do Mestrado Publicado na Revista Pharmaceutis Fator 5.8, qualis A1



pharmaceutics



Article

A Shortcut from Genome to Drug: The Employment of Bioinformatic Tools to Find New Targets for Gastric Cancer Treatment

Daiane M. S. Brito^{1,2}, Odnan G. Lima², Felipe P. Mesquita², Emerson L. da Silva², Maria E. A. de Moraes², Rommel M. R. Burbano^{3,4}, Raquel C. Montenegro^{2,5,*} and Pedro F. N. Souza^{1,2,*}

¹ Department of Biochemistry and Molecular Biology, Federal University of Ceará, Fortaleza 60020-181, Brazil

² Pharmacogenetics Laboratory, Drug Research and Development Center, Department of Physiology and Pharmacology, Federal University of Ceará, Fortaleza 60430-160, Brazil

³ Department of Biological Sciences, Oncology Research Center, Federal University of Pará, Belém 66073-005, Brazil; rommel@ufpa.br

⁴ Molecular Biology Laboratory, Ophir Loyola Hospital, Belém 66063-240, Brazil

⁵ Red Latinoamericana de Implementación y Validación de Guías Clínicas Farmacogenómicas (RELIVAF), Cyted, 28015 Madrid, Spain

* Correspondence: rcm.montenegro@gmail.com (R.C.M.); pedrofilhobio@gmail.com or pedrofilhobio@ufc.br (P.F.N.S.)

Abstract: Gastric cancer (GC) is a highly heterogeneous, complex disease and the fifth most common cancer worldwide (about 1 million cases and 784,000 deaths worldwide in 2018). GC has a poor prognosis (the 5-year survival rate is less than 20%), but there is an effort to find genes highly expressed during tumor establishment and use the related proteins as targets to find new anticancer molecules. Data were collected from the Gene Expression Omnibus (GEO) bank to obtain three dataset matrices analyzing gastric tumor tissue versus normal gastric tissue and involving microarray analysis performed using the GPL570 platform and different sources. The data were analyzed using the GEPIA tool for differential expression and KMPLOT for survival analysis. For more robustness, GC data from the TCGA database were used to corroborate the analysis of data from GEO. The genes found in in silico analysis in both GEO and TCGA were confirmed in several lines of GC cells by RT-qPCR. The AlphaFold Protein Structure Database was used to find the corresponding proteins. Then, a structure-based virtual screening was performed to find molecules, and docking analysis was performed using the DockThor server. Our in silico and RT-qPCR analysis results confirmed the high expression of the *AJUBA*, *CD80* and *NOLC1* genes in GC lines. Thus, the corresponding proteins were used in SBVS analysis. There were three molecules, one molecule for each target, MCULE-2386589557-0-6, MCULE-9178344200-0-1 and MCULE-5881513100-0-29. All molecules had favorable pharmacokinetic, pharmacodynamic and toxicological properties. Molecular docking analysis revealed that the molecules interact with proteins in critical sites for their activity. Using a virtual screening approach, a molecular docking study was performed for proteins encoded by genes that play important roles in cellular functions for carcinogenesis. Combining a systematic collection



Citation: Brito, D.M.S.; Lima, O.G.; Mesquita, F.P.; da Silva, E.L.; de Moraes, M.E.A.; Burbano, R.M.R.; Montenegro, R.C.; Souza, P.F.N. A Shortcut from Genome to Drug: The Employment of Bioinformatic Tools to Find New Targets for Gastric Cancer Treatment. *Pharmaceutics* **2023**, *15*, 2303. <https://doi.org/10.3390/pharmaceutics15092303>

Academic Editor: David Barlow

Received: 8 August 2023

Artigo publicado na revista Chemistry and Biodiversity Fator 2,8, qualis A3

doi.org/10.1002/cbdv.202301840

Review



www.cb.wiley.com

Recalculating the Route: Repositioning Antimicrobial Peptides for Cancer Treatment

Isadora de Almeida Gomes,^[a] Ana Beatriz da Lima,^[a] **Dalane Maria da Silva Brito,**^[a, b] Arlene Almeida Lima,^[a] Francisco Laio de Oliveira,^[a] Elmer Adilson Espino Zelaya,^[a] Luciana Magalhães Rebello Alencar,^[c] Débora Castelo Branco de Souza Collares Maia,^[d] Maria Elisabete Amaral de Moraes,^[a] Felipe Pantoja Mesquita,^[a] Pedro Filho Noronha Souza,^{*,[a]} and Raquel C. Montenegro^{*,[a]}

Resistance to antimicrobial drugs has been considered a public health problem. Likewise, the increasing resistance of cancer cells to drugs currently used in therapy has also become a problem. Therefore, the research and development of synthetic peptides bring a new perspective on the emergence of new drugs for treating this resistance since bioinformatics provides a means to optimize these molecules and save time and costs in research. Peptides have several mechanisms of action, such as forming pores on the cell membrane and inhibiting protein synthesis. Some studies report the use of antimicrobial peptides with the potential for action against cancer cells; suggesting a

repositioning of antimicrobial peptides to fight back cancer resistance. There is an alteration in the microenvironment, making its net charge negative for the survival and growth of cancer cells. The changes in glycoproteins favor the membrane to have a more negative charge, favoring the interaction between the cells and the peptide, thus making possible the repositioning of these antimicrobial peptides against cancer. Here, we will discuss the mechanism of action, targets and effects of peptides, comparison between microbial and cancer cells, and proteomic changes caused by the interaction of peptides and cells.

1. Introduction

Drug resistance is a problem for health professionals, as each year, there is a decrease in the production of new drugs, and those available on the market have increasingly lost their effects.^[1] One of the best-known drug resistances is Antimicrobial Resistance (AMR), which has been considered a public health problem since microorganisms have developed escape mechanisms for these drugs.^[2]

The Pan American Health Organization reports that in recent years, the main bacteria causing sepsis in hospitals have developed high levels of resistance to the antibiotics most commonly used to treat the infections they cause.^[3] Resistance

to cancer therapeutics has also become an ongoing problem, and resistance is now attributed to drug inactivation, altered drug targeting, and improved DNA damage repair, among others.^[4] Thus, new compounds have been developed for the treatment of this resistance. An example is the development of synthetic peptides that present an advantage over several drugs since they are formed by sequences of amino acids joined by peptide bonds and perform various functions, such as antimicrobial, antibiofilm, and anticancer activities, among others.^[5,6]

Antimicrobial peptides are found in all living organisms as components of defense systems (Figure 1A). These peptides assume several three-dimensional (3D) structures. The most common 3D structures assumed are α -helical, disordered, β -strand, and mixed (Figure 1B). The prospects of using peptides in treatments against diseases have grown lately. However, some difficulties were observed with its use, such as low oral bioavailability, short plasma half-life, and solubility. The advance in bioinformatics tools has made possible the modulation of peptide sequences to produce synthetic peptides to overcome previously mentioned problems.^[7] Thus, attention to these molecules and their repositioning is an excellent alternative for treating other pathologies such as cancer. Scientific research seeks hard means for cancer treatment, aiming at effectiveness and a good quality of life for the patient. Thus, antimicrobial peptides (AMPs) have been studied for their use against cancer cells, aiming at the ability of some AMPs to also present considerable actions against these cells from their mechanism of action by similarities between these two cells once both

[a] I. de Almeida Gomes, A. B. da Lima, D. M. da Silva Brito, A. Almeida Lima, F. L. de Oliveira, E. A. Espino Zelaya, Prof. Dr. M. E. Amaral de Moraes, Prof. Dr. F. Pantoja Mesquita, Prof. Dr. P. F. Noronha Souza, Prof. Dr. R. C. Montenegro
Pharmacogenetics Laboratory, Drug Research and Development Center (INPDM), Federal University of Ceará, Rua Coronel Nunes de Melo 1000, Fortaleza, CE, 60430-275, Brazil
E-mail: pedrofilho@biologia.ufc.br
rmontenegro@ufc.br

[b] D. M. da Silva Brito
Department of Biochemistry and Molecular Biology, Federal University of Ceará, Fortaleza 60020-187, CE, Brazil

[c] Prof. Dr. L. Magalhães Rebello Alencar
Laboratory of Biophysics and Nanosystems, Physics Department, Federal University of Maranhão, São Luís 65020070, Brazil

[d] Prof. Dr. D. Castelo Branco de Souza Collares Maia
Department of Pathology and Legal Medicine, Federal University of Ceará, Fortaleza, Ceará 60020-187, Brazil

Artigo publicado na revista Current Protein and Peptides Science, Fator 3.8, qualis B1

REVIEW ARTICLE

Natural and Synthetic Peptides to Control Drug-resistant Pathogens

Francisca J.F. de Sousa¹, Igor R.S. Costa¹, Francisco L.P. Cavalcante¹, Ana J.O. Silva¹, **Daiane M.S. Brito¹**, José Y.G. da Silva¹, José J.L. Silva¹, Camila G.L. Almeida¹, Felipe P. Mesquita^{1,2} and Pedro F.N. Souza^{1,2,*}

¹Department of Biochemistry and Molecular Biology, Sciences Center, Federal University of Ceará – Campus do Pici, CEP-60440-554, Fortaleza, Ceará - CE, Brazil; ²Drug Research and Development Center, Department of Physiology and Pharmacology, Federal University of Ceará, Fortaleza60430-275, Brazil

Abstract: Due to the excessive and inappropriate use of antibiotics in farming and clinic, pathogens developed resistance mechanisms to currently used drugs. Thus, because of this resistance, drugs become ineffective, leading to public health problems worldwide. According to the World Health Organization (WHO), microbial resistance to drugs is one of the most threats that humanity must face. Therefore, it is imperative to seek alternative methods to overcome microbial resistance. Here, the potential of natural or synthetic antimicrobial peptides to overcome microbial resistance will be discussed, and how peptides could be a source for new therapeutics molecules. In this context, antimicrobial peptides (natural or synthetic) are considered promising molecules based on their antifungal, antiviral, and antibacterial properties, making them eligible for developing new drugs. In addition, they can act synergistically with existing drugs on the market, revealing a broad spectrum of applications.

ARTICLE HISTORY

Received: March 20, 2023

Revised: April 28, 2023

Accepted: May 09, 2023

DOI:

10.2174/1389203724666230621121330

Keywords: Antibiotic resistance, antimicrobial peptides, multidrug-resistance pathogens, synthetic peptides, drugs, antifungal.

1. INTRODUCTION

1.1. Antimicrobial Resistance

In 1928, while studying the bacterium *Staphylococcus aureus*, the bacteriologist Alexander Fleming observed that one of his cultures was contaminated by mold. In this contaminated culture, he identified the presence of transparent halos, indicating that in the presence of mold, *S. aureus* did not grow [1]. In this case, Fleming identified the mold as a fungus from the genus *Penicillium*, which secreted a molecule that kills *S. aureus*. By chance, Fleming was responsible for discovering the first antibiotic in history: penicillin [2].

In the following decades, the therapeutic use of penicillin as an antibiotic marked the beginning of a revolutionary period in medicine [2]. The golden age of antibiotics, from 1950 to 1970, was marked by the discovery of other relevant molecules to fight infection, such as tetracycline, erythromycin, gentamicin, and vancomycin. Antibiotics dramatically reduced the death rates associated with many infectious diseases. Life expectancy also increased by 5 percent [3].

Despite advances in medicine and a wide range of antimicrobial agents available, infectious diseases still stand out as a major cause of morbidity and mortality. This problem may be driven by the current antimicrobial resistance crisis [4]. Antimicrobials were considered capable of establishing “miracle cures” when introduced into clinical practice [5].

Nevertheless, right after the discovery of penicillin, it became evident that bacteria could rapidly develop resistance mechanisms. It is now known that antimicrobial resistance is a natural evolutionary phenomenon in which pathogens exposed to chemical agents or other etiological stress develop diverse mechanisms to overcome this obstacle to survival. Thus, all classes of antibiotics are associated with the development of antimicrobial resistance [6].

This phenomenon is driven by the excessive and inappropriate use of antibiotics and by the inadequate therapeutic practices of health professionals, favoring the selection of more resistant strains [7]. Additionally, the use of antibiotics in agriculture or food animals significantly increases the development of antimicrobial resistance [8].

Antibiotic resistance acquired by pathogenic microorganisms, the alarming growth of fungal infections, and the emergence of viral diseases threaten public health worldwide and continue to be a major cause of human morbidity [4]. Therefore, the search for new antimicrobial agents and new therapeutic approaches against resistant microorganisms represents an urgent concern [9].

In this context, one of the most promising alternatives to fight infections caused by resistant microorganisms are an-

*Address correspondence to this author at the Department of Biochemistry and Molecular Biology, Sciences Center, Federal University of Ceará - Campus do Pici, CEP-60440-554, Fortaleza, Ceará - CE, Brazil and Drug Research and Development Center, Department of Physiology and Pharmacology, Federal University of Ceará, Fortaleza 60430-275, Brazil; Tel.: +55 (85) 3366 9816; E-mails: pedrofilhobio@gmail.com, pedrofilhobio@ufc.br

Artigos Aceitos para publicação

Atualmente existem dois artigos aceitos para publicação esperando apenas o processo de proofing.

Artigos submetidos

Atualmente existem 4 artigos submetidos em status de “under review”.